Investigating Cable Transfer Impedance and Layout for Microsatellite Applications

Silulami J. Doyi

November 2001

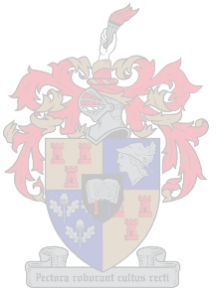

Thesis presented in fulfillment for the requirements of the degree of Master of Science in Engineering Science (Electronic) at the University of Stellenbosch

Study Leader: Prof. H.C. Reader

Co-study Leader: Mr. W.J.A. van Brakel

Declaration

I, the undersigned, hereby declare that the work contained in this thesis is my own original work unless otherwise indicated.

Abstract

Keywords: Electromagnetic Compatibility (EMC), Transfer Impedance, De-Embedding Procedure, EMC Integrated Test System (ITS)

The co-existence of electronic devices and their attached transmission cables requires a careful planning regarding the energy leakage across cable shields. This leakage poses potential serious problems and impedes system functioning.

This thesis pursues an investigation into the EMC cabling protocols for microsatellite systems. Network analysis techniques are applied in calibrating current probes and to recover the cable transfer impedance, Z_T. The calibration approach provides accurate results for frequencies up to 600MHz. The methods used to determine Z_T are based on injecting a disturbance current onto the outside of the cable-under-test (CUT) and measuring the corresponding voltage induced on the centre conductor. Useful results are obtained up to 80MHz with the use of a 0.5m length of cable. It is thus proposed that Z_T is a practical concept for shielding performance evaluation and for the testing of cable philosophy. The results are usable in classifying cables for verification and signal usage.

Further research involves a prediction tool called an EMC ITS that simulates the hardware of a microsatellite system to allow studies on design trade-offs, transmission cable criteria and placement of devices.

Opsomming

Sleutelwoorde: Elektromagnetiese Versoenbaarheid (EMV), Oordragsimpedansie, Onttrekkingsprosedure, EMV-geïntegreerde Toetsstelsel (GTS)

Die gelyktydige bestaan van elektroniese toestelle en hul aangehegte transmissielynkabels benodig deeglike beplanning met betrekking tot die lek van energie deur die kabels se afskerming. Hierdie lekkassie kan ernstige probleme tot gevolg hê en die stelsel se funksionering belemmer.

Hierdie tesis loods 'n ondersoek na die EMV bekabelingprotokolle vir mikrosatelliet-stelsels. Netwerk analise tegnieke word gebruik in die kalibrasie van stroom-probes en die verkryging van die kabel se oordragsimpedansie, Z_T. Die benadering wat gevolg is in die kalibrasie verskaf akkurate resultate tot en met frekwensies van 600MHz. Die metode wat gebruik word om Z_T te bepaal is gebaseer op die injeksie van 'n versteuringstroom op die buitekant van die toetskabel en die meting van die ooreenstemmende spanning wat opgewek word op die binne-geleier. Bruikbare resultate is tot en met 80MHz verkry met die gebruik van 'n kabel met 'n lengte van 0.5m. Daar word dus voorgestel dat Z_T 'n praktiese wyse is om afskermingsprestasie mee te evalueer, asook vir die toetsing van kabel-filosofie. Die resultate is bruikbaar in die klassifikasie van kabels vir verifikasie en seingebruik.

Verdere navorsing sluit in 'n voorspellingswyse wat 'n EMV GTS genoem word, wat die hardewaarde van 'n mikrosatellietstelsel simuleer om studie aangaande ontwerp-kompromieë, transmissielyn kriteria en die plasing van toestelle binne die gebruiksomgewing moontlik te maak.

Dedication

To my grandmother,
Mary Doyi
and
To the memory of my grandfather,
Vakele Willie Doyi
28 January, 1906 - 16 May, 1992

Your constant support and love stands as a cornerstone
in the foundation of my life.

Acknowledgements

Special thanks must be given to:

The Almighty God, for giving me strength and health to finish this project.

My family and my friends for supporting me through all the years of my education.

Prof. Howard Reader and Mr. Wessel van Brakel for their immeasurable assistance towards this research. Their guidance and valuable discussions, which have helped me develop both as a person and an engineer.

Mr. Jan Greyling for his advice on high frequency measurements and construction of test-jigs.

The Department of Communications of the Republic of South Africa, for both moral and financial support.

Contents

List of Figures

List of Tables

List of Photographs

List of Abbreviations & Acronyms

AC	Alternating Current
ADC	Analogue-to-Digital Converter
ANA	Automatic Network Analyzer
BCI	Bulk Current Injection
CISPR	Comité International Special desPerturbations Radioélectroniques (International Special Committee for Radio Interference)
CM	Common-Mode
CUT	Cable-Under-Test
DC	Direct Current
DM	Differential-Mode
EM	Electromagnetic
EMC	Electromagnetic Compatibility
EMI	Electromagnetic Interference
EMF	Electromotive Force
EQS	Electroquasistatic
GP	Ground Plane
GPIB	General-Purpose Interface Bus
HF	High Frequency
IC	Integrated Circuit
IEC	International Electro-technical Commission
IF	Intermediate Frequency
MQS	Magnetoquasistatic
PC	Personal Computer
PCB	Printed Circuit Board
RAM	Random Access Memory
RF	Radio Frequency
RFI	Radio Frequency Interference

Rx	Receiver
SA	Spectrum Analyszer
SE	Shielding Effectiveness
SG	Signal Generator
STP	Shielded Twisted Pair
SUNSAT	Stellenbosch University Satellite
TL	Transmission line
Tx	Transmitter
VHF	Very High Frequency
UHF	Ultra High Frequency

List of Symbols & Physical Constants

a	Transmission line radius (meters)
$\boldsymbol{a}, \boldsymbol{A}$	Area
$\boldsymbol{B}$	Magnetic flux density (tesla)
$\boldsymbol{B}_{actual}$	Actual $\boldsymbol{B}$-field at the probe
c	Velocity of light in free space $\approx 3 \times 10^8$ (meters/second)
C	Capacitance (farads)
C	Bounding contour
d	Distance (meters)
$\boldsymbol{E}$	Electric field (volts/meter)
$\boldsymbol{E}_{actual}$	Actual $\boldsymbol{E}$-field at the probe
EMF_{CUT}	Electromotive force at the terminals of the test cable (volts)
$EMF_{\boldsymbol{B}probe}$	Electromotive force at the $\boldsymbol{B}$-field probe terminals (volts)
$EMF_{\boldsymbol{E}probe}$	Electromotive force at the $\boldsymbol{E}$-field probe terminals (volts)
f_{res}, f_{nml}	Resonance frequencies (Hz)
$\boldsymbol{H}$	Magnetic field (amperes/meter)
h	Height (meters)
h_{GP}	Height of cable or conductor above ground plane (meters)
I	Identity matrix
I	Current (amperes)
I_1, I_2	Current applied at either port 1 or 2 (amperes)
I_{CM}, I'_{CM}	Common-mode current (amperes)
$I_{CM}(z)$	Common-mode current at z (amperes)
I_{DM}	Differential mode current (amperes)
I_{ext}	External disturbance current (amperes)
I_i	Injection current (amperes)
I_{source}	Source current (amperes)
$\boldsymbol{J}$	Current density (amperes/meter^2)

l	Transmission line length (meters)
ℓ	Length of transmission line or test-jig (meters)
L, L_1, L_2, L_3	Inductance (henries)
L_i	Internal inductance per unit length (henries/meter)
L_e	Leakage inductance (henries)
ℓ_L	Left side of the primary winding (meters)
ℓ_R	Right side of the primary winding (meters)
ln	Natural logarithm (base e)
log	Logarithm to base 10
M_1, M_2, M	Mutual inductance (henries/meter)
R_1, R_2, R_3	Direct current or low frequency resistance (ohms)
R_{BC}	Resistance of the return lead (ohms)
R_d	Surface transfer resistance (ohms)
R_{load}	Load resistance (ohms)
R_0	Characteristic resistance (ohms)
s	Separation distance (meters)
S, $\boldsymbol{S}$	Bounded surface
S	Scattering parameters
S_{11}, S_{22}	Reflection Coefficients
S_{12}, S_{21}	Transmission Coefficients
S_{ii}	Reflection coefficient seen looking into port i when all other ports are terminated in matched loads
S_{ij}	Transmission coefficient from port j to port i when all other ports are terminated in matched loads
t, t	Time (seconds)
V	Voltage (volts)
V_1, V_2	Open circuit voltages measured at either port 1 or 2 (volts)
V_1'' , V_1'	Voltage amplitude detected at port 1 (volts)
V_1^+ , V_2^+	Incident voltage wave at either port 1 or 2 (volts)
V_1^- , V_2^-	Reflected voltage wave at either port 1 or 2 (volts)

$V(z)$	Voltage source at z along the transmission line (volts)
V_{DM}	Differential-mode voltage (volts)
V_{load}	Voltage across the load (volts)
V_S	Source voltage (volts)
V_{probe}	Voltage produced at the probe's terminals (volts)
w	Width (meters)
x, y, z	Axes from origin zero (meters)
z	Distance along a line from origin (meters)
Z	Impedance parameters
Z_{02}	Port 2 termination (ohms)
Z_{12}, Z_{21}	Transfer impedance (ohms)
Z_{11}, Z_{22}	Impedance seen looking into either port 1 or 2 (ohms)
Z_{ii}	Input impedances seen looking into port i when all other ports are open-circuited
Z_{ij}	Transfer impedance between ports i and j when all other ports are open-circuited
Z_{in}	Input impedance (ohms)
Z_{int}	Internal impedance of $\boldsymbol{E}$-field probe (ohms)
Z_{load}	Load impedance (ohms)
Z_{loop}	CM loop or $\boldsymbol{B}$-field probe impedance (ohms)
Z'_{loop}	Differential mode loop impedance (ohms)
Z_0	Characteristic impedance of transmission line (ohms)
Z_{S1}	Port 1 source impedance (ohms)
Z_{ST}	System's transfer impedance (ohms)
Z_t	Transfer impedance (ohms)
Z_T	Cable transfer impedance (ohms/meter)
Z'_T	Differential transfer impedance (ohms/meter)
Z_{Term1}	Match termination impedance (ohms)
Z_{tt}	Transfer impedance of current probe (ohms)
Y_t	Transfer admittance ($ohms^{-1}$)

Φ	Magnetic flux (amperes/meter)
Φ_e	External magnetic flux encircling the return conductor
Φ_i	Internal magnetic flux encircling the signal conductor
Φ_M	Magnetic flux encircling coaxial conductors
ω	Angular frequency (radians/second)
θ	Phase delay (degrees)
λ	Wavelength of a single frequency (meters)
ε_0	Permittivity of vacuum (farads/meter)
μ_0	Permeability of vacuum (henries/meter)
α_{cable}	Cable attenuation (radians/meter)
π	3.14159265
i, j, k and n, m, l	Integer values

Chapter
1

Introduction

1.1 Background

Electromagnetic Compatibility (EMC) is the branch of science and engineering concerned with the proper functioning and co-existence of electrical and electronic devices, equipment or systems in all-electromagnetic (EM) environments. The official International Electrotechnical Commission (IEC) definition of EMC is [IEC 50(161)]:

> *The ability of a device, equipment or system to function satisfactory in its electromagnetic environment without introducing intolerable electromagnetic disturbances to anything in that environment.*

Present-day transmissions of data require high-speed signals, which are often associated with fast disturbances that can cause corrupted data and even system failure. However, it is worth noting that EMC is not only a high frequency (HF) phenomenon, it extends right down to low frequencies. A transmission cable may produce radiated fields that may couple significantly onto the on-board computer in a microsatellite. Conversely, the on-board computer is composed of many HF digital circuits that may create emissions that might couple significantly to the transmission cables, causing interference to the sub-systems interconnected by this cable.

The electrical reliability of a transmission cable shield can be defined as its ability to retain the required shielding properties under the effect of specified environment

conditions. The prediction of radiated fields from electrical circuits and their associated transmission cables is of paramount importance to proper electromagnetic interference (EMI) and radio frequency interference (RFI) control.

1.2 Problem Statement

The problem of determining the cable transfer impedance parameter is of utmost importance since the knowledge of such a parameter allows more information to be deduced regarding the EMC performance and characterization of different types and classes of transmission cables. Transfer impedance issues begin to emerge from 100's of kHz. Interconnecting transmission cables are invariably major routes for interference and important sources of radiation. Depending on their internal impedance, circuits and their associate transmission cables can produce, in their proximity, radiated fields that impact significantly on neighbouring circuitry, as well as on system cabling. These fields could be detrimental to the overall system of a microsatellite if clear guidelines are not followed in cabling and placement of devices or sub-systems during the developmental stages.

1.1 Hypothesis

This thesis will focus on an experimental investigation to verify that cable transfer impedance, Z_T, is the best tool for classifying transmission cables according to their signal usage and that it can be used to develop an EMC cabling layout protocol for electronic systems. The protocol will provide information on the selection of appropriate transmission cables to be used in predicted EM environments. If the cabling layout protocol is good it is likely that the transmission cable interconnecting sub-systems will give less radiated fields and more immunity as well. For the achievement of EMC, transmission cables and connectors must be carefully specified.

1.4 About this Thesis

The prime objective of this thesis is to set a starting point to investigate the protection, as well as the performance, of cabling as an integral part of a microsatellite design. The approach of the study is to design, firstly, a test fixture for calibration of current probes that are widely used for diagnostic testing. Secondly, reliable test techniques for the measurement of cable transfer impedance of various transmission cables will be investigated. Lastly, an enclosure system is designed to emulate the hardware flight model of the microsatellite for the purpose of EMC analysis.

Experimental evaluation of transmission cables forms a basis for a reliable and cost-effective technique of designing a cabling layout protocol that is expected to allow a development of clear guidelines on classifying transmission cable and their signal usage based on the performance parameter, Z_T.

The thesis chapter layout is structured as follows. In Chapter 2 the well-known theory of the transfer impedance concept is reviewed. A brief background on cable shielding is presented. The cable transfer impedance parameter is identified as the best parameter for the experimental evaluation of transmission cables. Special attention is given to the current-driven mechanisms involved and the measuring techniques that have been used before.

The project proceeds by looking at the investigation of a proposed experimental technique for the sensible calibration of current probes, a scattering and impedance models of the probe in Chapter 3. The two-port network analysis is discussed and implemented to facilitate the measurement procedure and understanding of the current probe's operation.

The design of two economical, frequency domain (FD) measuring techniques for the determination of cable transfer impedance is pursued in Chapter 4. Along with these, the effects of test-jigs are also investigated.

Theoretical and experimental techniques are developed to design a prediction tool for a microsatellite hardware flight model in Chapter 5. This chapter undertakes measuring emissions from various configurations of transmission cables in order to anticipate the correct choice of usage early in the design stage. A fundamental experiment for the demonstration of electrical noise produced by digital circuits is pursued.

Chapter 6 presents an in-depth analysis and discussion of the findings.

Chapter 7 concludes the thesis through reflecting on its contents and on the results obtained. Future recommendations are made and areas in which further studies can be done are identified.

Chapter

2

Cable Shielding - A Literature Review and Discussion of Relevant Theory

This chapter is based mainly on a literature survey study and its prime objective is to find the most important and predominant cable parameter(s) that can be useful in performing an experimental evaluation of different types and classes of cables.

2.1 Introduction

One of the predominant factors that can cause a device, equipment or system to malfunction, is poor compatibility of the device, equipment or system with its EM environment. The first thing an EMC engineer would be advised to do when correcting this problem would be to inspect the cable layout and placement of devices, equipment or systems. Hence, the first consideration when designing for good EMC is the placement of equipment and careful planning of the configuration for cable layouts. This is the most cost-effective approach if implemented at the design stage.

[Wil96] has presented three levels of EMC control measures for the proper design of an electronic instrument. The first level (primary level) involves circuit design, and the second level (secondary level) involves the interface between the internal circuitry and external cables and filtering. The third level (tertiary level) involves full shielding. Many authors [Mar01, Deu93, Wil96, and Hor98] identified the secondary level as the invariably major route for interference to enter or leave the electronic instrument. Thus, this invites further exploration

for the purposes of EMC research and development to bring innovations to the electrical and electronic manufacturing industries.

Shielded cables are commonly used to protect signals being transported between equipment from EMI [Rüt99]. But they are not the only class of cables e.g. unshielded twisted pair, ribbon, etc. are widely used in telecommunication networks and computers. Therefore, they should also be introduced and investigated for their performance. Signal integrity in information carrying cables (interconnection links) can be maintained if a number of precautions are taken before hand, e.g. cable layouts must be devised to provide immunity against conducted and radiated emissions (and not be a source of EMI as well).

Modern technologies are rapidly moving towards high-speed operating environments, clock pulses, integrated circuit (IC) switches, etc. Therefore, they are often potential sources of EMI. The fast disturbances generated externally by the switching noise of high frequency (HF) digital circuits could cause currents and charges to appear on the shields of interconnecting cables and, as the shields are not perfect, these external currents and charges could couple to the internal signal-carrying conductor(s). This will impede the proper system functioning. EMI can never be completely eliminated, due to the very nature and positioning of most electrical systems [Wal99]. The design of robust and reliable cabling protocols can play a vital role in reducing EMI to acceptable levels, taking into account that the need for cable layout depends on the particular EM environment of interest. Thus, the shielding performance of cables, their loop sizes and grounding philosophies in a circuit are very important for the achievement of EMC.

The leakage of EM energy to or from a cable in an electronic system is important as it describes how immune a cable is to interference and how much it contributes to additional, unwanted, signals in the ambient environment. Cables are often large and effective antennas, carrying common-mode (CM) currents to or from the apparatus [Deu93]. These currents may induce electrical noise not only at the input and output circuits directly connected to the leads, but also deeper inside the apparatus. Thus, these currents contaminate the wanted signals inside the apparatus. The literature from [Wil96,

p124] and [Hor98] has reported that CM emission from these cables often dominates the direct radiation from the printed circuit board (PCB). Because of their lengths, they are more efficient at interacting with the EM environment. To alleviate EMC problems in a piece of equipment, thorough research on coupling parameters should be conducted to assist in the selection of appropriate cables, cable layout and grounding philosophy.

2.2 Transfer Impedance Concept

2.2.1 Theoretical Background

The work presented by Tsaliovich [Tsa95] suggests that, if little or no information about the specific cable applications is known, the shield transfer function may be the only way to evaluate and compare different shields. On the other hand, if the application data is available, the transfer function serves as a cornerstone to develop *system-specific shielding effectiveness* parameters with the required relevance to a specific task. Several characteristics, which would belong to the transfer function category, have been known and widely used for many years. One such characteristic that is often used is *transfer impedance*, Z_t, first introduced by Schelkunoff [Tsa95].

In the 1930s, Schelkunoff recognised that the impedance concept could be extended to EM fields in a systematic way and noted that impedance should be regarded as a characteristic of the type of field, as well as of the medium in which the waves propagate [Poz98]. Vanlandschoot [Val97] describes Z_t as representing magnetic field (inductive) coupling and transfer admittance, Y_t, as representing electric field (capacitive) coupling between the cable and its environment. The former is identified as the best practical tool and useful measure of the shielding effectiveness (*SE*). Moreover, the measure of Z_t is more robust than measurements of Y_t, the latter being more environmentally sensitive [Ben97, p137]. These transfer parameters can be expressed in current and voltage relation as follows:

$$V = Z_t I \tag{2.2.1.1}$$

$$I = Y_t V \tag{2.2.1.2}$$

Electric field coupling dominates with high impedance circuits, low current loads. Thus, Y_t will be equal to zero. Magnetic field coupling dominates with low impedance circuits, high current loads. For the purpose of simplifying analysis, quasistatic conditions are assumed. Quasistatic refers to the situation where circuit dimensions are much less than a wavelength.

- Magnetoquasistatic (MQS) conditions imply that capacitive coupling is negligible small.
- Electroquasistatic (EQS) conditions imply that inductive coupling is negligible small.

The concept of Z_t forms an important link between field theory and transmission line (TL) or circuit theory. For a solid, non-magnetic material, tubular shield, the electrostatic shielding is much greater than the magnetostatic shielding, and as a result, the transfer impedance term dominates at low frequencies [Tes97, pp. 451-455]. Therefore, the contribution of Y_t to the total response of the cable is very small.

The two cable parameters mentioned above have a significant role in describing the field coupling mechanism from a CM to differential-mode (DM) circuit and vice-versa. General definitions of these parameters for cable shielding engineering are as follows:

- Y_t describes the process by which the portion of the induced charge on the cable shield finds its way onto the internal conductor(s) inside the shield.
- Z_t describes the process by which the portion of the induced current on the cable shield finds its way onto the internal conductor(s) inside the shield.

In Figure 2.2.1.1 the current driven mechanism that leads to the definition of Z_t is depicted. V_{DM}, is the induced voltage per unit length, ℓ, inside the shield due to the disturbing current, I_{CM}, flowing along the outer surface of the shield.

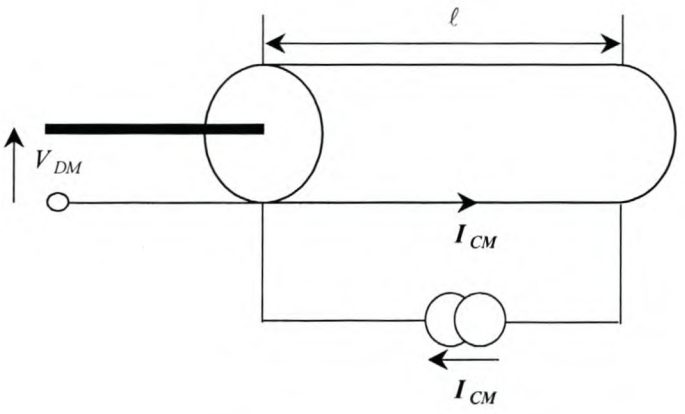

Figure 2.2.1.1: Conceptual illustration of the coupling mechanism that leads to the definition of transfer impedance.

The DM and CM circuits can be distinguished according to the current distributions and their properties as follows [Clo99]:

- DM excitation - the current has, at each instant along the cable or structure, the same amplitude but flows in opposite directions. Thus, the net current through an enclosed loop surrounding the cable or structure is zero.
- CM excitation - the current has, at each instant along the cable or structure, the same amplitude and flows in one direction. Thus, the net current through an enclosed loop surrounding the cable or structure is not zero. Often the coupling via the large CM loop is the most important in EMC problems.

The DM currents are the desired currents while the CM currents are not intended, but will be present in practical systems. Figure 2.2.1.2 shows the circulation of currents in the DM and CM circuits formed by a coaxial cable and the environment in which the cable is situated.

Design analyses and correction of EMC problems cannot be implemented without identifying the current paths and types of currents flowing in wire loops, harnesses and routing.

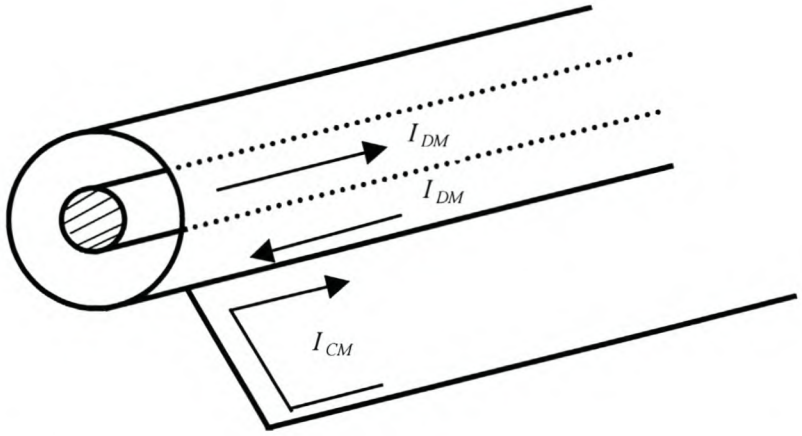

Figure 2.2.1.2: A coaxial cable forming two circuits with the environment (after [Deu93]).

The DM current (I_{DM}) returns via the interior of the cable shield while the CM current (I_{CM}) flows on the outer surface of the cable shield. I_{DM} is associated with less radiation problems because its net current is zero, whilst I_{CM} is associated with more radiation problems since it usually flows in large loops and its net current is not zero.

From the illustration of Figure 2.2.1.2, three functions of the cable shield can be identified, be it coaxial or parallel conductor pair cables. First, it serves as a return path for I_{DM}. Second, it forms a part of the CM circuit, i.e. it closes the CM loop to allow for current flow. Third, it may shield the interior of the cable against external EM fields. The grounded shield should carry the main part of I_{CM} and prevent it from reaching the cable signal lead and thus from entering the apparatus [Deu93].

2.2.2 Types of Transfer Impedance

[Rüt99] attempted clarification on the seemingly conflicting definitions of transfer impedance concepts and differing notions were found to be complementing each other. It was reported there that the 'transfer impedance' as a single concept is subdivided as follows:

- 'differential transfer impedance', Z'_T
- 'cable transfer impedance', Z_T
- 'system transfer impedance', Z_t

The 'differential transfer impedance' is defined for an infinitesimal section of shielded cable and is purely a cable shield parameter, determined by the shield geometry. Thus, it does not account for all the factors involved in the *system-level shielding*.

$$Z'_T = \frac{1}{I_{CM}} \left(\frac{dV}{d\ell} \right)_{I_{DM}=0} \quad \Omega/\text{m} \qquad (2.2.2.1)$$

Wavelength effects at higher frequencies require that Z'_T be integrated over the total cable including end connections, taking into account the phase. The 'cable transfer impedance' is defined as a measure of the *SE* of an actual cable, including any end connections. Alternatively, [Wil96] refer to 'cable transfer impedance' as a 'surface transfer impedance' which is a measure of the voltage induced on the inner conductor(s) of the cable DM circuit by an interference current flowing down the cable's outer shield. This transfer impedance will vary with frequency.

The illustration shown in Figure 2.2.2.1 is usually used for theoretical analysis and experimental determination of Z_T. For instance, Morrielo [Mor97] gives an expression for Z_T as the quotient of the series *EMF* (electromotive force), V_{DM}, induced per unit length, ℓ, inside

the shield to the disturbing current, I_{CM}, flowing along the outer surface of the shield in an electrically short piece of cable with connectors:

$$Z_T = \left(\frac{V_{DM}}{I_{CM} \ell} \right)_{I_{DM}=0} \tag{2.2.2.2}$$

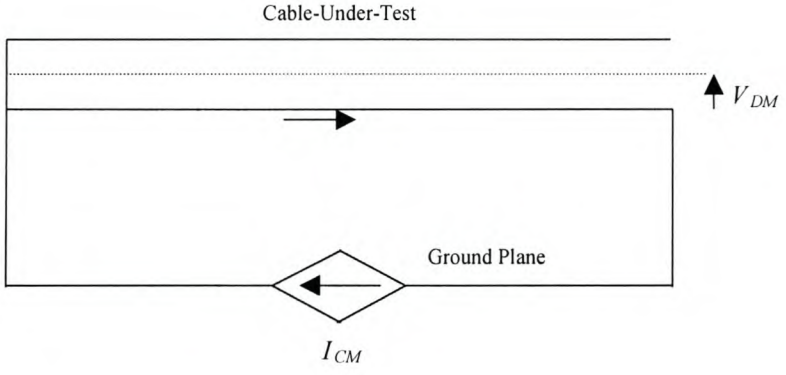

Figure 2.2.2.1: Cable transfer impedance of various screen types (after [Wil96]).

From the cable transfer impedance illustration of Figure 2.2.2.1 one end of the cable is deliberately short-circuited (signal conductor to return conductor). The other end is open-circuited i.e. a representation of a high impedance termination into measuring equipment such as an oscilloscope. Hence, this satisfies the condition that the DM current must be zero (I_{DM} = 0) for the experimental determination of Z_T. The voltage, V_{DM}, is developed between the signal and return conductors. This cable property is usually called the 'surface transfer impedance' by many authors and will be expressed in per unit length for comparison with published data.

The 'system transfer impedance' is defined as the ratio of the total disturbance voltage in the DM circuit (i.e. the DM voltage produced without applying an input signal to the DM circuit) and the CM current causing it [Rüt99]:

$$Z_t = \left.\frac{V_{DM}}{I_{CM}}\right|_{I_{DM}=0} \qquad (2.2.2.3)$$

Z_t can be determined experimentally by exciting a current I_{CM} and measuring the resulting voltage V_{DM}. The value of Z_t depends on the three-dimensional geometry of both the injection and the DM circuit [Hel95]. The 'system transfer impedance' includes the effect of the entire cable and the surrounding equipment, e.g. equipment housing and/or other connections to grounding structures [Rüt99]. This property is generally referred to as just the transfer impedance. Although Z_t may be useful as it accounts for all the factors involved in the *system-level shielding*, Z_T is of prime importance as it provides information about the actual cable performance (without system effects) and properties, which contributes to the overall *system-level shielding*.

2.2.3 Transfer Impedance Approach to Transmission Cables

The study and measurements of 'cable transfer impedance' Z_T and 'system transfer impedance' Z_t will provide us with the appropriate data to classify cables according to their signal usage and the EM environment of interest. As soon as equipment is fitted with external cables with lengths exceeding the largest equipment dimension, it is highly probable that these cables will become the largest contributors to radiated emissions, and susceptibility as well [Mar92, p33]. To shield against EM field interference, usually both ends of the shield are grounded. This is the most important technique in practice for preventing EM field coupling.

Figure 2.2.3.1 emulates two pieces of equipment (or two parts of a single piece of equipment) communicating with each other via a parallel TL link. The source, cable and load form the DM circuit, while the cable and environment form the CM circuit. The source and the load are connected to the ground plane (GP). The way that the cable shield is terminated at the connector interface is critical in maintaining the shielding

properties of the cable. The literature shows that coaxial and multi-conductor cables with more than one shield offer a lower Z_T [Deu93].

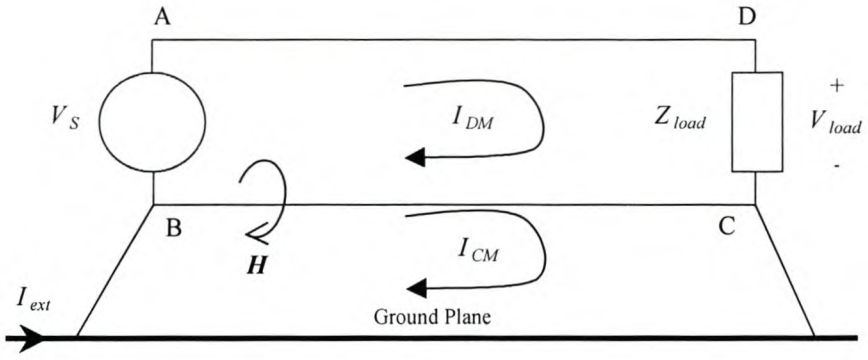

Figure 2.2.3.1: Illustration of two-parallel leads above GP, transporting a signal from a source to a load (after [Laa98]).

Two parallel leads transport a signal from a source V_S to a high-impedance load Z_{load}. In addition to the DM current I_{DM}, a CM current I_{CM} may flow over the lower lead. The current I_{CM} causes a magnetic flux between the parallel leads, which corresponds to a mutual inductance part of Z_t. An interference voltage equal to $Z_t I_{CM}$ shows up across the load Z_{load}.

From Figure 2.2.3.1, two distinct TL's can be defined: an external line (CM circuit) having currents and charges flowing on the exterior of the cable shield, together with a GP return, and an internal line (DM circuit) formed by ABCD that carries the intended signal current I_{DM}. In the Figure, I_{CM} may be the current due to external EMI fields in the large CM loop, or to a current I_{ext}. Thus, the internal line acts as a pickup loop antenna. This leads to an undesired response of the circuit configuration shown by Figure 2.2.3.1. The mechanism discussed in this section could be reciprocated when the cable acts as a transmitting antenna. This will occur when the internal line gives rise to radiated emissions.

In Figure 2.2.3.1, the signal circuit consists of two-parallel leads, with I_{CM} flowing through the lower lead BC. To determine the interference voltages, Faraday's induction law is applied to a properly chosen closed contour and is expressed as follows:

$$\oint \boldsymbol{E} \cdot dl = -\frac{\partial}{\partial t} \oiint \boldsymbol{B} \cdot d\boldsymbol{S} = -\frac{\partial \Phi}{\partial t} \tag{2.2.3.1}$$

in which Φ is the magnetic flux enclosed by the contour, while $\boldsymbol{E}$ and $\boldsymbol{B}$ are the electric and magnetic field vectors respectively. Equation (2.2.3.1) is applied to contour ABCD: through the source V_S, the signal lead, the load Z_{load}, and back through the grounded lead. The high-impedance load Z_{load} is chosen such that I_{DM} is negligible small. A flux appears in the signal circuit due to the magnetic field $\boldsymbol{H}$ caused by the current I_{CM}. Integrating the $\boldsymbol{H}$-field ($\frac{I_{CM}}{2\pi a}$) over the area enclosed by the contour, one finds

$$\Phi = \mu_0 \oiint \boldsymbol{H} \cdot d\boldsymbol{S} = \mu_0 \frac{I_{CM} l}{2\pi} ln \frac{s}{a} \tag{2.2.3.2}$$

with l the length of the cable, s the separation of the two leads, and a the radius of each lead.

When the single return lead is replaced by a coaxial cylinder around the signal lead, as shown in Figure 2.2.3.2, I_{CM} is evenly distributed around the signal lead AD shown in Figure 2.2.3.1. The magnetic field $\boldsymbol{H}$ due to I_{CM} remains largely outside the cable shield and thus outside the signal circuit. This reduces Z_T drastically since the $\boldsymbol{H}$-field causes only little flux inside the DM (or signal) circuit. But, if 'pigtails' are used at the ends of the coaxial shield, they will largely contribute to Z_T. A 'pigtail' refers to a non-360° connected outer of a cable at an interface, causing increased magnetic coupling between interior and exterior circuits.

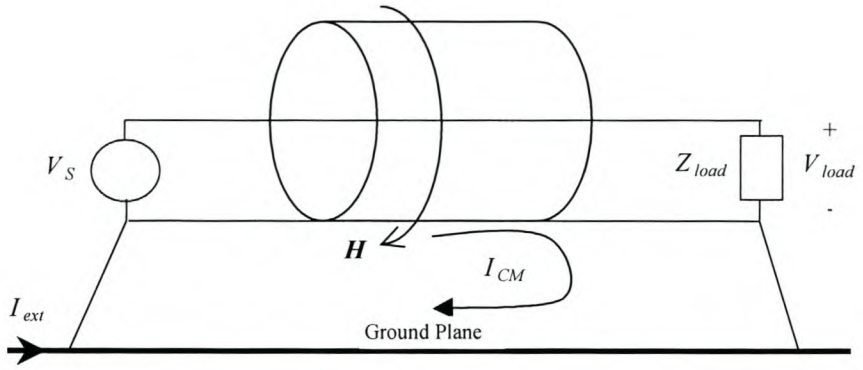

Figure 2.2.3.2: A coaxial lead replaces the return lead BC in Figure 2.2.3.1 ([after [Laa98]).

At HF 'pigtails' may be as bad as having no connection of the cable outer at all. From an EMC perspective, the leakage of EM energy from a circuit to the ambient environment is an undesired phenomenon, since it give rise to radiated emissions. Hence, measurements of Z_T are important, because they allow more information to be deduced about the cable shielding performance. This cable coupling parameter, Z_T, can be encountered with any cables, e.g. twin-flex, shielded twisted-pair, etc.

For a braided shield, the current pattern is complex due to the overlapping of individual strands of the shield; it results in less shielding with an increase in frequency. Some accurate models for calculating the surface resistance term of cable transfer impedance have been developed by [Van78] for many cable types. Predictions of the transfer mutual inductance term are much more difficult, especially when inhomogeneous shields such as braided ones are involved. Computation of Z_T is therefore often impossible and it is usually this quantity that has to be determined by measurement techniques.

2.3 Transmission Line Theory

2.3.1 Theoretical Description

For the purposes of simplification the analysis of the measurement systems are based on the TL approach as depicted by Figure 2.3.1.1, field theory and two-port network analysis. The theoretical prediction is based on the assumption that the length of the TL, ℓ, is only a fraction of a wavelength long, i.e. $\ell << \lambda$. If this condition applies the system may be modelled by a simple lumped element circuit, instead of a generally distributed element circuit. The model is invalid if the test cable lengths are comparable to a wavelength.

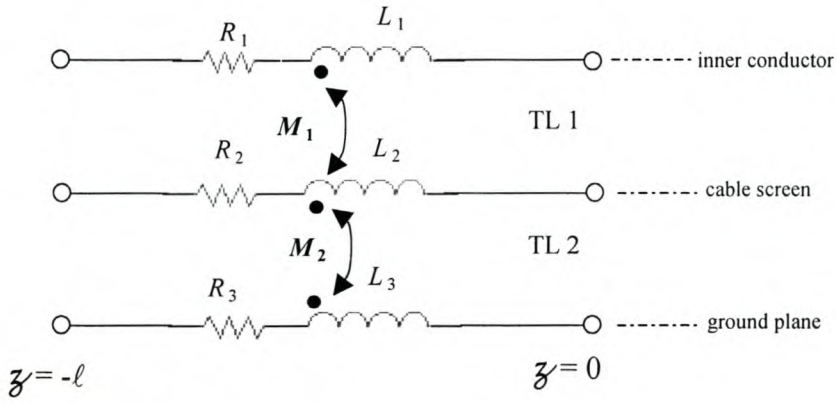

Figure 2.3.1.1: Lumped circuit model for the two transmission-lines approach (after [Mil98]).

In the chosen frequency range the experimental setup can be modelled with lumped TL parameters as illustrated in Figure 2.3.1.1. The inductors L_1, L_2 and L_3 are specified as properties of closed loops (i.e. TL1 and TL2). R_1, R_2 and R_3 are the usual direct current (DC) or low frequency resistances for the inner conductor, cable screen and GP, respectively. The mutual inductor terms M_1 and M_2 represent the magnetic field coupling that occurs between parts of the configuration test system as depicted by Figure 2.3.1.1

[Ram94, p175]. Vance [Van78, p45] gave an expression for the characteristic impedance of the shield-ground TL:

$$Z_0 = 60\cosh^{-1}\left(h_{GP}/a\right) \tag{2.3.1.1}$$

The shield-ground TL (or CM loop) characteristic impedance can be calculated using equation (2.3.1.1), where a is the radius of the cable and h_{GP} is the height (in air) above the GP. The following approximation can be used if the height of the test cable above ground is much greater than the radius a of the test cable.

$$Z_0 \approx 60log(2h_{GP}/a) \quad \left(h_{GP} >> a\right) \tag{2.3.1.2}$$

For measurements at higher frequencies [Val97], the impedance variations in the inner and outer TL's must be taken into account for correct determination of the magnitude of cable transfer impedance, Z_T. For correct modelling at higher frequencies, Figure 2.3.1.2 shows the required TL model used by [Ben96].

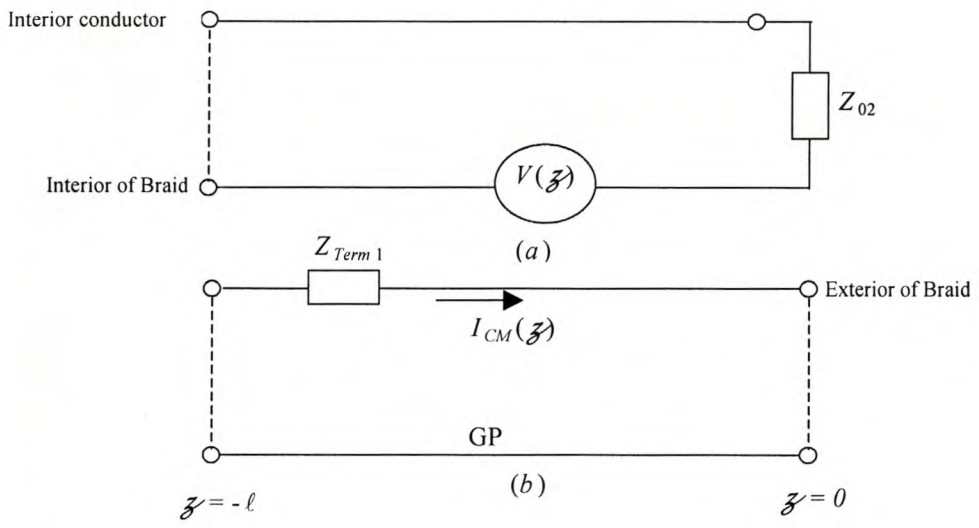

Figure 2.3.1.2: Distributed voltage $V(z)$ and current $I_{CM}(z)$ required for modelling at higher frequencies (after [Ben96]).

From Figure 2.3.1.2(*a*), $V(z)$ is the voltage source at z induced between the test cable interior screen and inner conductor. This is due to the disturbing current $I_{CM}(z)$ at z flowing over the test cable screen that returns via the GP. Z_{02} is the internal impedance of the measuring equipment. Figure 2.3.1.2(*b*) shows the short-circuited TL with the matching resistor Z_{Term1}.

2.4 Exploration of Z_T - Review of Measurement Techniques

A test fixture for measuring cable transfer impedance must be designed to minimise spurious coupling between the excitation source and the detection circuits. In a review of Z_T, measurements that are carried out with network analyzers, or similar data acquisition equipment, currents tend to leak out of the driving cables and flow over the outside of the test fixture and onto (and into) the coaxial cable carrying the measured internal signal. It is thus advisable to use protection, such as an EMC cabinet to prevent contamination of the desired signal(s).

As Z_T is such a useful parameter in the evaluation of the *SE* of cables, many measurement techniques, which emulate more or less the actual EM environment, have been proposed over the years. Some of these techniques are the:

1. Current Probe Technique
2. Triaxial Test Cable Technique
3. Wire-Injection Technique.
4. Standard Triaxial Technique.

The first two are summarized in this section.

There have been several stated requirements for techniques to investigate the effectiveness of a cable shield, including [Atk84]:

1. Repeatability.
2. Potential for test automation.
3. Simplicity of equipment setup and test sample preparation.
4. Low time and labour consumption.
5. Low cost.
6. Straightforward physical interpretation of the test results and their connection with the product quality.

Chapter 4 describes and evaluates two measurement techniques that go some way toward meeting these goals. The test of cable shielding procedure is summarised in the form of a flow diagram in appendix A based on the above-mentioned requirements. The measurement results that were presented using the above-mentioned setups are mainly designed for shielded braided cables. This invites exploration and development of measuring techniques suitable for both shielded and unshielded cables.

In the case of multi-conductor cables, all the inner conductors have to be shorted at both ends [Kle93]. This simplifies the TL analysis because all the inner conductors are regarded together as one single conductor. When preparing the cable-under-test (CUT), the non-driven end of the cable is terminated in a way that corresponds to the measurement technique (Z_{load} = 0, 50 or $\infty\Omega$). The case where the CUT is terminated into a 50Ω-matched load is challenging for Z_T measurements, because its effect must be removed from the actual measured Z_T values.

2.4.1 Triaxial Test Cable Technique

This method was proposed by Martin and Mendenhall and is another variation on the standard triaxial technique [Coa96]. In this approach, the CUT has the braid from another length of the test cable 'milked on' or 'pulled on' over its insulating jacket. The 'milking on' process is difficult and care must be taken not to damage the cable or braid. This technique is more versatile than any other as any type or length of cable can be used. However, the results obtained may not be accurate as the 'milking on' process disturbs the braid. This suggest that this method does not fully satisfy the requirements set out above, particularly points (3) and (4). So, the 'Current Probe Technique' was developed to overcome these complications.

2.4.2 Current Probe Technique

The current probe technique was originally proposed by Atkinson [Atk84] at Sheffield University in 1984. The original technique has been simplified and extended by authors such as Cheng [Che95]. This technique could theoretically be used on any length of a cable. The experimental part of the technique is quick and easy to carry out as required by industrial specifications.

2.5 Concluding Remarks

The computation of Z_T is often impossible; hence it is determined by ways of measurement. Transfer impedance is reciprocal, and thus applies equally to emission and susceptibility (immunity). Z_T can be accurately determined if other effects such as CM currents and capacitive coupling are carefully avoided or characterized in the test-system; the effects of test-jigs must be distinguished from the measured results. All of the techniques discussed do yield values of cable transfer impedance to a reasonable degree

of accuracy. However, most of them are complicated to setup and are not easy to interpret.

Triaxial based test fixtures are associated with complications such as the preparation of the test cable sample, milking on process that may disturb the braid structure, etc. The current probe technique, an extended version of which will later be introduced, meets the above-mentioned requirements. According to Morriello, its circuit model is the same as that of the triaxial device, which is complex. Moreover, at HF it requires a correction factor that may introduce severe errors in the calculations, rendering the analysis unreliable. This is a challenge for all these techniques to be improved; or new techniques need to be developed to be recommended by EMC international standards.

The contribution of Y_t to the total response of the cable is usually small. For this reason the investigation to be pursued in the following chapters will concentrate on Z_t. Low values of Z_t or Y_t imply a low interaction between the cable and its EM environment. Thus, a good quality cable should have a low Z_T measured value. Therefore, the quality of a shielded or unshielded cable can be characterised by its cable transfer impedance.

The Z_T of cables is a local parameter along the DM circuit, its value depends on the type of the DM circuit (bifilar pair or coaxial) and on the end terminations used. The measurement of Z_T is a practical tool for shielding performance evaluation and its result can be used to classify cables.

Chapter

3

Current Probe Calibration Techniques

In this chapter, the general fundamental concepts regarding current probes are discussed along with the experimental evaluation of the current probes' transducer factors (i.e. the transfer impedance, Z_{tt}) using a proposed measurement technique. EMC applications of the transformer and important problems pertaining to the reliability and performance of the measurement procedure are addressed. The conversion of scattering (S) to impedance (Z) parameters proves to be useful in obtaining the Z_{tt} frequency domain (FD) response.

3.1 Introduction

A current probe is usually built on a toroidal core and is designed to convert the current-under-investigation to a voltage, which can be detected by a measuring instrument. Current probes provide means of accurately measuring net (common-mode) radio frequency (RF) current flowing on a conductor or bundle of conductors without requiring a direct connection to the conductor(s) of interest.

Current probes are widely used not only in emission measurements but also for current injection purposes. Bulk Current Injection (BCI) techniques have gained wide acceptance in aerospace, commercial and military EMI testing, because they provide an economical way of verifying the immunity against radiated interference [Cer01]. Besides the regulatory aspects of this test, it is particularly adopted for pre-compliance testing during product prototype stages to quickly establish the susceptibility of the equipment under test.

Practical experience has also shown that the process of applying current probes in pre-compliance testing of equipment reduces the number of expensive failures in electronic designs. Current probes are simply clamp-on, calibrated transformers. The official International Special Committee on Radio Interference (CISPR) definition of current probes is [CISPR 16]:

> *Current probes can be used to make measurements of asymmetric (common-mode) disturbance currents on conductors without making ohmic contact with the conductor or having to break the conductor (clamp-on current transformer).*

Industrial and research applications require a quick, simple, economical and sensible technique to evaluate the transfer impedance parameter, Z_{tt}, of current probes. Because of this, development of a test-jig technique for the evaluation of Z_{tt} for current probes is pursued. The proposed measurement technique provides good results for frequencies below 600MHz with a calibration fixture (jig) of simple design.

3.2 Calibration for Measurement Purposes

The primary measurement range of these current probes is in the 30Hz to 100MHz region as reported by CISPR specifications. However, CISPR recommends that general EMC measurements be made between 30Hz and 1000MHz. For probe measurements above 100MHz, care must be taken to position the probe so as to measure the maximum current. It is desirable that the frequency response of a current probe be as flat as possible across the passband. CISPR 16 specifies that its Z_{tt} must be in the region of 0.1Ω to 5Ω in the 30Hz to 1000MHz range and 0.001Ω to 0.1Ω below it (measured with a 50Ω system).

The calibration of a current probe implies experimental determination of Z_{tt} of the particular measurement probe using a special calibration fixture. The parameter, Z_{tt}, of these devices is defined as the ratio of secondary voltage (generally across a 50Ω resistive load) to the primary current [CISPR 16], i.e. it relates the current on the cable to be measured to the voltage at the

transducer terminals. The measured response of Z_{tt} for the probe can be useful for characterising, as well as determining, the sensitivity of various current probes. To obtain maximum sensitivity, Z_{tt} should be as high as possible.

The proposed measurement technique is applied to an EMCO[1] model 94111-1L series current probe in the region of 300kHz-1GHz. The current probe is a broadband RF transformer for use with EMI test equipment and can measure RF currents on cables without physically disturbing the circuit. The calibration is done on a test-jig, which is made of ≈1mm thick brass, forming a rectangular fixture with two open sides. The present technique is verified and validated by comparing the measured results with the data provided by the manufacturer of the current probe.

[1] For the probe's technical specifications and description refer to appendix B.

3.3 Experiment and Analysis Descriptions

The configuration of the experimental setup is shown in Figure 3.3. The dedicated jig is essentially a conducting enclosure made of brass with *SMA* connectors fixed to two opposite faces to allow the instrumentation connection.

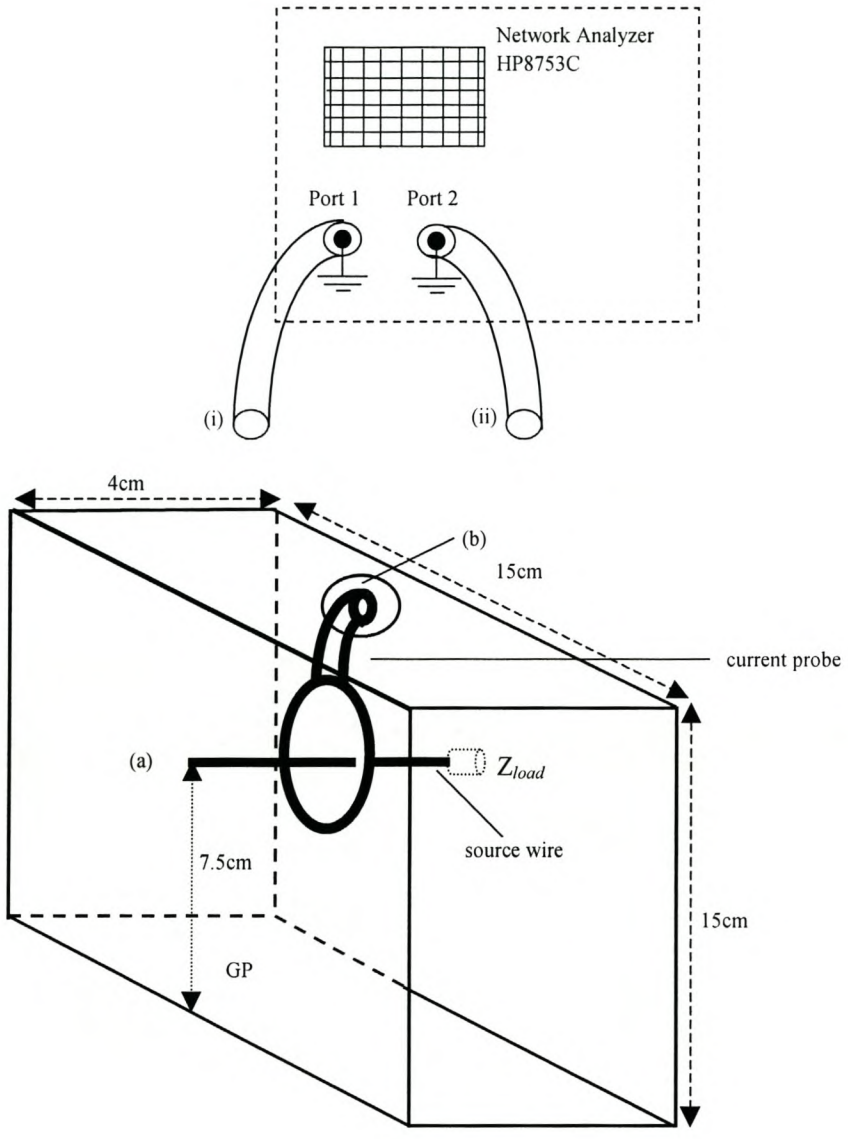

Figure 3.3: Configuration of the experiment with the geometry of the calibration fixture and the equipment required for measurements.

The enclosure is a double-open-sided box, thus providing access to the source wire. The source wire of about 3mm in diameter is centrally positioned inside the enclosure. It connects the centre conductors of the coaxial ports and is maintained at a constant height of 75mm above the GP. The non-driven end of the source wire is terminated in a 50Ω load, Z_{load}. Semi-rigid coaxial cables, 0.5m in length and with low cable transfer impedance, Z_T, lead to the test fixture and connect with the reference calibration points (i) and (ii) to (a) and (b) planes, respectively.

The chosen physical geometry of the test-jig is dictated by the size of the current probe. Thus, the jig has a largest physical dimension of 0.15m. The wavelength at the upper frequency (1GHz) limit is 0.3m, so the jig is said to be electrically small. The jig has a metallic shielding lid with an insulated hole and its diameter was determined by the size of the N-type output connector of the current probe. The purpose of the lid is to ensure some EM shielding of the probe-under-test from fields produced by CM currents on the feed cables and screening of stray capacitance. The insulation prevents electrical contact between the probe and jig structure. The probe is positioned at the centre of the source wire and is not disturbed during measurements. Photograph 3.3 depicts the setup within the screened room.

The experiment is performed by measuring the system's *S*-parameters on a calibrated HP8753C automatic network analyzer (ANA) in the frequency range from 300kHz to 1GHz. These *S*-parameters are recorded and converted to *Z*-parameters. The ANA was linked to an HPVee PC program through an IEEE 488 General-Purpose Interface Bus (GPIB) connection, which allowed for automatic collecting and storage of data onto a disk.

In the following sections three description models are introduced. The first is the *S*-parameter model, which facilitates the measurement procedure by treating the system as a two-port network and can be determined by direct measurements. The second is the field theory model, which is primarily intended to describe the operation of the probe. The third model is the *Z*-parameters, which are derivable from the measured *S*-parameters. The implementation of the calibration is based on network analysis techniques (i.e. the combination of *S* and *Z*-parameter

models) to obtain a full description of the measuring system. Hence, an S to Z-parameter conversion procedure will be used to derive the Z_{tt}.

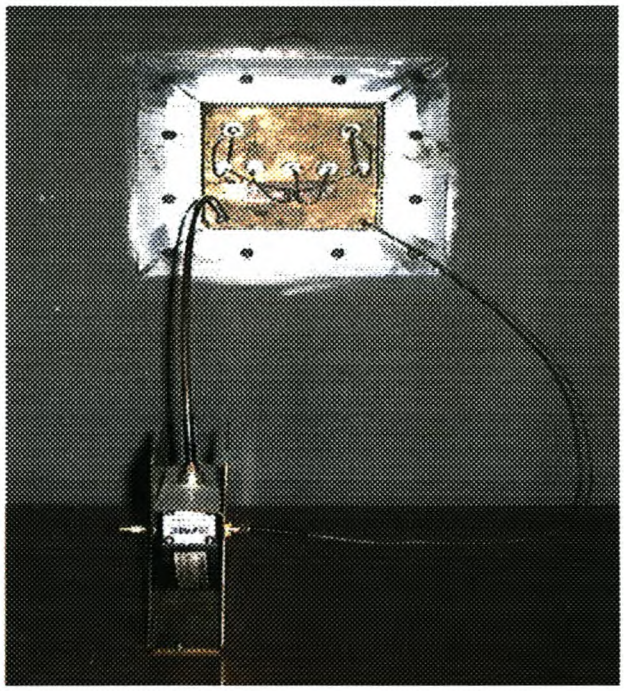

Photograph 3.3: Current probe configuration setup within the screened room.

3.3.1 Scattering-Parameter Model

When a probe clamps over the conductor or cable in which current is to be measured, the conductor forms the primary winding of the test measuring system concerned. Therefore, this discussion will refer to the source wire current as just the primary winding [EMCO, 97], and the probe as the secondary winding as depicted in Figure 3.3.1.1.

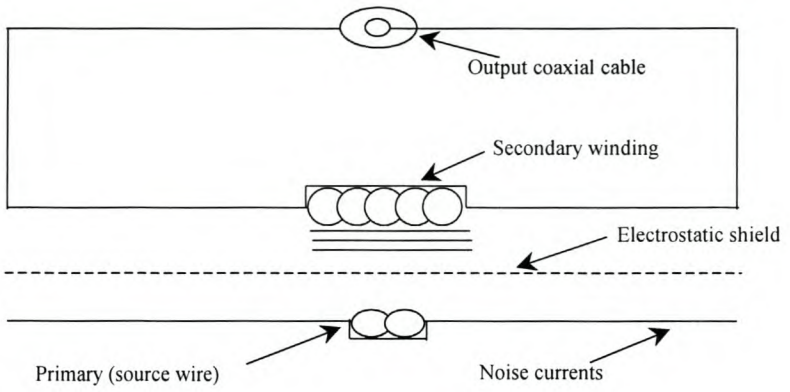

Figure 3.3.1.1: Basic RF transformer representation for the EMCO current probe.

To recover the parameter Z_{tt}, the operational configuration of the probe shown in Figure 3.3.1.2(a) is considered. The probe clamps onto a standard line, whose characteristics are theoretically known. The entire measuring system can be seen as a connection of three subsystems: a three-port network representing the probe, a two-port network representing the left (ℓ_L) side of the primary winding and another two-port network for the right (ℓ_R) side of the primary winding as also pointed out in the report by Cerri *et. al* [Cer01]. Note that the term 'port' refers to a pair of wires exiting from a source circuit for which a voltage and current can be defined [Tes98].

The current probe can be seen as a 'black box', whose *S*-parameters are determined by measurements without knowing anything about its internal components as shown in Figure 3.3.1.2(b) (after [Cer01]). Thus, the following *S*-parameter matrix describes the measuring system.

$$\begin{bmatrix} V_1^- \\ V_2^- \\ V_3^- \end{bmatrix} = \begin{bmatrix} S_{11} & S_{12} & S_{13} \\ S_{21} & S_{22} & S_{23} \\ S_{31} & S_{32} & S_{33} \end{bmatrix} \begin{bmatrix} V_1^+ \\ V_2^+ \\ V_3^+ \end{bmatrix} \qquad (3.3.1.1)$$

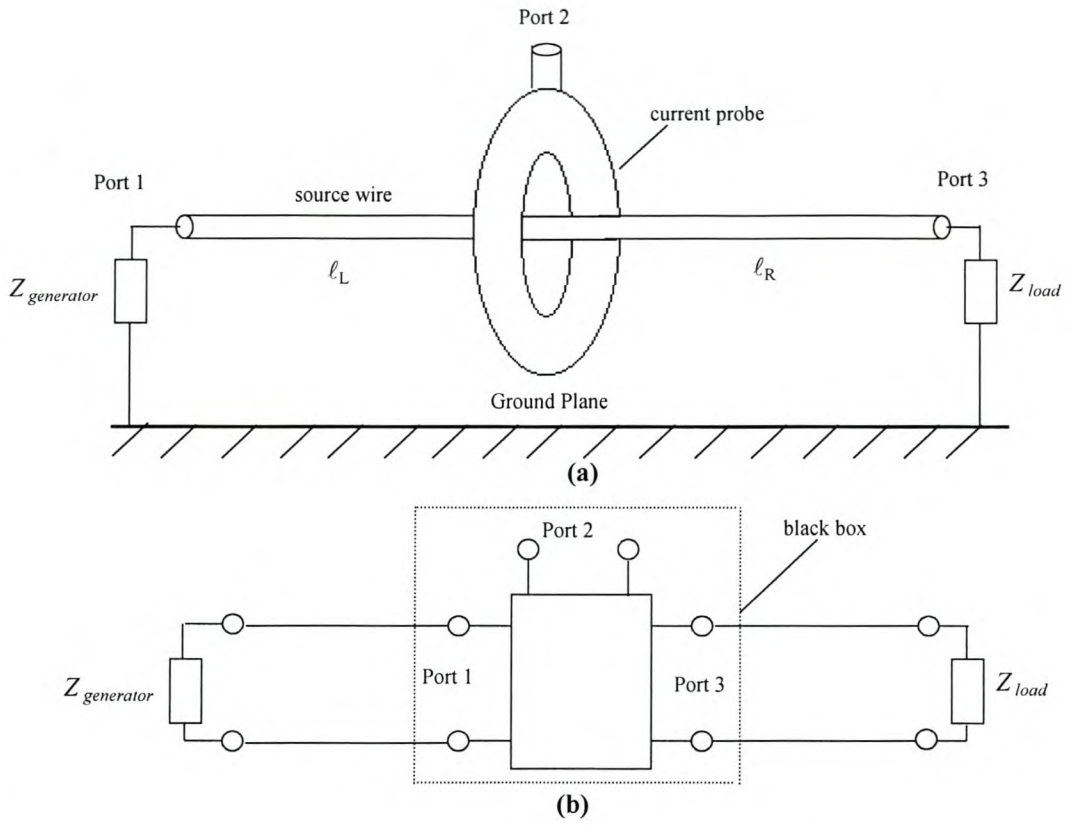

Figure 3.3.1.2: Three port representation of the measuring system. (a) Operational configuration of the current probe clamps a source wire over the GP. (b) Equivalent circuit for the current probe setup (after [Cer01]).

The specific elements of the [*S*] matrix can be directly determined from measurements as reported by [Poz98, pp. 196-198]

$$S_{ij} = \left.\frac{V_i^-}{V_j^+}\right|_{V_k^+ = 0 \text{ for } k \neq j} . \tag{3.3.1.2}$$

Thus, S_{ij} is found by driving port j with an incident voltage wave V_j^+, while measuring the reflected voltage wave, V_i^-, coming out of port i. The incident voltage waves on all ports except the jth port are set to zero. Also, S_{ii} is the reflection coefficient seen looking into port i when all other ports are terminated in matched loads, and S_{ij} is the transmission coefficient

from port j to port i when all other ports are terminated in matched loads. The S-parameters depend on the type of network, its operating conditions, and frequency of the signal.

The reduction of a three-port sub-system to a two-port sub-system will simplify the problem analysis, and reduce the measurement time and computation. The following considerations must be taken into account when reducing three to two-port sub-systems, which are easier to deal with:

- The reflection coefficient response at port 1 (S_{11}), seen by the ℓ_L side of the primary winding, will be the same as the reflection coefficient response at port 3 (S_{33}), seen by the ℓ_R side of the primary winding, when all the other ports are terminated in 50Ω loads.
- The transmission coefficient response between the excitation port 1 and port 2 (S_{21}) through the ℓ_L side of the primary winding, should be the same as the transmission coefficient response between the excitation port 3 and port 2 (S_{23}) through the ℓ_R side of the primary winding.
- The current probe must be centrally positioned around the primary winding such that ℓ_L equals ℓ_R in length for the above-mentioned conditions to hold.

These considerations will hold if the orientation and positioning of the current probe is not disturbed during the measurement and the characteristic impedance Z_0 of ℓ_L and ℓ_R is identical. Then for convenience, the characteristic impedance will be set to $Z_0 = 1$. Thus, equation (3.3.1.1) can be reduced to a two-port network as follows:

$$\begin{bmatrix} V_1^- \\ V_2^- \end{bmatrix} = \begin{bmatrix} S_{11} & S_{12} \\ S_{21} & S_{22} \end{bmatrix} \begin{bmatrix} V_1^+ \\ V_2^+ \end{bmatrix} \qquad (3.3.1.3)$$

The two-port network of equation (3.3.1.3) provides a complete description of the network as seen at its 2 ports.

3.3.2 Field Theory Approach to Current Probes

Current probes make use of Ampère's integral law [Cla92, p416]. This law is clearly described and reported by [Hau89, p19]:

$$\oint_C \boldsymbol{H} \cdot d\boldsymbol{s} = \int_S \boldsymbol{J} \cdot d\boldsymbol{a} + \frac{d}{dt} \int_S \varepsilon_0 \boldsymbol{E} \cdot d\boldsymbol{a} \qquad (3.3.2.1)$$

where C is the contour bounding the open surface S. The first term on the right hand side of equation (3.3.2.1) describes the total electric current through S while the second term describes Maxwell's displacement current with ε_0, the permittivity of vacuum measured in farads/meter. Ampère's law shows that a magnetic field can be induced around a contour by either the net conduction current passing through the surface spanning the contour or the net displacement current that penetrates the open surface S, as illustrated in Figure 3.3.2. The displacement current is produced by the time-varying electric field. If no time-varying electric field penetrates this surface, the induced magnetic field is directly related to the conduction current passing through the loop. Current probes use this principle in order to measure the net current.

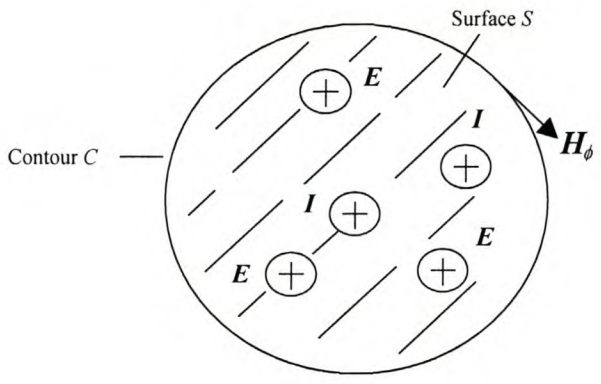

Figure 3.3.2: The current probe - illustration of Ampère's law (after [Cla92]).

From Figure 3.3.1.2(a) the current that passes through the source wire (forming a loop with the jig), produces a magnetic field that is concentrated in and circulates around the probe's core, according to the quasistatic form of Ampère's law. This law relates the time-varying current to the magnetic field it generates in the following way:

$$\oint_C \boldsymbol{H} \cdot d\boldsymbol{s} = \int_S \boldsymbol{J} \cdot d\boldsymbol{a} \tag{3.3.2.1}$$

Several turns of wire are wound around the core of the probe, so that the time-varying magnetic flux that circulates around the core induces, by Faraday's law, an electromotive force (*EMF*) that is proportional to this magnetic flux. The voltage at the output port of the probe is given by:

$$EMF = -\frac{d}{dt}\int_S \boldsymbol{B} \cdot d\boldsymbol{a} \tag{3.3.2.2}$$

with $\boldsymbol{B}$ the magnetic flux vector passing through the loop area, $d\mathbf{a}$ an infinitesimally small section of the area vector enclosed by the loop surface S and, for a single frequency, d/dt equals $j\omega$. The *EMF* result is measured as a voltage V_{probe} over the current probe's terminals. This induced voltage is related to the injection current I_i in the source wire by the transfer impedance Z_{tt} as:

$$Z_{tt} = \frac{V_{probe}}{I_i} \tag{3.3.2.3}$$

Experimentally, simply pass a current of known magnitude and frequency through the probe and measure the resulting voltage produced at the terminals [Cla92]. The result is a calibration curve that relates the ratio of the voltage V_{probe} to the current I_i as in equation (3.3.2.3). The quantity Z_{tt} has units of ohms.

3.3.3 Impedance Parameters and the Equivalent Circuit Model

Circuit models are useful for predicting system responses. One of the useful models is a two-port representation – the two-port representation of circuits forms a basic foundation for developing models for EMC predictions. Two-port circuit theory is an extension of the Thévenin and Norton representation of a single-port circuit. The application of network analysis techniques facilitates and simplifies the derivation of equations. The *S*-parameter data is recorded and converted to *Z*-parameters according to the formula [Poz98, p199]

$$Z = R_0(\mathrm{I} + S)(\mathrm{I} - S)^{-1} \tag{3.3.3.1}$$

where R_0 is the characteristic impedance of the system, I the identity matrix and S is the *S*-parameter matrix. Figure 3.3.3.1 shows a two-port representation of the present measuring system.

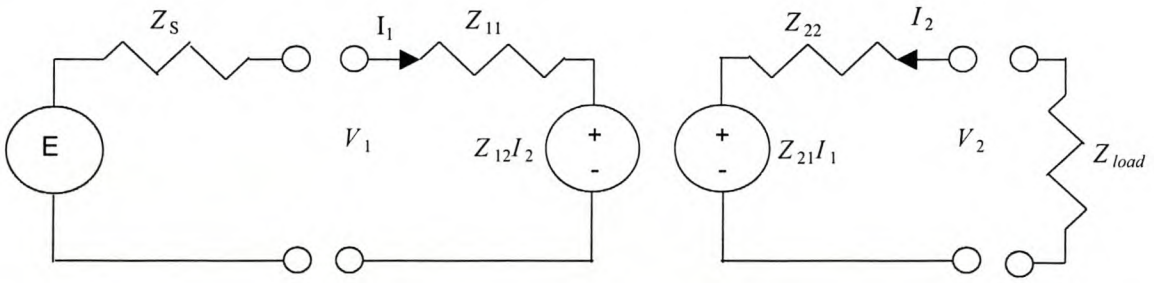

Figure 3.3.3: Equivalent circuit model for a two-port network in terms of its *Z*-parameters (after [Mar98, p4-13]).

The advantage of doing a conversion to *Z*-parameters is the compensation for the test system's mismatches due to discontinuities in the two-port network through these parameters, i.e. the conversion plays a significant role in de-embedding the system. In the FD the characteristic equations describing a two-port network are:

$$V_1 = Z_{11}I_1 + Z_{12}I_2 \tag{3.3.3.2}$$

$$V_2 = Z_{21}I_1 + Z_{22}I_{22} \tag{3.3.3.3}$$

or in matrix notation

$$\begin{bmatrix} V_1 \\ V_2 \end{bmatrix} = \begin{bmatrix} Z_{11} & Z_{12} \\ Z_{21} & Z_{22} \end{bmatrix} \begin{bmatrix} I_1 \\ I_2 \end{bmatrix} \tag{3.3.3.4}$$

where the elements Z_{ij} are called the open circuit parameters. The matrix is referenced as the [Z] matrix of the two-port network and its elements can be found by the following expression:

$$Z_{ij} = \left. \frac{V_i}{I_j} \right|_{I_k = 0 \text{ for } k \neq j} \tag{3.3.3.5}$$

Thus, (3.3.3.5) states that the Z_{ij} can be found by driving port j with the current I_j, open-circuiting all other ports (so $I_k = 0$ for $k \neq j$) and measuring the open-circuit voltage at port i. Thus, Z_{ii} is the input impedances seen looking into port i when all other ports are open-circuited, and Z_{ij} is the transfer impedance between ports i and j when all other ports are open-circuited. The following points give the basic description of the Z-matrix in regard to the present measurement technique:

- The Z-matrix is passive [Tes98, p51].
- Reciprocity theorem shows that Z_{ij} equals Z_{ji} for linear networks.
- Z_{tt} of the current probe can be obtained from the system's transfer impedance Z_{ST} (Z_{21} or Z_{12}) with an open circuit termination at either port:

$$Z_{ST} = \left. \frac{V_2}{I_1} \right|_{I_2 = 0} \left(= \left. \frac{V_1}{I_2} \right|_{I_1 = 0} \right) \tag{3.3.3.6}$$

The problem is that I_2 does not equal zero in the actual circuit connection. But I_2 can be solved for as follows when port 2 is terminated in a finite termination Z_{load}:

$$I_2 = -\frac{V_2}{Z_{load}} \tag{3.3.3.7}$$

The current probe transfer impedance is defined by the following expression into 50Ω equipment,

$$Z_{tt} = \frac{V_2(\text{loaded})}{I_1} \tag{3.3.3.8}$$

If V_2 from equation (3.3.3.8) is loaded by Z_{load} (i.e. when port 2 is loaded), then it is reduced by a voltage divider influence

$$V_2(\text{loaded}) = V_2\left[\frac{Z_{load}}{Z_{load} + Z_{22}}\right] \tag{3.3.3.9}$$

with the reduction factor $Z_{load}/(Z_{load} + Z_{22})$, where Z_{load} is the measuring termination. Therefore, to achieve the transfer impedance of a current probe, the following equation derived from a two-port network in terms of Z-parameters is applied:

$$Z_{tt} = \frac{Z_{21}}{1 + Z_{22}/Z_{load}} \tag{3.3.3.10}$$

which is from the equivalent circuit for a two-port network. The conversion is computed using MATLAB.

3.4 Experimental Results and Discussion

The results presented in this section were obtained through the combination of *S* and *Z*-parameter models. Regarding the former model, the probe matrix is determined by positioning the probe at the centre of the source wire and performing the measurements of the overall matrix. The use of the ANA makes this type of measurement easier and more time efficient compared to a setup with a separate generator and detector. The results of the proposed measurement technique start from 300kHz, which is the lowest operating frequency of the ANA used. The following ANA settings were used to perform all measurements inside a screened room.

- 10Hz Intermediate Frequency (IF) bandwidth was used.
- The reference generator output signal of +20dBm.
- 51 sample points.
- Averaging factor of 8.

With these settings, after calibration, including isolation terms, the noise floor level is approximately -120dBm with the cables disconnected. Figure 3.4.1 shows short circuit standard repeatability test results after performing a full two-port calibration. This test can also be done with an open circuit or 50Ω load calibration standards. To perform the repeatability test the cable attached to port 1 was terminated in the short circuit standard and the reflection coefficient response was measured. The same principle applies to port 2 to obtain a similar measured response.

The purpose of a repeatability test is to verify that the calibration is correct and repeatable. This is done by comparing the response of a short, open circuit and the load to what is expected theoretically. Figure 3.4.1 shows a short circuit response in a logarithmic and Smith chart format. These results are expected when comparing calibrations since the short is supposed to give a 0dB reference in logarithmic format after the calibration while it is supposed to sit in the left top part on the Smith chart format.

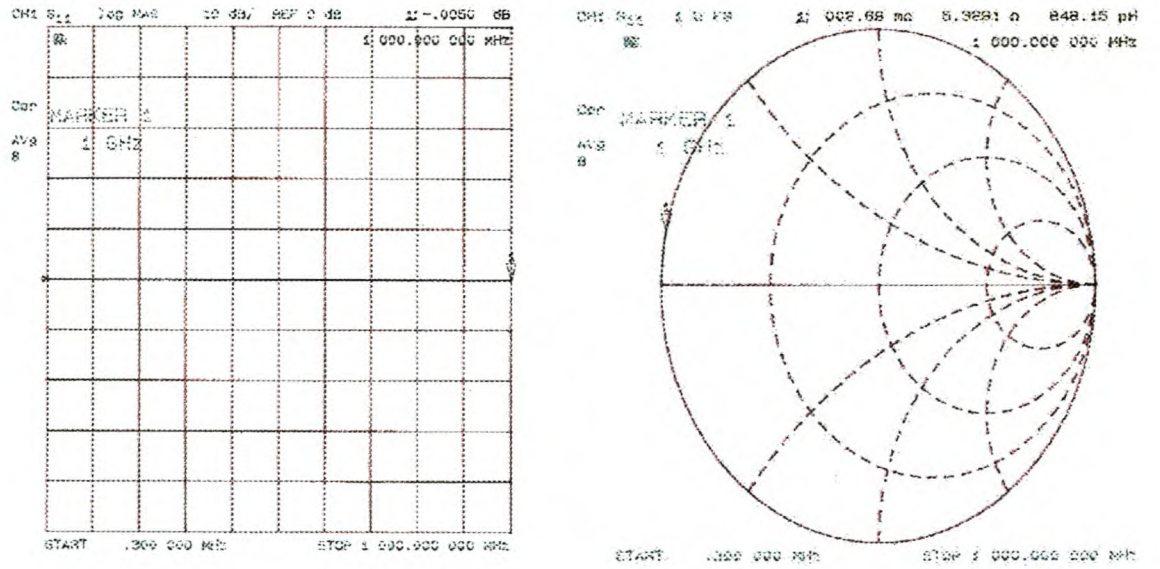

Figure 3.4.1: Short circuit repeatability test results for port 1 in a logarithmic magnitude and Smith chart format.

The physical length of the short circuit connector standard stays the same. What does change is the effective length in terms of wavelength. At low frequencies the phase delay ($\theta = \omega t$) is low, because the short circuit connector is a small percentage of the wavelength whereas at microwave frequencies it will be noticeable.

After going through the calibration procedure, reference points (i) and (ii) from Figure 3.3 are connected to points (a) and (b) respectively, for measuring the system's *S*-parameters. The measurements carried out include *S*-parameters for the calibration fixture in isolation and with the probe centrally positioned, as well as the transmission between the probe and calibration fixture ports.

The measured reflection coefficient S_{11} is shown in Figure 3.4.2, both in isolation and with the current probe centrally positioned.

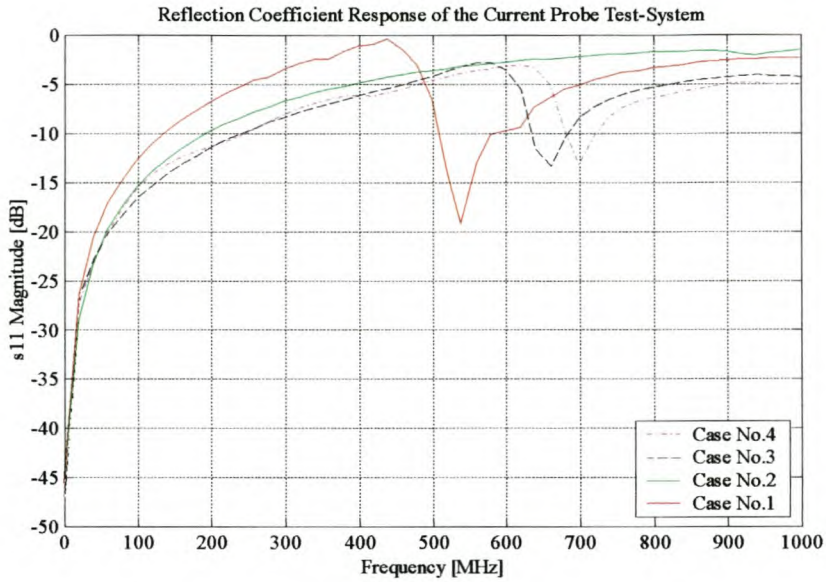

Figure 3.4.2: Measured reflection coefficient S_{11} for different configurations of the calibration fixture.

These results show discrepancies that occur at 540MHz, 660MHz and 700MHz, with case 1, 3 and 4, respectively as described below. Case 2 shows a smooth response across the band.

1) The calibration fixture in isolation without the lid
2) The calibration fixture in isolation with the lid
3) The calibration fixture with probe centrally positioned and the lid on. Chokes were also clamped on feed cables for this case.
4) The calibration fixture with the lid on and probe centrally positioned.

When the lid is off (case 1), a response worse than cases 2, 3 and 4 is observed, as shown by the experimental results of Figure 3.4.2. This is an indication of measurement inaccuracies and a small change in the test fixture's characteristic impedance, Z_0. It is suspected that stray capacitance exists between the screened room wall and the desired current path of the test fixture. Thus, a shielding lid must be used to provide electrostatic shielding and a constant Z_0. The measured response of case 1 shows that the desired current path is exposed to a direct capacitive coupling to the screened room wall, hence differences between case 1 and 2. The

capacitive coupling effect contaminates the measured signal. Its effect becomes evident when ferrite chokes are used to suppress unpredictable CM currents (caused by charges excited on cable exteriors) in case 3 by increasing the impedance of the measuring cable. This resulted in a resonance peak that shifted from 700MHz down to 660MHz.

It is apparent that the presence of a lid gives an effective improvement of the response of S_{11} across the frequency range of interest. The shielding lid effectively reduces the unwanted stray capacitance between the screened room metal wall and the current return path and the probe metallic body. The difference between case 2 and 4 indicates that the probe is also a source of additional reflections in the jig. The metallic body of the probe introduces discontinuities along the source wire, which behaves as a two-wire transmission line with its GP, resulting in different propagation conditions for the injected signal with respect to the case where the probe is absent.

Figure 3.4.3 shows the transmission coefficient measurements that indicate the EM coupling level between the primary winding and secondary winding

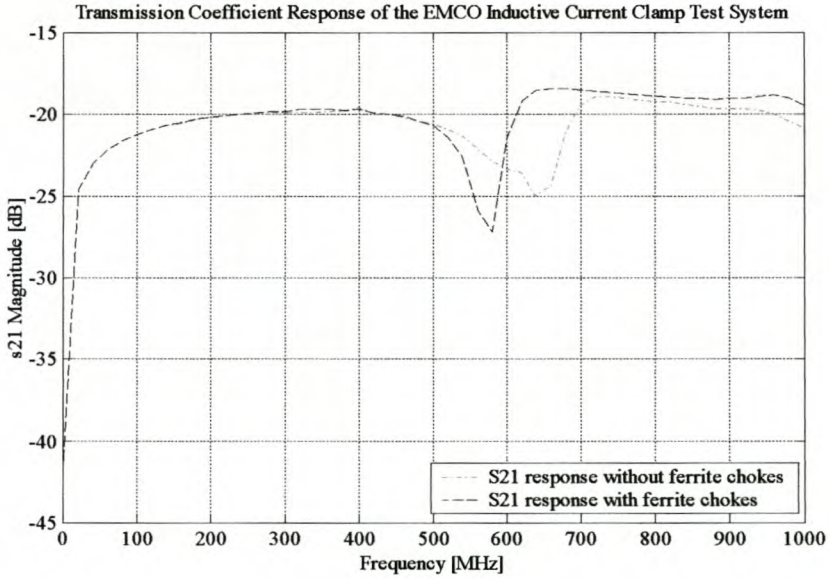

Figure 3.4.3: Frequency behaviour of the measured transmission coefficient of the test-setup.

Measured results were obtained for the best case as evident from case 4 of Figure 3.4.2. Care must be taken when performing transmission measurements. The CM currents tend to leak out of the feed or driving cable and flow outside of the test fixture and onto (and into) the cable carrying the measured signal. Thus, this contaminates the measured signal received at either port. The cable connecting to the ANA receiving port must follow a direction orthogonal to the primary winding in order to minimize the radiated field coupling between the calibration fixture current path and the cable connecting to the receiving port. For a linear, passive network S_{21} equals S_{12}.

The measured transmission response show that the effect of clamping ferrite chokes over the measuring cables shifts the dip from 640MHz down to 580MHz. Therefore, this reduces the influence of capacitive coupling to the desired measurements. Figure 3.4.4 shows the Z-parameter response of the test system after converting the measured S-parameter data.

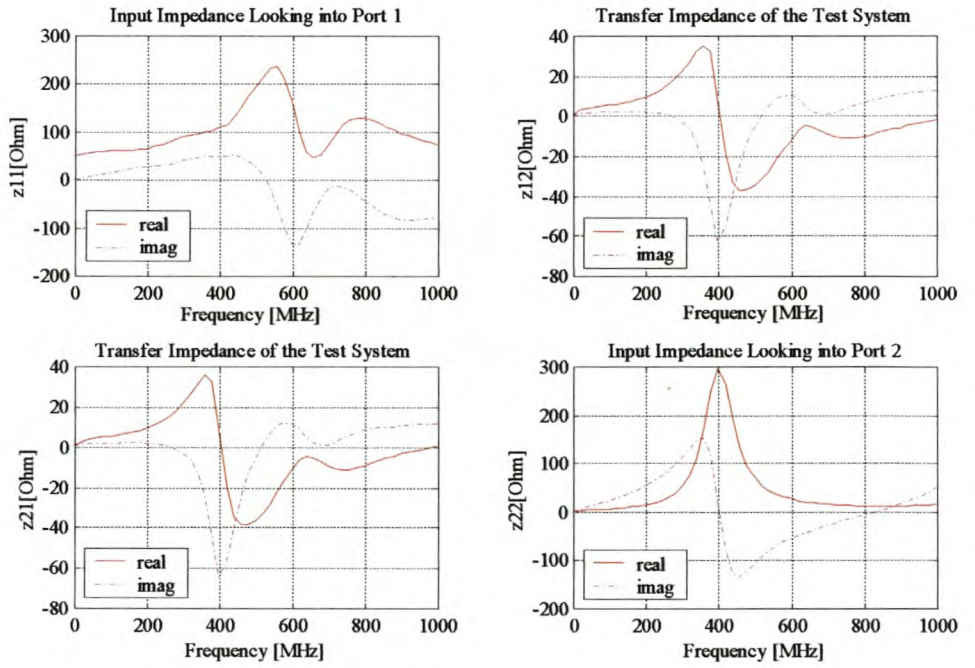

Figure 3.4.4: *Z*-parameter response for the test configuration setup obtained using the calibration technique.

The test system is passive and reciprocal ($Z_{12} = Z_{21}$), which means that the roles of the primary winding and secondary winding can be interchanged without changing the test system's characteristics. The measurement of Z_{11} and Z_{22} describes the input impedance seen looking into the respective ports when either port is terminated into an open circuit. Therefore, Z_{11} gives the response of the source wire while Z_{22} gives the response of the current probe.

The values of Z_{tt}, measured with the present technique are computed from equation 3.3.3.10 and the experimental results are graphically illustrated in Figure 3.4.5 and Figure 3.4.6 as a function of frequency. In Figure 3.4.5, the agreement can be seen over the narrow frequency range, where measured results were found to be consistent, repeatable and well correlated with the manufacturer's data.

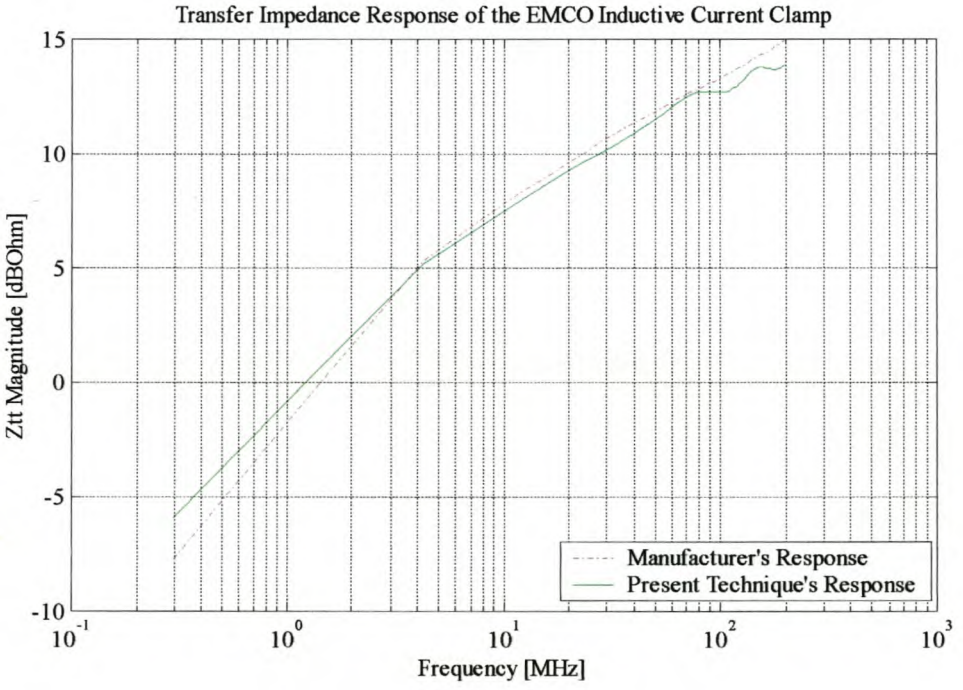

Figure 3.4.5: Comparison of Z_{tt} measured frequency response with the results provided by the probe's manufacturer.

A detailed comparison of the measured results, over a broader frequency range, is depicted in Figure 3.4.6 and shows a discrepancy in measurements of about ± 2dB. The measurements were found to be repeatable up to ≈ 200MHz. From the measured results, it is apparent that including more ferrite chokes over the driving cable to eliminate CM current causes a reduced resonant frequency according to equation (3.4.1). This is because of extra inductance with loss above hundreds of MHz.

$$f_{res} = \frac{1}{2\pi\sqrt{LC}} \tag{3.4.1}$$

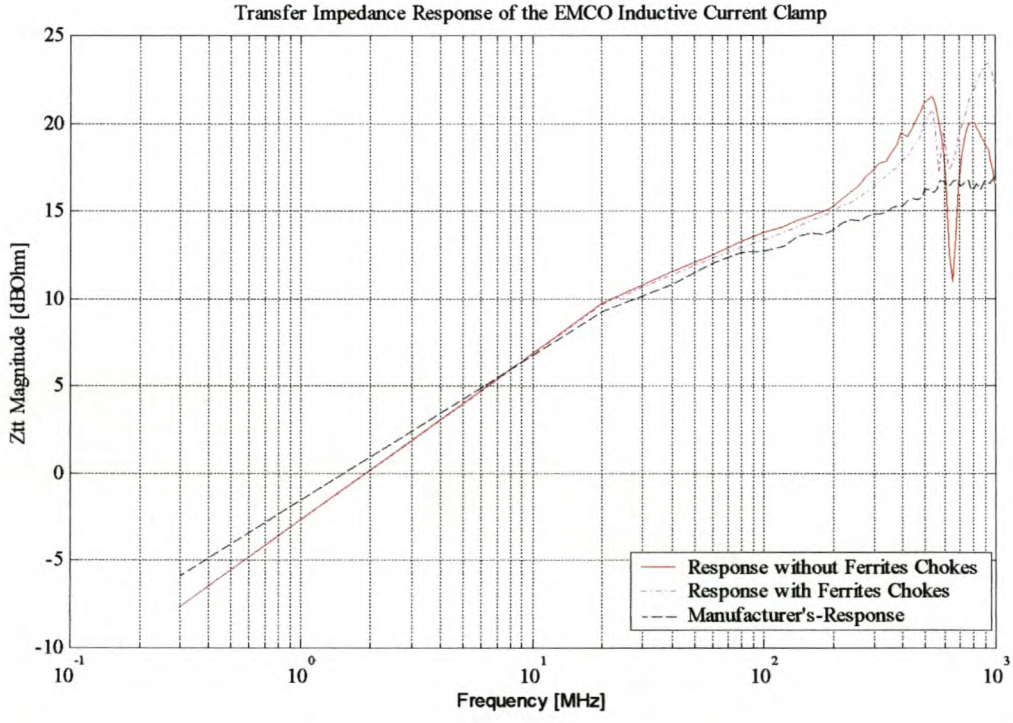

Figure 3.4.6: Comparison of Z_{tt} measured response for the current probe, with the results provided by the probe's manufacturer over a broad frequency range.

Although the uninsulated current clamp's N-type connector and cable connector(s) do not come in contact with the GP or other nearby conductors, it is clear that the clamp becomes

environmentally sensitive at higher frequencies. It is the only part exposed to the driving cable or the screened room wall, when the jig is covered with the lid. The measured results from Figure 3.4.6 depict a property of being independent of the return path in the region below 200MHz.

The measurement discrepancies at higher frequencies are a property of capacitive coupling that exists between the clamp's connector, driving cables and laboratory environment. Moreover, another contribution is due to the jig structure that no longer satisfies the condition of being electrically small at higher frequencies. Thus, the equivalent circuit from the network analysis model applied, fails when the excitation signal becomes comparable to the largest physical dimension of the calibration fixture. This becomes important above 500MHz, since the dimensions of the calibration fixture are approaching $\lambda/2$.

At higher frequencies, capacitive coupling effects increase. In particular, stray capacitance exists between the clamp's N-type connector and driving cable, which then resonate with the driving cable's inductance, hence more CM current will flow over the calibration fixture. The resonance at higher frequencies makes the interpretation of results difficult and renders the present measurement inaccurate. Also, the mismatches can become increasingly significant. Another factor that contributed to the discrepancies between the manufacturer's data and the present technique is the difference in our two specific configurations.

From previous sections it was noted that the current probe is essentially the secondary winding of a transformer. Maree [Mar98, p4-14] reports that the secondary winding is thus reflected into the primary. It must thus be ensured that the insertion impedance is small in comparison with the combination of source and load impedance of the cable that is measured. This is to prevent the current probe from impeding the current flowing in the test cable. For this particular probe a maximum added impedance of 0.75Ω is specified, when the probe is terminated in a 50Ω system. This will have an insignificant effect on the measurements undertaken.

3.5 Concluding Remarks

Measured results show that the experimental technique has met the prime objective of reproducing sensible and reliable values of Z_{tt} comparable to that of the manufacturer, although over a reduced frequency range. However, care must be taken to alleviate other effects such as capacitive coupling and CM current since they cannot be calibrated out of the test system. The CM currents are not predictable at resonance and the use of ferrite chokes just shifts the resonant point to a lower frequency. The lack of damping also points to the low loss of these chokes at this frequency.

The *S* to *Z*-parameter conversion approach permits the transfer impedance to be corrected for mismatch effects associated with the coaxial inputs of the calibration fixture and the primary winding. However, more accurate models at higher frequencies still remain a challenge to account for resonance effects.

The applicability of the proposed measurement technique depends on both the frequency range of interest and the detailed geometry of the measurement calibration fixture. This technique shows improved measured results for frequencies below 600MHz. It has also been shown that the use of a partial enclosure to form the test-jig improves the measurements to a higher upper frequency limit. The technique is economical, easy to construct and suitable for use during the development stages of electronic products.

Chapter

4

Cable Transfer Impedance – An Experimental Evaluation

Many cable transfer impedance measurement methods have been proposed over the years and each has its relative strengths. This chapter focuses on an investigation of two FD measurement techniques for an experimental evaluation of interconnecting leads for EMC performance. Experimental results show that both techniques produce repeatable and measurable Z_T for frequencies below 80MHz and a good agreement is achieved up to 50MHz with test cables of about 0.5m.

4.1 Introduction

The focus of the chapter is the experimental determination of cable transfer impedance, Z_T, which is derivable from system transfer impedance, Z_t. In chapter 2, different methods used to measure Z_T were explored, e.g. the standard triaxial, current-injection method, pulled-on braid, current probe method, etc.

A new, wire-loop antenna technique, and a current-injection technique (originally described in [Hel95, p22] as the wire-injection method) are investigated. The latter method is improved and versatile as any type of cable can be used, and it is suitable for vector and scalar measuring equipment. Ready-made interconnecting leads can be evaluated for the purposes of cable certification and classification, quality control and EMC trouble-shooting [Fou98]. Both techniques are economical and simple to analyze. For the new method a dedicated test-jig is required, which is straightforward to prepare.

No special construction of the cable is necessary, however, the CUT has to be fitted with appropriate connectors. An effort was made to ensure that factors such as CM currents and capacitive coupling do not interfere with the measurements of Z_T.

The screening performance measurements are expressed in terms of Z_T and are conducted for two types of TL's that are widely used in telecommunications engineering:

i. Parallel conductors, e.g. twisted-pairs.
ii. Coaxial conductors.

The specific situation, which led to the development of these techniques, illustrates the problem in a satellite system's research and development stages. Low cost leads are typically used to connect to analogue-to-digital converters (ADCs) and are susceptible to interference. The experimental study and evaluation will make a proper selection of interconnecting leads for a known, or predicted EM environment, possible.

Measurements are reconciled between two different techniques using an ANA and spectrum analyzer (SA). Published data was also used to compare measured results.

4.2 Wire-Loop Antenna Technique

The test fixture is shown in Figure 4.2. The experiment was performed by measuring system *S*-parameters on a calibrated HP8753C ANA in the frequency range from 300kHz to 100MHz. The measured *S*-parameters (201 sample points) were then converted to *Z*-parameters [Poz98].

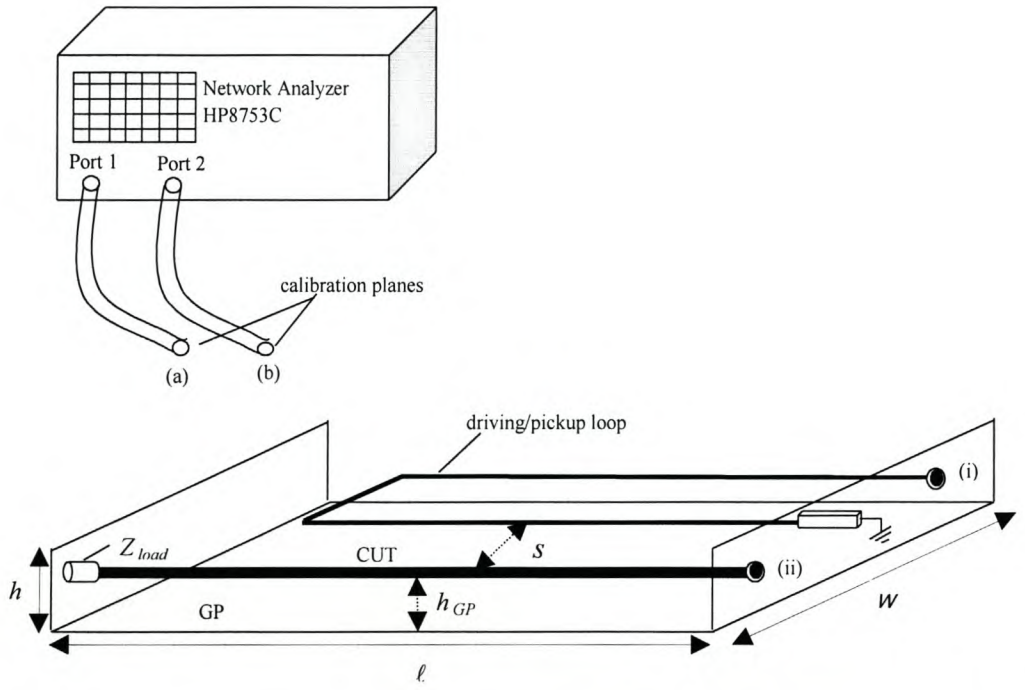

Figure 4.2: Experimental configuration and geometry of the wire-loop technique.

The proposed wire-loop measurement technique represents more or less an actual EM environment for the analysis of emission and immunity problems. Its principle of operation is similar to that of the current probe method. However, in this implementation an excitation line (or drive-line) is obtained by using a wire-loop antenna (insulated copper wire) terminated into a 50Ω chip resistor. For ease of understanding, circuit theory and field theory approaches are used for the technique's theoretical discussion and predictions.

In Figure 4.2 the wire-loop antenna is $\approx 0.48 \times 0.02$m in size and positioned at s meters (≈ 0.02m) from the CUT. The mounting of the CUT and the wire-loop is maintained at a constant height (h_{GP} = 5cm) above a perfectly conducting GP. The measuring semi-rigid coaxial cables leading to the test-jig are $\approx$ 5m in length, with low Z_T. The reference calibration planes (a) and (b) connects to plane (ii) and (i), respectively.

The largest physical dimension (ℓ) is $\approx$ 0.5m. With a wavelength at 100MHz of 3m, MQS conditions can be assumed [Hau89, p71], so the experimental setup can be modelled with lumped parameters.

4.2.1 Analysis Descriptions

A roughly matched test-system is achieved by terminating the non-driven end of the CUT in its characteristic impedance (Z_{load} = 50Ω), thus providing a reduced reflection system with a uniform distribution of currents in the inner conductor. The cables leading to the test fixture are well screened with very low Z_T. For this reason, insignificant CM current flows, thus corrupting the measured signal minimally. This point was confirmed by fitting ferrite chokes over the measuring cables – no changes were observable. Ferrite chokes absorb magnetic fields and add more CM impedance to the measuring cables. The CUT with its environment is considered as a three-conductor system, whereby the inner conductor, cable screen, and environment are the conductors.

The inner conductor and cable screen forms the DM loop. The cable also forms a part of a larger circuit, the CM loop in EMC terms, which closes via the environment of the metal sheet. The excitation line formed by the shield-ground loop can behave like a two-wire TL depending on the wavelength of the excitation signal. Hence, [Kle93] interprets this entire system as two TL's (loops), which are joined with a mutual conductor. The situation depicted in Figure 4.2.1 explores the practical situation where the cable screen is grounded at both ends.

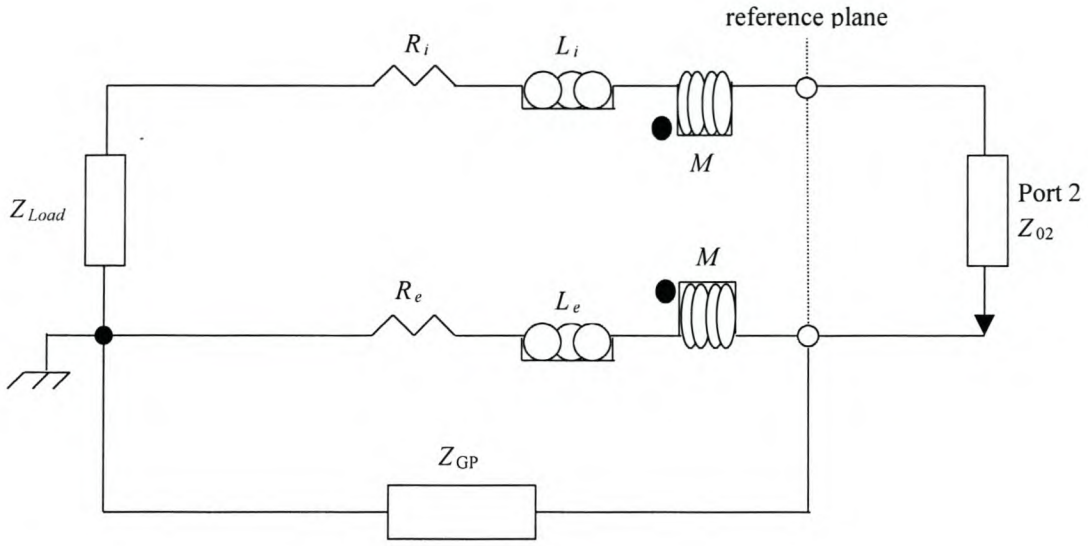

Figure 4.2.1: CUT current lumped model for the experimental setup in Figure 4.2.

The resistances R_i and R_e are physical resistances of the signal and return conductors respectively. Inductance L_e is the leakage inductance, and is caused by the external flux (Φ_e) encircling only the return or external conductor [Mil98, p328], whereas L_i is the internal inductance per unit length caused by the internal flux (Φ_i) encircling only the signal or internal conductor(s). The literature from [Mil98] presents the parameter Φ_M as the flux encircling both conductors of a coaxial line, since it forms a perfectly coupled transformer with winding inductance equal to the mutual inductance M. It is worth noting that the parameter M is unaffected by scaling the dimensions of the cable or test-jig housing.

With reference to Figure 4.2, the approach to experimentally determine Z_T is that of exciting a CM current in the large shield-ground TL (CM loop) of the system. This is accomplished by an external interfering magnetic flux, $\partial\Phi/\partial t$, generated by an interfering current that is injected in the wire-loop antenna. An *EMF* voltage is induced onto the inner conductor of the CUT due to its Z_T and the CM current flowing down the outer shield-ground TL.

The metal sheet provides a well-defined and efficient GP (return path) for the CM currents. The use of low impedance circuits allows the determination of Z_T, whilst minimizing the effects associated with Y_t. Most of the discussion in this section will relate directly to the notion that a cable shield-ground loop can act as a receiving antenna, but the results developed can also be applied to the same CM loop when it acts as a transmitting antenna. To correctly extract Z_T, a general method to account for system effects is derived through the de-embedding procedure described in the next section.

4.2.2 De-Embedding Procedure and TL Modelling of the Test System

De-embedding procedures are used to remove system effects. For the purposes of this experiment they are used to remove the effects of the test-jig fixture and only leave the cable transfer impedance, Z_T. The test-system is linear, passive and reciprocal, which means that the roles of the CUT and the wire-loop can be interchanged without changing the system characteristics (and Z_T remains unchanged). The derivation of equations for de-embedding the system is based on 50Ω coaxial cables and the measurement of reverse transmission coefficient (S_{12}) i.e. exciting port 2 with port 1 loaded. The same principles apply for the derivation based on the transmission coefficient, S_{21}.

4.2.3 Configuration Setups for the De-Embedding Procedure

For the setups illustrated in this section, the magnitude of the induced *EMF* voltage is dependent on both the area of the victim loop (through which the shared flux passes) and the rate of change of the disturbance current in the wire-loop antenna. The victim (or sensing) loop here, is the shield-ground TL with respect to the radiating wire-loop antenna. Therefore, the system transfer impedance, Z_t, changes with the changes in the geometry of the DM and CM loops formed by the CUT and the environment.

4.2.3.1 Wire-Loop Antenna Configuration Setup

Figure 4.2.3.1 (setup (*i*)) shows a schematic model of the wire-loop that is used in the current-driven mechanism as a driving wire-loop antenna above a perfectly conducting GP. The loop is made from a standard SWG 22 insulated copper wire. The current injected from port 2 of the ANA becomes equivalent to the DM current of that circuit, thus:

$$I_i = I_{DM} \tag{4.2.3.1}$$

where I_i is called the injection current.

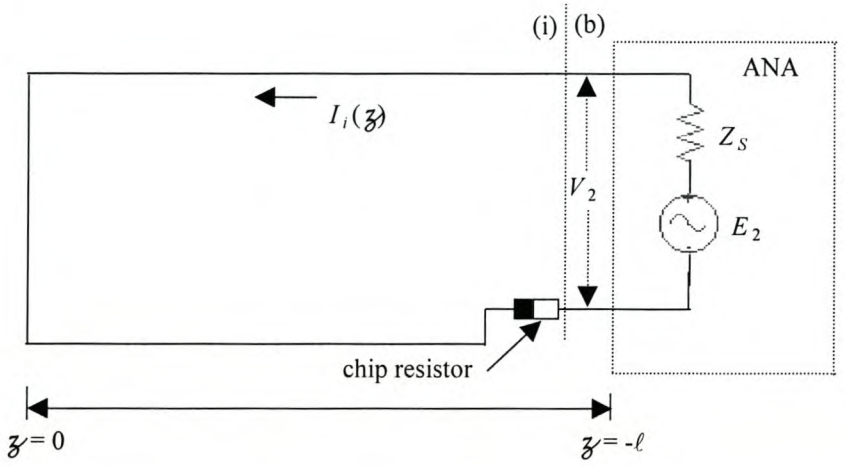

Figure 4.2.3.1: Cross-sectional schematic view for the circuit model of the wire-loop antenna, setup (*i*).

The operation was implemented in such a way that the current I_i flows in the loop from the source to the load (50Ω chip resistor), forming a small loop antenna that is quite effective at HF. Thus, the wire-loop antenna provides the external source of interference or emission in this system. It may be noted that the area of the loop influences the available signal strengths and was chosen empirically. The chip resistor was chosen over an ordinary carbon resistor because of its better frequency response across the frequency

range of interest. At low frequencies the chip resistor will roughly match the wire-loop to the internal impedance of the source. It is important to note that the chip resistor and loop inductances does not provide a perfect match, but does improve the measurement conditions.

4.2.3.2 Test-Cable Configuration Setup

Figure 4.2.3.2 (setup (*ii*)) illustrates a schematic side view for the configuration of the CUT mounted for the test measurements. The TL model of the CUT incorporates CM-DM coupling. The system transfer impedance, Z_t, can be extracted from the measurements of this system. The GP is made of a metal sheet. The upright terminating plates of the test-jig at the far ends divert the CM current from the CUT screen outer surface to return via the GP.

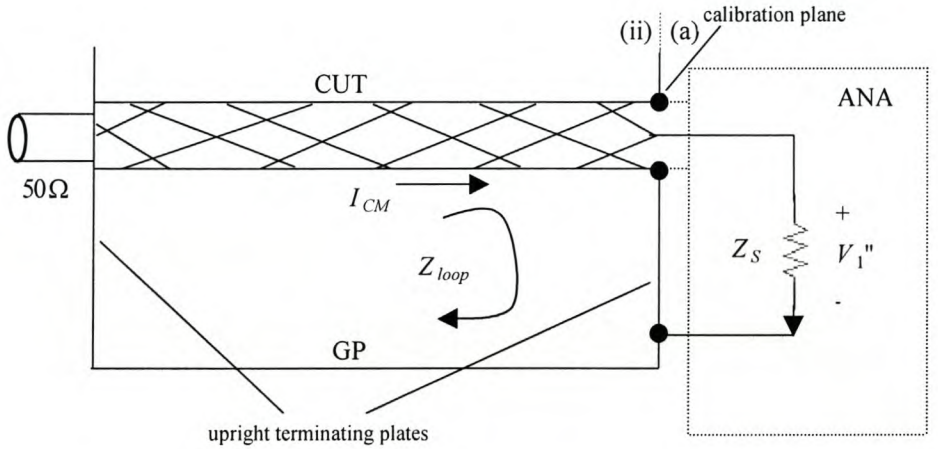

Figure 4.2.3.2: Cross-sectional view of the configuration for the CUT reverse transmission measurement, setup (*ii*).

The actual Z_T can be deduced by manipulating the circuit theory expressions for the measured system transfer impedance of both setups in Figure 4.2.3.2 and Figure 4.2.3.3.

4.2.3.3 De-embedding Circuit Configuration Setup for Correct Determination of I_{CM}

Figure 4.2.3.3 (setup (*iii*)) shows a schematic side view for the practical configuration that is used to introduce a correction for the system effects in order to isolate Z_T. A simple cable 'coax-braid' is prepared by disconnecting the inner conductor of a coaxial cable from the connector centre pins to only leave the braid. Disconnection, rather than complete removal, helps to maintain the braid's structure. The 'coax-braid' is fitted with BNC connectors and replaces the CUT. It is short-circuited at the end connected to port 1 (driven end) of the ANA while the other end is open-circuited and attached to the GP.

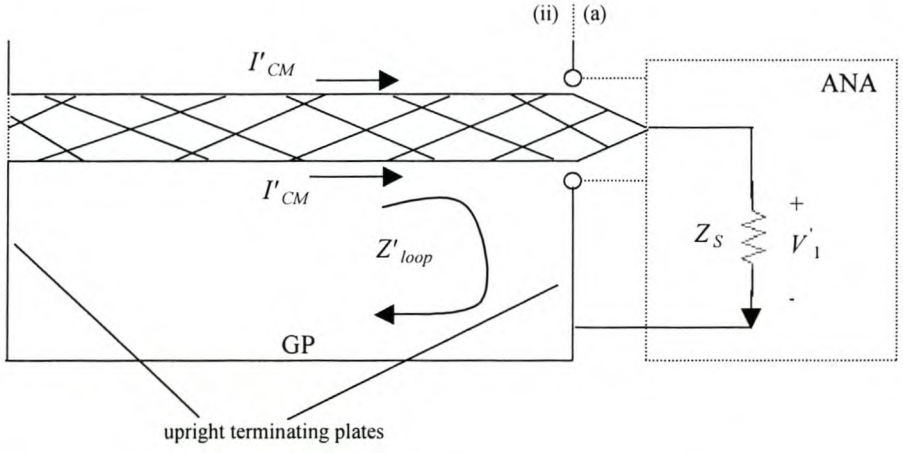

Figure 4.2.3.3: Cross-sectional view of the configuration setup for the de-embedding circuit model, setup (*iii*).

This 'coax-braid' is used to approximate the actual pick-up area of the magnetic flux produced by the wire-loop antenna. Hence, I_{CM} can be measured if the loop impedance Z_{loop} of the shield-ground TL is known. As port (a) is calibrated, Z_S equal to 50Ω is at plane (ii). In Figure 4.2.3.3 Z'_{loop} indicates the loop impedance of the shield-ground line through which the excited CM current flows. This replacement, measuring I_{CM}', helps in

determining the I_{CM} that is going to flow in the shield-ground loop of the setup shown in Figure 4.2.3.2. This requires that the induced *EMF* in both configurations in Figure 4.2.3.2 and Figure 4.2.3.3 is approximately the same. Faraday's integral law,

$$\oint_C \boldsymbol{E} \cdot d\boldsymbol{S} = -\frac{\partial}{\partial t} \iint_S \boldsymbol{B} \cdot d\mathbf{A} \tag{4.2.3.3.1}$$

define the electric (***E***) field generated in a closed loop cut by a time-varying ***B***-field. For a high impedance load, the measured *EMF* between loop terminals is:

$$EMF = \int \boldsymbol{E} \cdot d\boldsymbol{S} \tag{4.2.3.3.2}$$

For the *EMF* to be the same in both configurations, Faraday's law requires that the pick-up area $d\mathbf{A}$ for both configurations in setup (*ii*) and (*iii*) be the same, i.e. the shield-ground loop areas should approximately be the same. Assuming this is true, I_{CM}' equals I_{CM}. With the 'coax-braid' in place, the system transfer impedance Z_t can be determined exactly for setup (*iii*).

4.2.4 Derivation of Equations

The *EMF* voltages induced into the CM loops, by the time-varying ***B***-field of the wire-loop antenna in configuration setups (*ii*) and (*iii*) when driving port 2, remain the same as discussed in the previous section and are expressed as follows:

$$EMF_{Z_{loop}} = Z_{loop} I_{CM} \tag{4.2.4.1}$$

$$EMF_{Z'_{loop}} = Z'_{loop} I'_{CM} \tag{4.2.4.2}$$

where $Z'_{loop} \approx Z_{loop} + Z_S$ is the DM loop impedance for configuration setup (*iii*) and Z_{loop} is the CM loop impedance for the configuration of setup (*ii*). The CM currents I'_{CM} and I_{CM} flow in the closed CM loops of configuration (*iii*) and (*ii*) respectively. Realising that the *EMF* induced into the two loops is the same and the injected signal current (I_i) remains constant, equations 4.2.4.1 and 4.2.4.2 yield:

$$I_{CM} = \frac{\left(Z_{loop} + Z_S\right)}{Z_{loop}} I'_{CM} \tag{4.2.4.3}$$

For the two configuration circuit models described, the system transfer impedance can be defined by the following equations for setup (*ii*) and (*iii*) respectively:

$$Z_t = \frac{V_1''}{I_i} \tag{4.2.4.4}$$

$$Z'_t = \frac{V'_1}{I_i} \tag{4.2.4.5}$$

The voltages V_1'' and V_1' are detected at port 1 of the ANA for setup (*ii*) and setup (*iii*) respectively. The configuration of setup (*ii*) also allows a direct description of an expression for the cable transfer impedance, Z_T. The ratio of the voltage detected at port 1 and the CM current flowing in the shield-ground loop result into the definition of Z_T.

$$Z_T = \frac{V_1''}{I_{CM}} \tag{4.2.4.6}$$

From equations (4.2.4.4) and (4.2.4.5) the following expression can be obtained:

$$Z_t = Z_t' \frac{V_1''}{V_1'} \tag{4.2.4.7}$$

The following results when equation (4.2.4.6) is substituted into equation (4.2.4.7):

$$Z_t = Z_T Z_t' \frac{I_{CM}}{V_1'} \tag{4.2.4.8}$$

Substituting equation (4.2.4.3) into equation (4.2.4.8) and solving for Z_T yields:

$$Z_T = \frac{Z_t Z_{loop}}{Z_t'\left(Z_{loop} + Z_S\right)}\left(\frac{V_1'}{I_{CM}'}\right) \tag{4.2.4.9}$$

From the result expressed by equation (4.2.4.9), two important definitions of terms can be made. Firstly the ratio of the detected voltage at port 1 and CM current ($\frac{V_1'}{I_{CM}'}$) for the *'coax-braid'* configuration equals $Z_{loop}' \approx Z_{loop} + Z_S$. Secondly, the loop impedance Z_{loop} can be obtained from the loop's input impedance derivable from the reflection coefficient (S_{11}) for setup (*ii*) and is as follows:

$$Z_{in} = Z_0 \frac{\left(1 - S_{11}\right)}{\left(1 + S_{11}\right)} \tag{4.2.4.10}$$

Thus, from equation (4.2.4.10) Z_{loop} equals Z_{in}. Hence for the description of the system from Figure 4.2.3.2, the formula for computing the cable transfer impedance from the measured *S*-parameter data, after converting to *Z*-parameters, is given as follows:

$$Z_T = \frac{Z_t Z_{in}}{Z_t'} \tag{4.2.4.11}$$

These equations are based on circuit theory and are not valid when the largest dimension of the test-jig becomes comparable to the wavelength of the excitation signal.

4.3 Current-Injection Technique

The schematic view of the proposed measurement technique for Z_T is shown in Figure 4.3, which also illustrates more or less an actual EM environment. The EM environment is well defined and stable. Its principle of operation is similar to that of the current-injection method proposed by [Hel95]. However, in this implementation an excitation line is obtained by devising a well-defined path for the CM current (i.e. shield-ground plane) instead of a nearby return conductor. This is achieved by mounting the test cable above a conducting flat GP, thus forming a shield-ground (two-wire) TL.

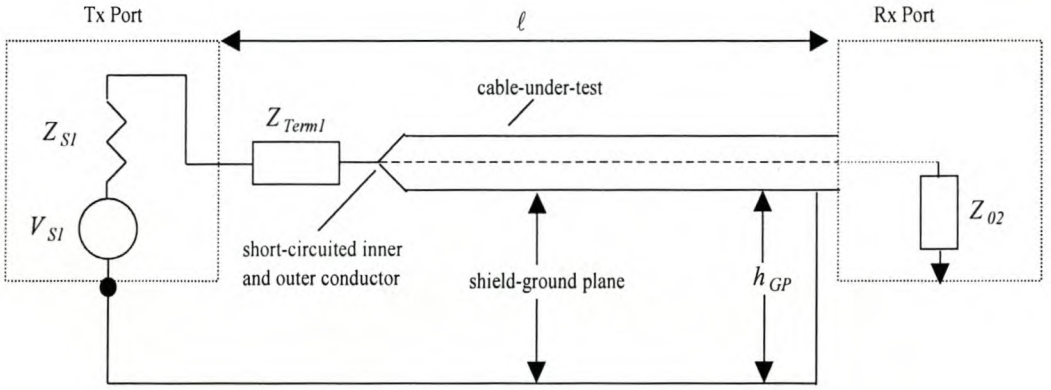

Figure 4.3: Schematic view of the proposed current-injection measurement technique.

The fundamental principle employed by the proposed measurement technique is that of deliberately exciting a CM current, I_{CM}, which varies with frequency and flows down the cable screen, and measuring the corresponding voltage induced onto the inner conductor(s). The CUT can be presented as a victim line whilst the shield-ground plane can be presented as a source of emission or interference, emulating a real situation. The

driven end of the CUT is short-circuited and a 50Ω resistor is connected in front of the short circuit to roughly match the system and to ensure a uniform excitation of I_{CM} across the frequency band of interest. The other end is connected to a 50Ω detector. The CUT is fitted with appropriate connectors as in the conventional operation. The physical construction of the jig for the configuration test setup shown in Figure 4.3 permits the test cables to be maintained at a constant spacing ($h_{GP} \approx 0.05$m) above, or be kept firmly against, the metallic GP. This limits the test cable to a length of ≈ 0.5m.

4.3.1 Theoretical Description – Two-Port Analysis Approach

The application of two-port network analysis makes the experiment analysis description more understandable. The measurement technique focuses on measuring the *S*-parameters of the configuration test-setup and converts them to *Z*-parameters using the formula [Poz98]:

$$Z = R_0(\mathrm{I} + S)(\mathrm{I} - S)^{-1} \tag{4.3.1.1}$$

where R_0 equals 50Ω, the characteristic impedance of the system, I the identity matrix and S is the *S*-parameter matrix. The numerical computation of the conversion is done in Matlab. The following TL equations describe the measuring system in the FD:

$$V_1 = Z_{11} I_{CM} + Z_{12} I_{DM} \tag{4.3.1.2}$$

$$V_2 = Z_{21} I_{CM} + Z_{22} I_{DM} \tag{4.3.1.3}$$

and in matrix notation

$$\begin{bmatrix} V_1 \\ V_2 \end{bmatrix} = \begin{bmatrix} Z_{11} & Z_{12} \\ Z_{21} & Z_{22} \end{bmatrix} \begin{bmatrix} I_{CM} \\ I_{DM} \end{bmatrix} \tag{4.3.1.4}$$

Figure 4.3.1 shows a representation of the current-injection method in the form of *Z*-parameters.

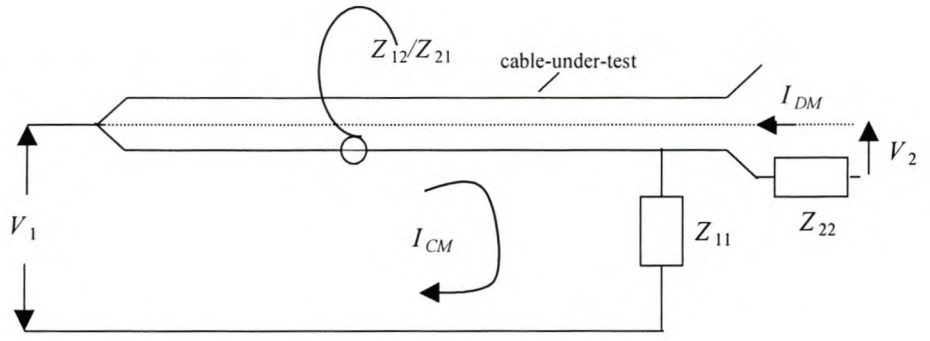

Figure 4.3.1: *Z*-parameter representation of the current-injection method.

Z_{11} and Z_{22} are the input impedance at the network ports determined by ratios of the open circuit voltages (V_1 and V_2) and currents (I_{CM} and I_{DM}) at the same ports. Z_{12} and Z_{21} are the system transfer impedances determined by the ratio of the open circuit voltages (V_1 and V_2) and currents (I_{CM} and I_{DM}) at the opposite ports. Z_{12} and Z_{21} describe the coupling between both TL's. Linear passive networks are reciprocal, thus $Z_{12} = Z_{21}$. Since electrically short cables ($\ell << \lambda$) are assumed, Z_T per unit length can be obtained from the system transfer impedance. For a finite termination, Z_{21} must be reduced by a voltage divider influence at the receiving port as follows:

$$V_2(\text{loaded}) = V_2 \frac{Z_{02}}{(Z_{02} + Z_{22})} \tag{4.3.1.5}$$

with Z_{02}, the internal impedance of the measuring instrument. Then Z_T will be related to the equivalent parameters in the following way.

$$Z_T = \frac{Z_{21}}{1 + Z_{22}/Z_{02}} \tag{4.3.1.6}$$

Equation (4.3.1.6) expresses an important result for the numerical computation of the cable transfer impedance and must further be divided by the length of the CUT to obtain Z_T in Ω/m.

4.3.2 Application of the Current-Injection Technique

The measurement technique has been implemented both by scalar and vector instrumentation in the FD using a SA and an ANA. The measuring cables leading to the test-jig are well screened semi-rigid coaxial with lengths of ≈ 0.5m. The L-section plate of the jig reduces CM current to insignificant levels. Insignificant signal changes when ferrite chokes are clamped over the cables leading to the test setup also suggest the absence of CM current.

4.3.2.1 Current-Injection Technique – ANA Measurements

The ANA *S*-parameter measurements were performed with a HP8753C ANA as depicted in Figure 4.3.2.1. The dimensions of the jig are ($\ell \times w \times h$) ≈ 0.5 × 0.15 × 0.3m. Points (a) and (b) indicate the calibration planes while points (i) and (ii) indicate coaxial connection points on the test jig for the CUT.

The calibration was done for the frequency range from 300kHz to 100MHz. *S*-parameter measurements were taken (51 sample points) at the two SMA connector planes as indicated in Figure 4.3.2.1 and converted to *Z*-parameters using the formula given in equation (4.3.1.1).

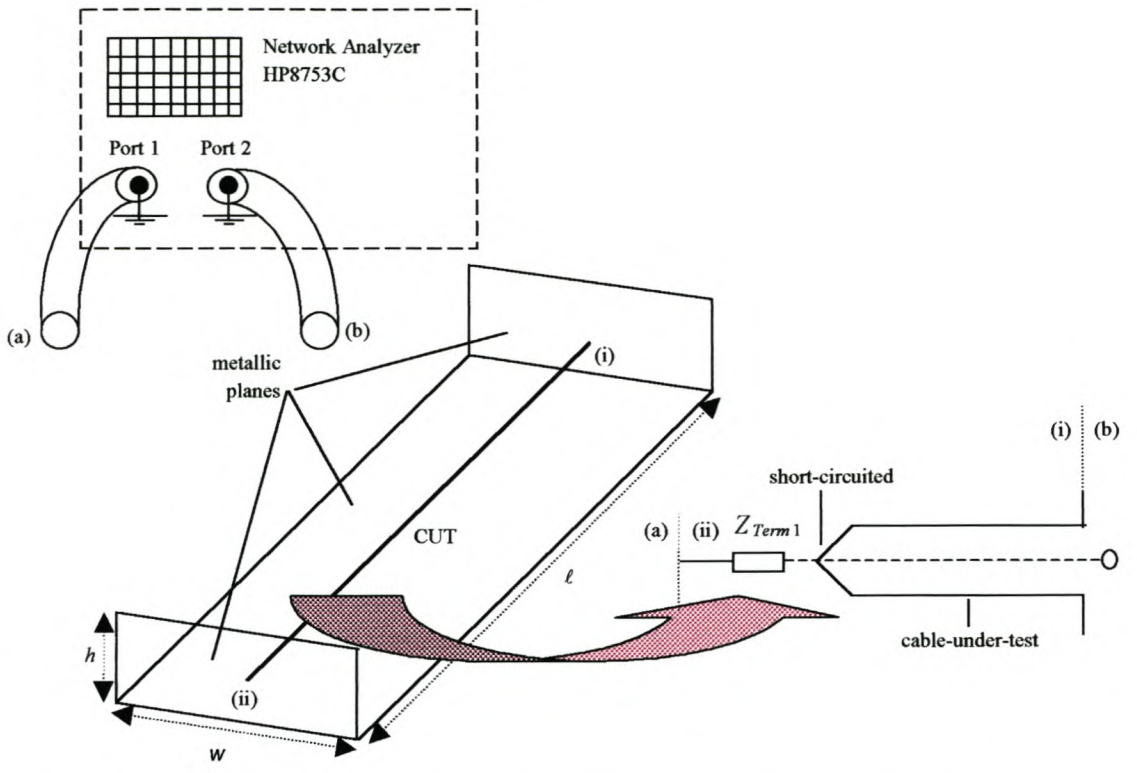

Figure 4.3.2.1: Experimental configuration and cross-sectional geometry of the test setup using an ANA.

The use of an ANA has advantages compared to other detectors or analyzers and are as follows:

- Easier means of measurement since it treats the test-system as a two-port network.
- Calibration is well established.
- Magnitude and phase measurement can easily be obtained.

A good dynamic range was achieved by using a high quality calibration kit, an IF bandwidth of 10Hz and averaging which was set to 8. A good workable dynamic range of 120dB was achieved for a full 2-port calibration with the above-mentioned settings.

Two types of measurements were performed for the configuration test-setup illustrated in Figure 4.3.2.1.

1) The CUT was placed on the test-jig configuration test-setup. The reflection coefficients S_{11} and S_{22} at the input of the shield-ground TL and the short-circuited TL (CUT), respectively, were measured.
2) Thereafter, the transmission through the CUT screen S_{21} and S_{12}, respectively were measured.

4.3.2.2 Current-Injection Technique – SA Measurements

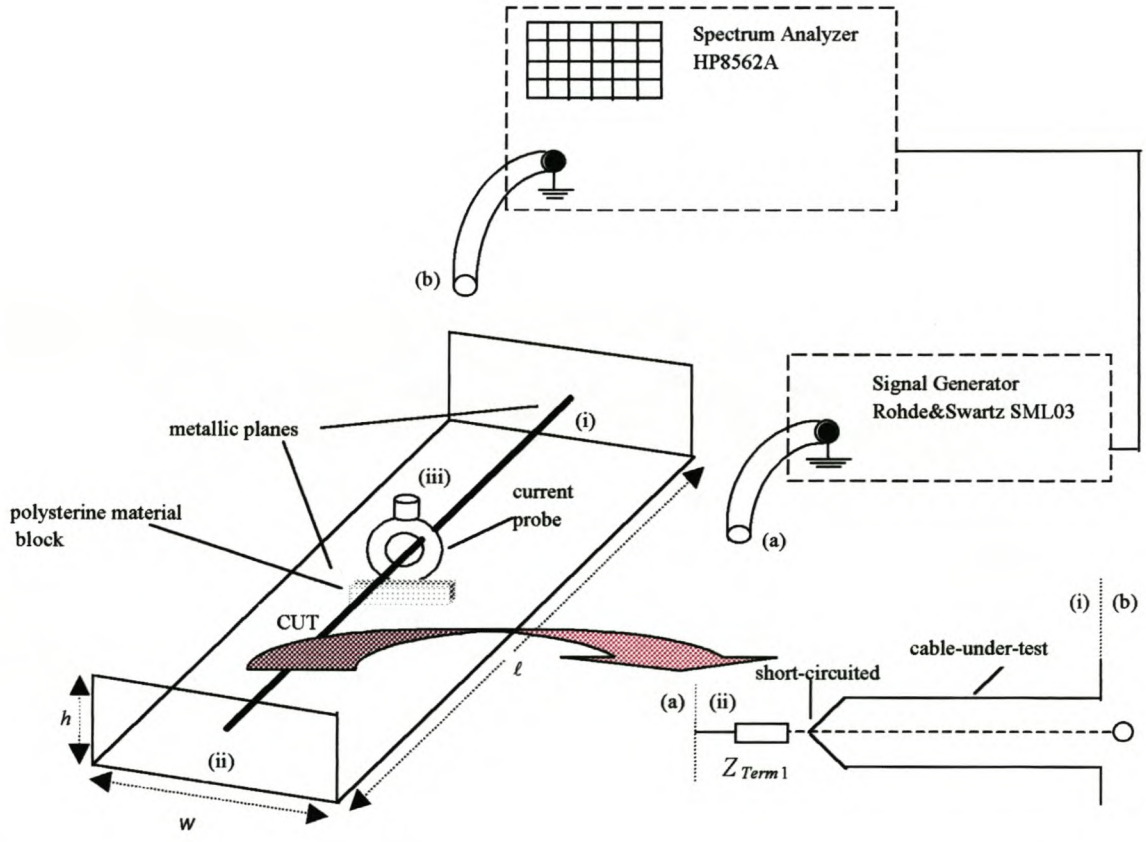

Figure 4.3.2.2: Experimental configuration and cross-sectional geometry of the current-injection test setup using a SA.

The configuration test-setup depicted in Figure 4.3.2.2 results in a lower cost when compared to the ANA setup. A SA, type HP8562A, is used. The SA was also linked to an HPVee PC program.

Points (a) and (b) indicate the calibration planes while points (i), (ii) and (iii) indicate coaxial connection points for current injection, the CUT's output end and CM current monitoring, respectively.

According to its specifications the SA's input port cannot handle a DC component at its input, without sustaining damage. A SUHNER DC-block is thus routinely connected at the input port. The block is specified to work properly without distorting the input signal in the frequency range 5MHz to 5000MHz. This implies that the block starts attenuating signals just below 5MHz, which is within the frequency range of interest.

An addition of a 50Ω signal generator (SG) (9kHz-3.3GHz) for the test-setup is required because the 50Ω SA (1kHz-22GHz) does not generate the signals that are being observed. When combined with SG, a SA becomes useful for checking the HF response of circuit networks. Moreover, it allows a study of the properties of a two-port system. An EMCO 94111-1 current probe is used to monitor the CM current flowing down the screen of the CUT. A 3dB attenuator was connected at the output port of the SG to improve its 50Ω impedance characteristic.

The configuration uses the same test-jig as in the ANA configuration test-setup. A calibration with 601 sample points is achieved by making a through connection of calibration points (a) and (b) in order to get a reference point. The measurements were performed for the frequency range of 10kHz to 100MHz with an output power of 13dBm from the SG. Because of the DC block cut-off frequency specification, the reliable result will start from 5MHz and above. It was observed that performing the measurement without synchronising the two instruments results in measurement inaccuracies and a longer time for the overall measurement. To synchronise the instruments, the trigger of the SG was connected to the external trigger input of the SA. The SG was set to linear steps of 50kHz and the SA was set to a continuous sweep

mode (maximum hold) plus a sweep time of 50ms. Therefore, the overall measurement time improved and the synchronisation of the two instruments was achieved. Two types of measurements are performed for the configuration test-setup illustrated in Figure 4.3.2.2.

1) The CM current flowing down the screen of the CUT is monitored. A current probe with a known transfer factor, Z_{tt}, is used whilst the CUT receiving end is terminated into a 50Ω matched load.
2) Next, the transmission through the CUT screen is measured. This implies that a transfer function is realised by applying a signal onto the shield-ground TL and measuring the corresponding voltage induced onto the CUT inner conductor while the probe is terminated in a 50Ω-matched load.

4.4 Metrology Issues Associated with Test-jigs

The prime objective of this section is to investigate the common measurement errors that may arise, especially at HF, when using test-jigs. One problem that can occur demonstrates a difficulty when attempting to reduce the flow of CM current onto the measuring equipment's coaxial cables. This occurs in the current-injection technique and is depicted in Figure 4.4.1.

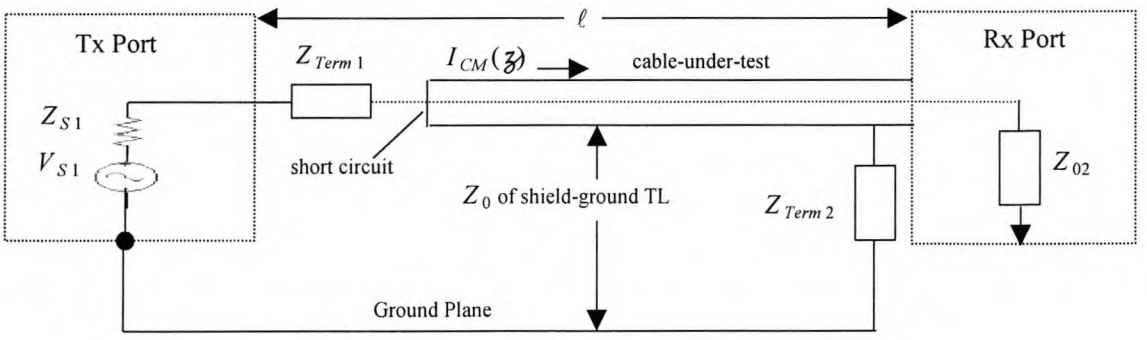

Figure 4.4.1: Schematic of the proposed metrology demonstration.

The original feed-through at the terminating plate on the port 2 side was not sufficient in that it allowed CM current to flow on the cable attached to port 2. A piece of PCB was used to isolate this cable's ground connection from the setup, while Z_{Term2} allowed a path for the CM current to flow. Figure 4.4.2 shows the actual configuration setup used in this investigation with the effective resistance Z_{Term2} built into the shield-ground loop. The dimensions of the test-jig are the same as mentioned in the previous sections. Z_{Term2} is obtained by using two 100Ω resistors in parallel. The original purpose of Z_{Term1} (equals 50Ω) for this measurement sequence was to prevent driving the system hard into a short circuit. Note, with Z_{Term2} present in the circuit as well, a 100Ω loading is presented to port 1.

The PCB carrying Z_{Term2} is mounted to fit around the circumference of the CUT connector (Rx port side), such that it shares the same GP with the jig. There is no means of using a gasket between the jig metal plate and PCB since it is made of plastic material.

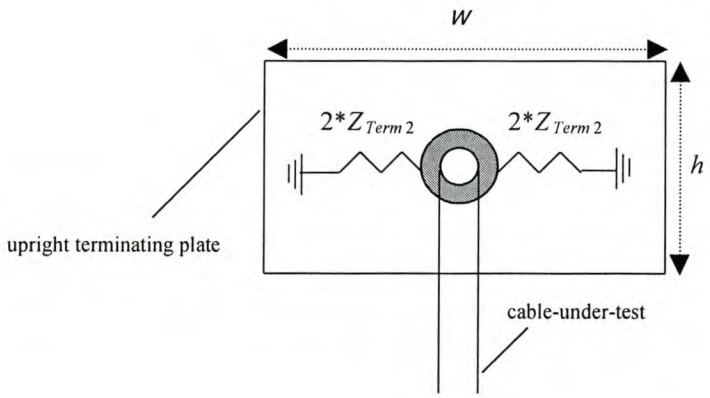

Figure 4.4.2: Cross-sectional view of the experimental configuration demonstrating the jig construction for mounting the PCB.

Because of the 'open' connection on the port 2 side caused by the PCB used, some part of the CM current still finds its way onto the measuring cable. One essential means to reduce this is to put CM chokes on the Rx cable and make that a high impedance path too. Properly designed chokes over the band would be first choice. The path for the CM current is via the

measuring cable to the Rx port and over the equipment housing of the ANA and internal circuitry. It was found difficult to isolate the measurement from the CM current by clamping ferrite chokes over the measuring cable. A proper return path confines the CM current within the desired points of the shield-ground TL. Measurements for both systems were done and compared in the next section.

4.4.1 Analysis Findings and Observations

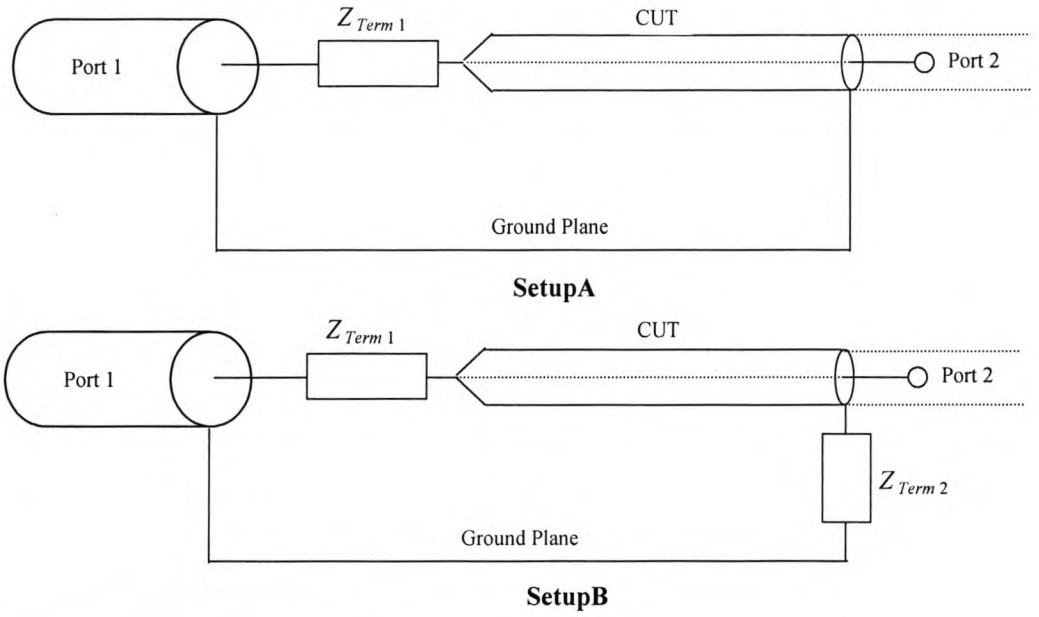

Figure 4.4.1.1: Comparison of configurations shown by Figure 4.3 (setup A) and Figure 4.4.1 (setup B). Schematic side view.

Figure 4.4.1.1 shows the experimental configurations to determine Z_T: Setup A yields correct Z_T values while setup B is associated with measurement errors that cannot be calibrated out of the test system. For configuration setup A, resonance show up in the response of the input impedance seen looking from port 1 (Z_{11}) at approximately 75MHz. The resonance corresponds to $\lambda/4$, that transforms the short circuit to an open circuit. This $\lambda/4$ resonance effect causes the CM current in the shield-ground TL to form a standing wave pattern.

It can be noted that more current will flow in the CM loop of setup A than in setup B, because of an added resistor Z_{Term2} in setup B. Both these configurations yield similar results at low frequencies. But discrepancies are noticeable as soon as the frequency reaches a few tens of MHz.

4.5 Experimental Results and Discussions

The magnitude of Z_T, as a function of frequency for a range of common 50Ω coaxial cables with single braided screens and parallel wire pairs, was measured with the proposed experimental techniques. Figure 4.5.1 shows measured Z_T values with the wire-loop antenna technique.

From these measurement results it is clear that the RG 58A/U cable shows a better performance response compared to the RG 58C/U cable since it has lower Z_T values on average across the frequency range of interest. At low frequencies, the responses for the cables are almost the same, but as the frequency increases, the responses differ by approximately 0.2Ω/m at 50MHz. This is expected, because the names of the cables suggest that the overlapping of the braid wire strands is different, which contributes significantly to the 'porpoising' effect that dominates in the desired frequency range.

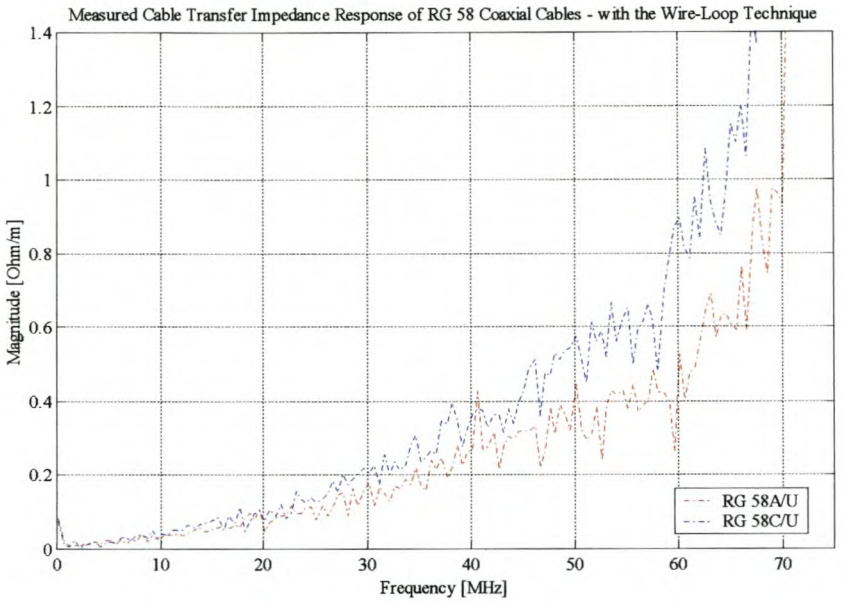

Figure 4.5.1: Experimental Z_T magnitude response for coaxial cables using the wire-loop antenna technique.

The measured results tabulated in Table 4.5 compare the values obtained using the wire-loop antenna technique only for RG 58C/U to values obtained by other authors using different measurement techniques and different lengths of the same cable, below the 50MHz range.

Table 4.5: Visual comparison of Z_T [Ω/m] of the RG 58C/U values with the wire-loop and published results.

Frequency	Benson [Ben96]	Fourie [Fou98]	Wire-loop
10MHz	0.1	0.056	0.035
20MHz	0.16	0.10	0.09
30MHz	0.2	0.16	0.21
40MHz	0.3	0.22	0.3
50MHz	0.4	0.32	0.56

The response for both cables increases linearly with frequency, but the curves are not smooth across the desired frequency band. This feature may be due to impedance variations in the test system. Therefore, TL effects must be taken into account. Unfortunately, the attempt to de-embed all the effects was unsuccessful. The current-injection measurement technique is first used to evaluate the reflection coefficient response with the 50Ω coaxial cables in place.

Current-injection method results of Z_T are presented in Figure 4.5.2 and 4.5.3. Both configurations show that the response for each cable increases linearly with the frequency. The measured result of RG 58 cables shows a cut-off frequency at ≈ 2MHz for the C/U and ≈ 5MHz for the A/U, whereas the RG 316 has a cut-off frequency at ≈ 700kHz. This suggests that the overlapping of the braid wire strands and the optical coverage of the RG 316/U coaxial cable are different from the RG 58 coaxial cables.

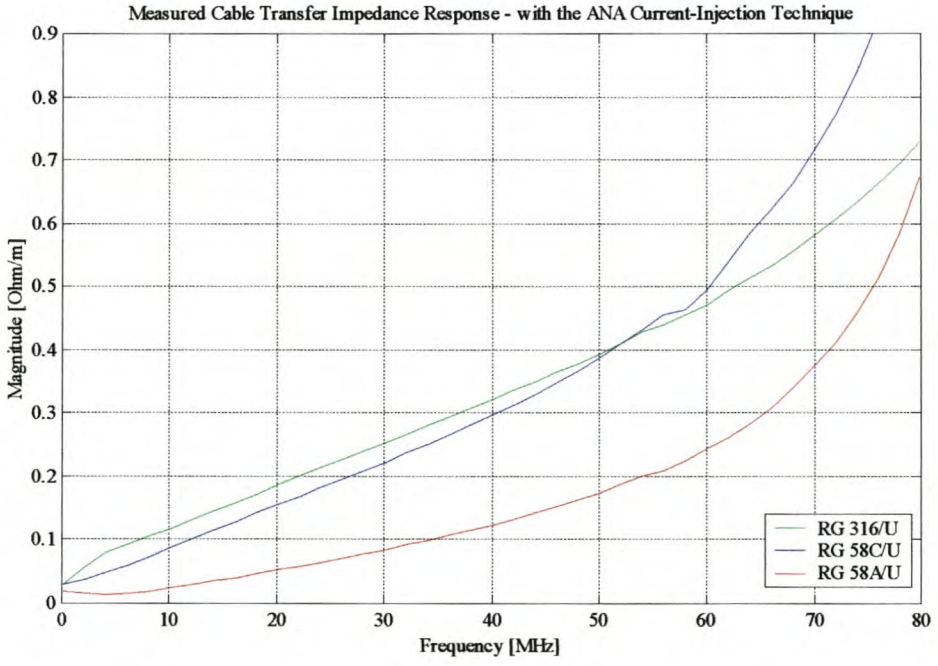

Figure 4.5.2: Magnitude response of measured Z_T versus frequency for RG coaxial cables with the ANA setup.

The only advantage of the RG 316/U against the RG 58 cables is that it is flexible and easy to work with. The most reliable and repeatable Z_T results are below 50MHz for both configuration test-setups. Assuming electrically small cables ($\ell << \lambda$), external EM fields see a braided cable screen as a complete screening enclosure. Thus, coupling of external disturbances occurs mainly by diffusion and 'porpoising' effect due to the braid woven strands.

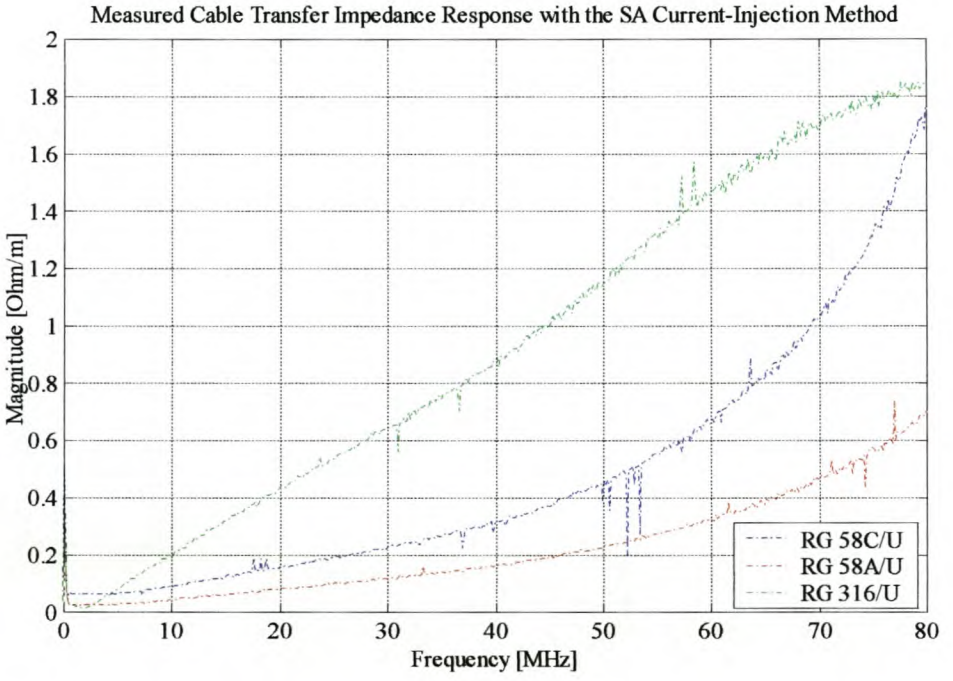

Figure 4.5.3: Magnitude response of measured Z_T versus frequency for RG coaxial cables with the SA setup.

Figure 4.5.4 shows measured magnitude response of Z_T for parallel conductor pairs. The experiment investigated the influence on ordinary wires of twisting the ground return with its outgoing signal wire uniformly. The twist tends to make local environment EMI contributions cancel out, since the induced voltage in each incremental twist area is approximately equal and opposite to its neighbour. This is the best practice for unshielded ordinary wires and is also evident from the measured results.

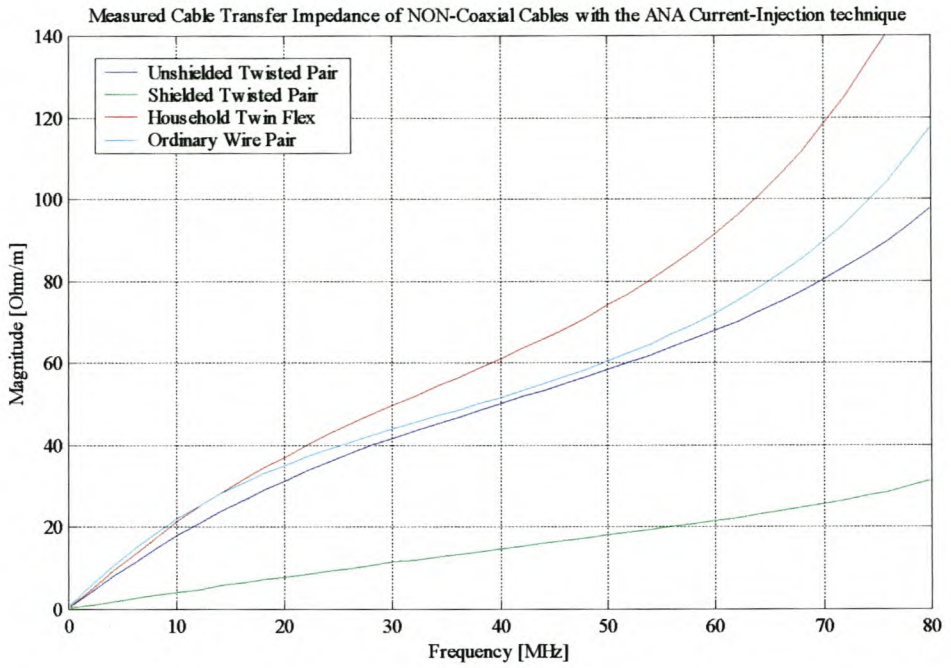

Figure 4.5.4: Magnitude response of measured Z_T versus frequency for non-coaxial cables with the ANA configuration test-setup.

Magnetic coupling occurs between parallel conductor loops because of Faraday's law. The twisting reduces the inductive pickup, hence the reduction in Z_T. The results indicate that the shielded twisted pair (STP) has got a better performance than the other cables across the frequency range, while the household twin flex shows the worst measured result. The shielding additionally reduces capacitive coupling.

4.5.1 Cable 1 – RG 58C/U

This 'single-braided' 50Ω coaxial cable is widely used. The measured results for RG 58C/U obtained by both current-injection configurations are presented in Figure 4.5.1.1 and correlate well for frequencies below 50MHz. The magnitude of Z_T rises linearly with

increasing frequency. Thus, it is apparent that the cable becomes more EM leaky with frequency since the cable screen is common to both the internal (DM) and external (CM) circuits. The discrepancy at HF is attributed to the λ/4 resonance, the effect of which shows up above 50MHz.

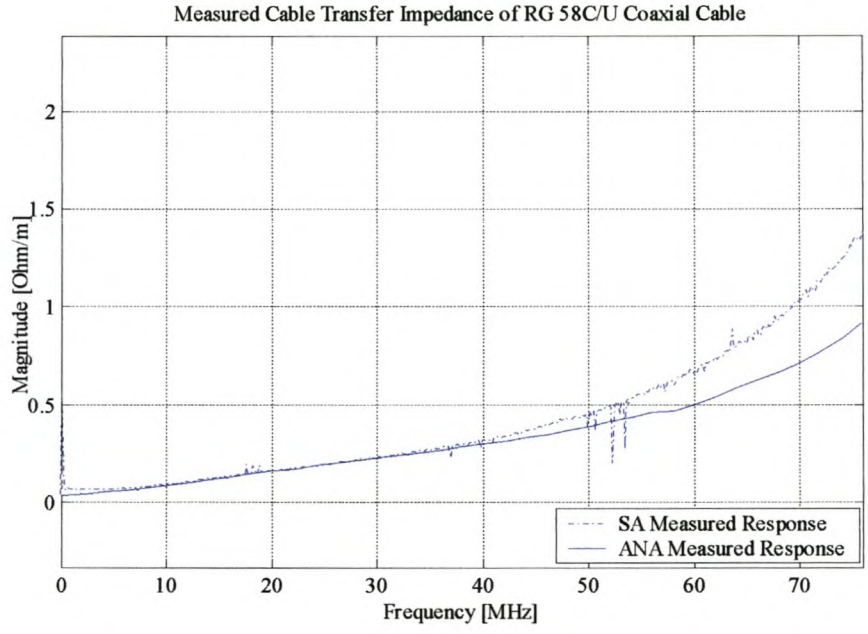

Figure 4.5.1.1: Magnitude response of measured Z_T versus frequency for RG 58C/U cable.

4.5.2 Cable 2 – RG 58A/U

The measured results for RG 58A/U obtained by both current-injection configurations are presented in Figure 4.5.2.1 and agree to within 0.1Ω/m in the worst case for frequencies below 50MHz. Thus, both configurations setups show a good Z_T agreement.

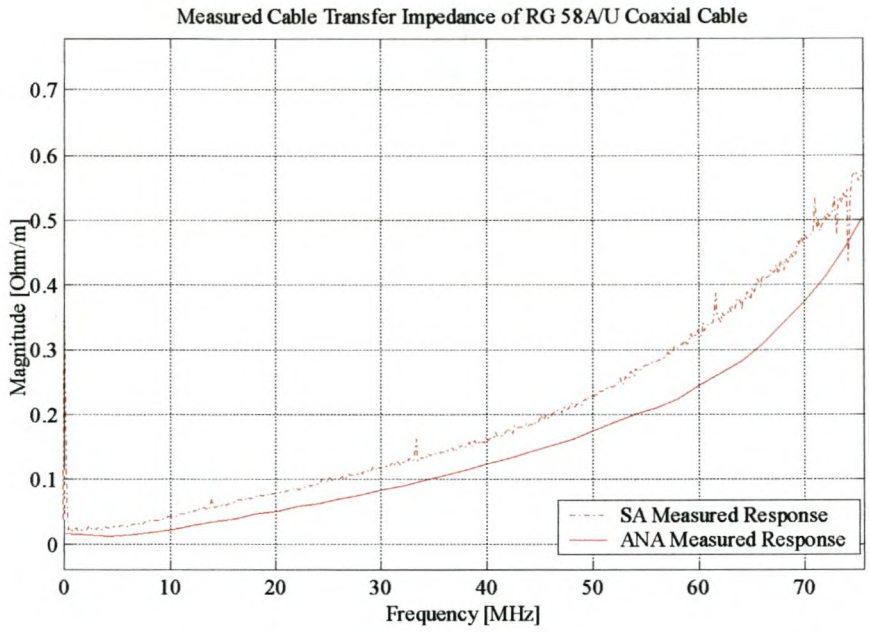

Figure 4.5.2.1: Magnitude response of measured Z_T versus frequency for RG 58A/U cable.

4.5.3 Cable 3 – Shielded Twisted-Pair

The shielded twisted wire-pair, called STP, with an aluminium foil as a screen, is now tested. Measured results are shown in Figure 4.5.3.1 and are $\approx 10\Omega$/m (20dB) worse than the RG coaxial cables across the frequency band. Again, the ANA and SA are in good agreement with a difference of less than $\pm 3\Omega$/m across the frequency band.

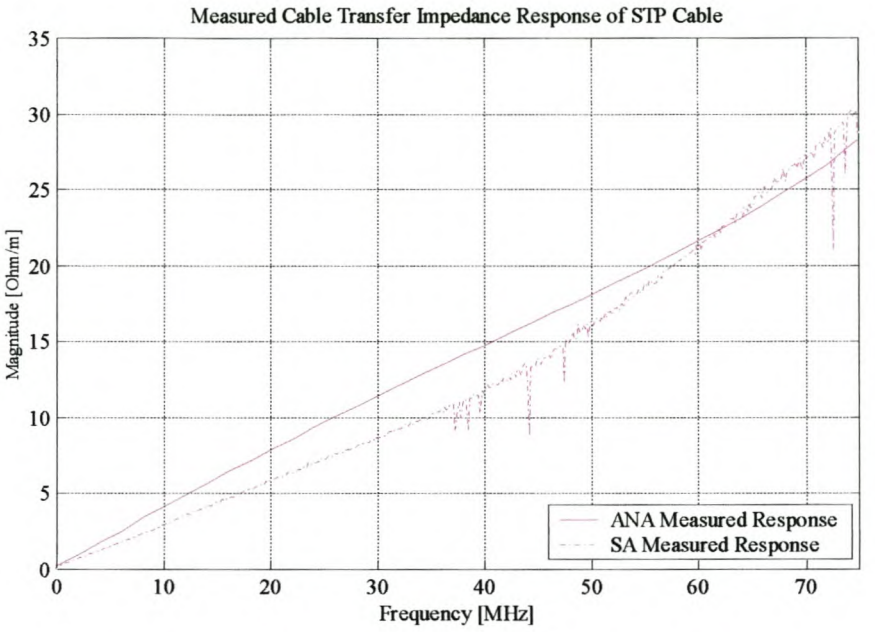

Figure 4.5.3.1: Magnitude of measured Z_T versus frequency for parallel conductor pair.

4.5.4 Cable 4 – RG 316/U

This is a 'single-braided' 50Ω flexible coaxial cable. The measured results for RG 316/U are obtained by the SA configuration test setup with the cable sample fitted with different end gold SMA connectors on the Rx port side, only. This was done to examine the contribution of cable end connectors to the total magnitude of Z_T.

Figure 4.5.4.1 shows that the measured magnitude response of Z_T is different for each and connector cable sample – showing their influence. This underscores the fact that this is cable transfer impedance.

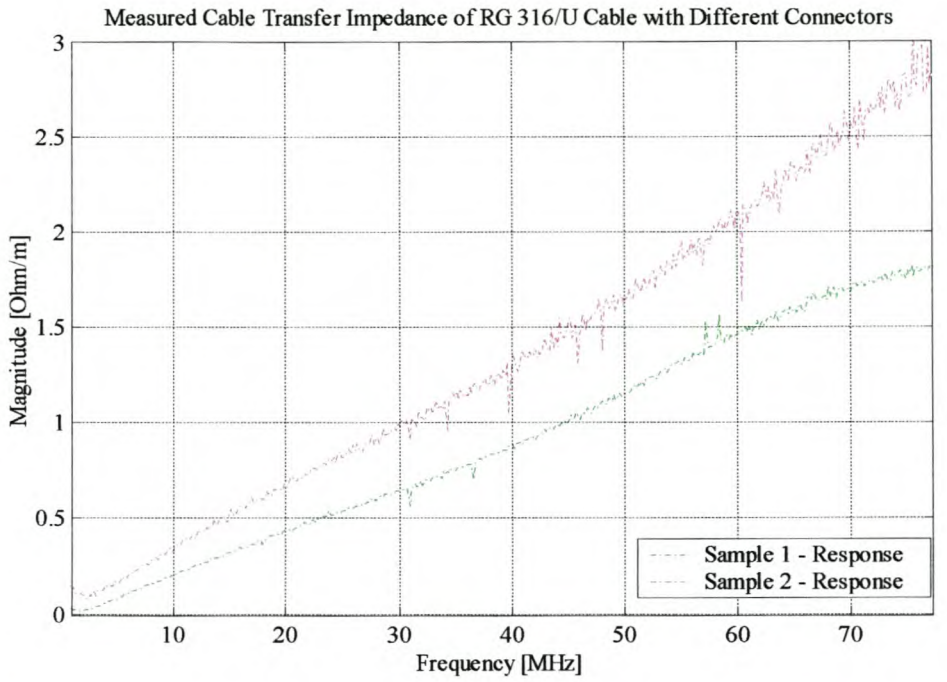

Figure 4.5.4.1: Magnitude of measured Z_T versus frequency results obtained with SA setup for an RG 316/U cable fitted with different connectors.

4.5.5 Demonstration of Test-Jig Effects

In Figure 4.5.5.1, measured results for the theory developed in section 4.4, are shown. The 50Ω resistor Z_{Term2} built into the shield-ground TL gives rise to unpredictable CM currents that negatively affect the measurements. These results indicate clearly that the clamping of CM ferrite chokes over the measuring cable did not reduce the unwanted CM current sufficiently.

The configuration setup A and B from Figure 4.4.1.1 yield a comparable Z_T response below 20MHz, as shown in Figure 4.5.5.1. But as the frequency increases the CM current influence prevails, thus leading to measurement inaccuracies to the magnitude response of Z_T. The following section compares the measured results obtained by the different measurement methods.

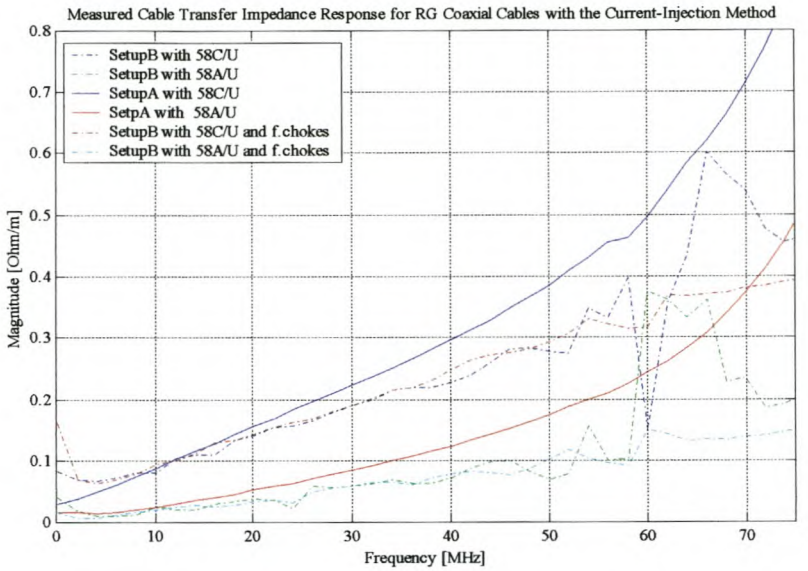

Figure 4.5.5.1: Measured magnitude response of Z_T under the influence of CM current using the ANA setup.

4.5.6 Comparison of Measurement Methods

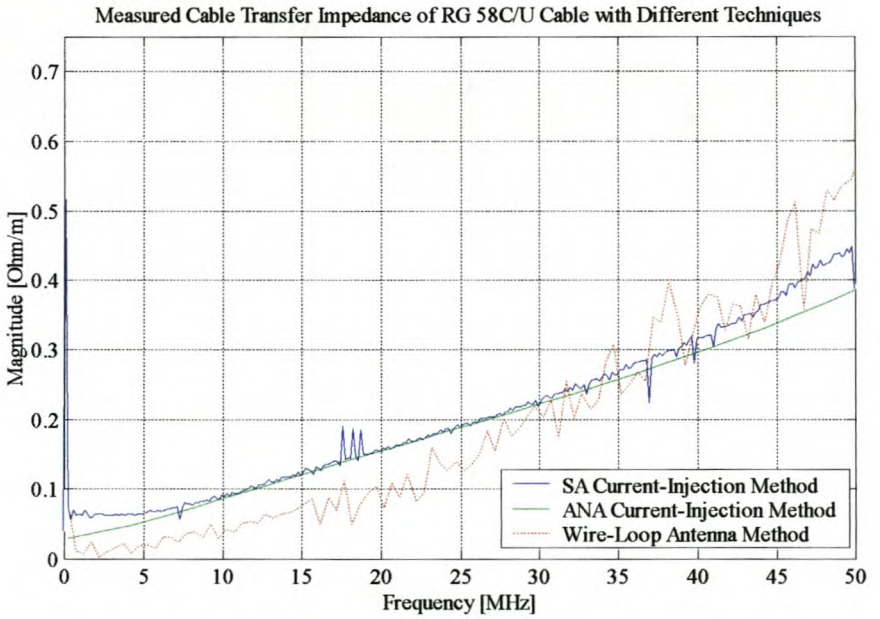

Figure 4.5.6: Typical values of Z_T frequency obtained using different methods.

The measured results for RG 58C/U obtained by both current-injection and wire-loop configuration methods are presented in Figure 4.5.6.1 for comparison, and agree to within $\approx 0.15\Omega/m$ in the worst case for frequencies below 50MHz. Furthermore, the current-injection approach correlates well to the Z_T values gathered from the literature, as seen in Table 4.5.6.

Table 4.5.6: Visual comparison of Z_T [Ω/m] values of the RG 58C/U values with the current-injection approach against published results.

Frequency	Benson [Ben96]	Fourie [Fou98]	ANA Current-Injection	SA Current-Injection
10MHz	0.1	0.056	0.08	0.09
20MHz	0.16	0.10	0.16	0.16
30MHz	0.2	0.16	0.22	0.22
40MHz	0.3	0.22	0.30	0.31
50MHz	0.4	0.32	0.39	0.42

4.6 Concluding Remarks

Techniques for measuring the cable transfer impedance of shielded and unshielded cables have been introduced. The measurement systems require simple construction and common laboratory instruments. The main advantage over existing techniques is the ease of mounting and connecting the cables in the test setup. The CM current, I_{CM}, injected and the DM voltage, V_{DM}, generated is measured directly i.e. no estimation is required. Although the magnitude response of Z_T was found to be measurable and repeatable up to 80MHz, the proposed techniques have shown to produce best results at frequencies below 50MHz when using 0.5m length of cables. The upper frequency limit of the current-injection technique is higher than the wire-loop antenna technique, but this depends on

factors inherent in each measuring system (wire-loop antenna operational frequency range).

Two configuration test-setups that use different measuring equipment have been introduced and compared. Both are economical and straightforward to set up. Measured results achieved with both configurations have shown good agreement in the current-injection case and interesting agreement with the wire-loop approach. The wire-loop antenna measurement technique suffers from an upper frequency limit due to resonance. If shorter cable samples are used an improvement can be achieved. The ANA enables rapid measurements compared to the SA.

It has been shown that the measurement of cable transfer impedance, Z_T is a practical tool for shielding performance evaluation and its result can be used to classify cables for verification or development of a cable matrix. This will form a basis for their choice in given applications. The measured results depicted a distinct response for each test cable sample, thus permitting a comparison of various cable shields.

Chapter
5

Development and Evaluation of an EMC Integrated Test System

Satellite designs are required to meet aerospace mission specifications. On this basis the Stellenbosch University Satellite (SUNSAT) was required to meet a design structure of 45cm maximum cubic side [Mil93]. Theoretical and experimental techniques will be developed to study the coupling between transmission cables and neighbouring circuitry of the satellite hardware structure. However, the emphasis of the investigation covered is primarily a development of measuring techniques rather than an in-depth theoretical (or mathematical) analysis model of the system.

5.1 Introduction

During the integration stage of a satellite system, EMC engineers play an important role in providing guidelines concerning aspects such as screening of the fast bus that carries micro-processor signals, cable layout protocols, placement of devices and prototyping of the electronic hardware, etc. The investigation of EMC problems associated with transmission cable layout protocols in a complex system such as the final design of a satellite may be frustrating, expensive and time consuming for electronic integration engineers.

An EMC Integrated Test System (ITS) is a 'satellite' hardware emulating tool designed to evaluate the response of circuits and transmission cables for EMC purposes. It is a well-defined EM environment that simulates a real situation.

The idea behind the EMC ITS mechanical structure is that it would theoretically allow itself to be treated as a Faraday cage [Mil98, p293], preventing the internal signals from coupling to the external environment and vice versa. For example, the signals that are internal to the satellite environment may couple significantly to the antennas that are situated externally on a satellite. However, the treatment of this theory is beyond the scope of this thesis.

In order to understand how a transmission cable or an electronic sub-system inside an enclosure radiates externally, it is first necessary to understand how a transmission cable or an electronic sub-system excites the environment internal to the enclosure. Partial or complete enclosures are used for EM shielding to reduce fields inside (or outside) the space enclosed. The experimental work pursued will use a cubic structure for the design of an enclosure, thus meeting the satellite specification mentioned above, with the hope of making a meaningful contribution to future satellite research and development projects.

The significance of the measurements undertaken will help anticipate the impact of emission on neighbouring circuitry and, possibly, careful placement of devices. The implementation and evaluation used involves the coupling between two magnetic loops, and also between two electric monopoles which are introduced into the enclosure. Further investigation into radiated emission from digital circuits is also presented.

5.2 Experiment and Analysis Descriptions

The complete enclosure was first evaluated theoretically for the prediction of resonance frequencies. The resonance frequencies f_{nml} of a closed cubic enclosure with side L are given by [Oly99]

$$f_{nml} = \frac{c}{2L}\sqrt{n^2 + m^2 + l^2} \tag{5.2}$$

with n, m, l equals to 0, 1, 2, ··· but with maximally only one sub-index equal to zero, and c the propagation velocity in vacuum. For a box with L equals to 0.45m, these resonance frequencies up to 1GHz together with their degree of degeneracy are tabulated in Table 5.2. The degree of degeneracy is the number of combinations of n, m, l giving the same resonance frequency.

Table 5.2: Resonance frequencies and their degeneracy for a cubic enclosure with a 0.45m side length.

Name	Frequency [MHz]	Degeneracy
f_{110}	471.4	3
f_{111}	571.4	1
f_{210}	745.4	6
f_{112}	816.5	3
f_{220}	942.8	3
f_{221}	1000	3

5.2.1 Geometry and Dimensions of the EMC ITS

The dimensions of the enclosure are ($\ell \times w \times h$) $\approx$ 45(z) $\times$ 45(y) $\times$ 45(x)cm and are shown in Figure 5.2.1.1. The enclosure was made from an aluminium sheet with thickness of $\approx$ 1.5mm. In constructing the enclosure, four side panels were bent from the same piece of metallic sheet and joined at one joint to form a double-open-sided cubic box. One of the open sides was then closed with a metal sheet to form the back panel. The joints were then carefully fastened with a gasket, closely spaced screws and a metallic tape to prevent EM energy leakage.

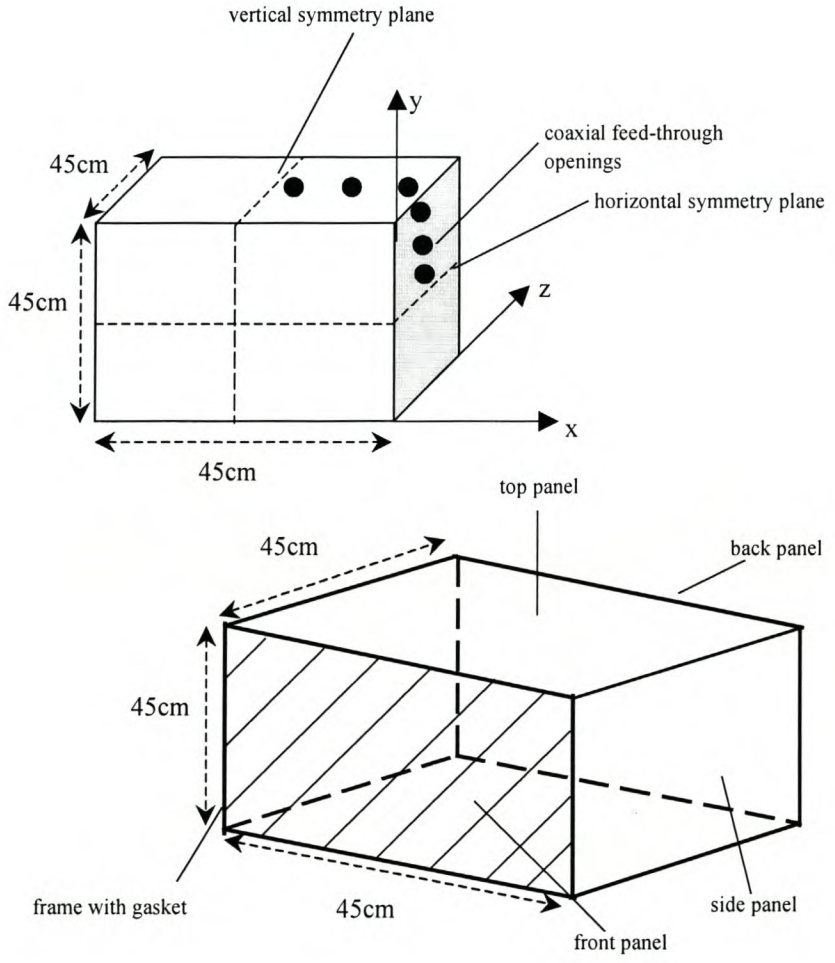

Figure 5.2.1.1: Geometry and dimensions of the test enclosure.

The other open side was used as a front panel and was constructed to have a lid, allowing access inside the enclosure. The lid was also fastened with gasket, closely spaced screws and metallic tape to the front panel frame, ensuring good contact between the lid and the enclosure.

The enclosure was designed to house two sub-enclosures made from tin material. The outer enclosure forming the Faraday cage is used as an EMC cabinet that protects the measuring equipment from interference produced by internal signals while the inner EMC cabinets (sub-enclosures) shown in Figure 5.2.1.2, controls the CUT environment. However, in most cases the level of integration in a satellite does not permit a construction of each function into a 'black box' and screening it from the exterior as it is the case in this situation. Hence, the use of sub-enclosures in the experiment is intended for the prevention of direct coupling between the transmit (Tx) circuit, receive (Rx) circuit and the CUT. This prevents the contamination of the measured near-field strength by undesired signals. The CUT interconnects the two modules (sub-enclosures) that are properly grounded to the chassis.

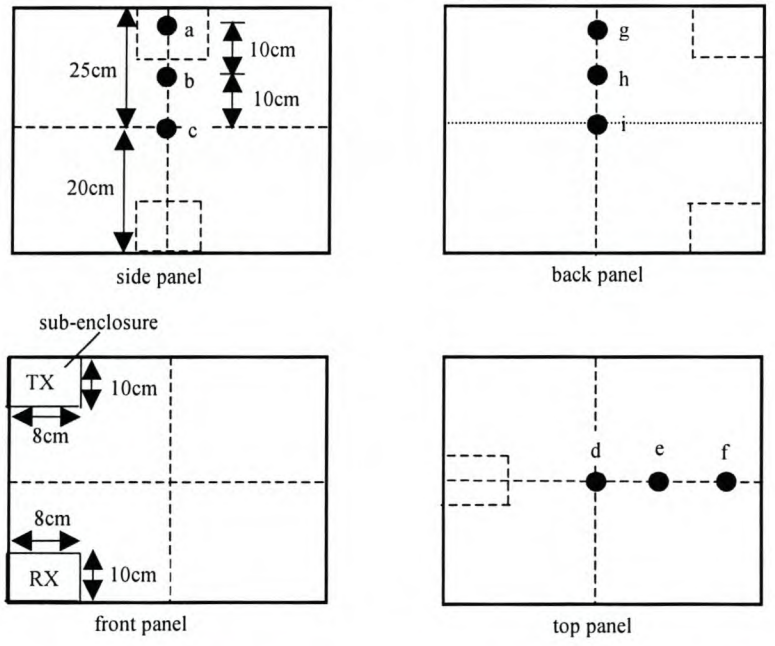

Figure 5.2.1.2: Geometry and dimensions of all side panels and sub-enclosures.

The dimensions of the sub-enclosures are ($\ell \times w \times h$) $\approx$ 10(z) $\times$ 8(y) $\times$ 10(x)cm. The sub-enclosures are attached along one side panel as seen in Figure 5.2.1.2. The side that attaches the sub-enclosure to the EMC cabinet side panel is each constructed to have a lid, allowing access to the internal environment of the sub-enclosure.

Circular apertures, (a) to (i) of $\approx$ 1cm in diameter were drilled through the enclosure for insertion of 'sniffer' probes that will sense near-field strength inside. The interval distance shown in Figure 5.2.1.3 between the measuring points (P1, P2, P3 and P4) located along the measuring cable is $\approx$ 10cm. This measurement is by nature very empirical, but nevertheless gives a useful indication of energy within the EMC ITS arising from different cable classes. The position P1 is situated at the measuring cable's SMA connection to the 'sniffer' probe. Due to the vertical and horizontal symmetry of the enclosure, the apertures were chosen to be on one half of each side of the enclosure.

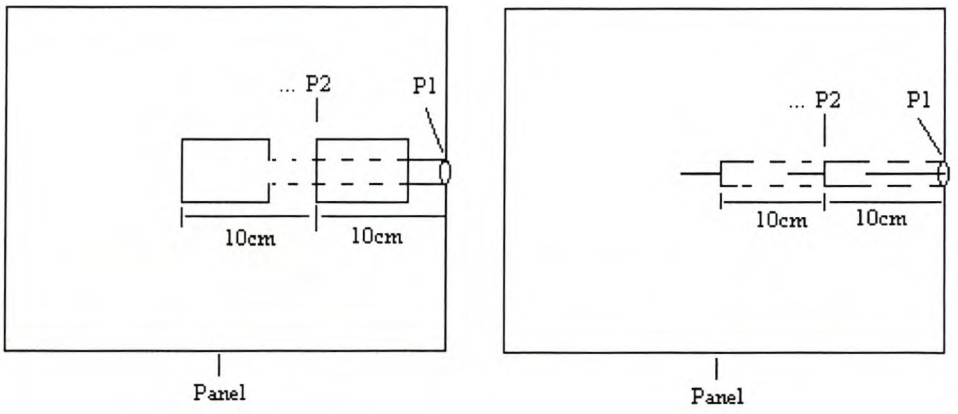

Figure 5.2.1.3: View of the panels with the *B*-field sensor (left) and *E*-field sensor (right) probing one aperture to different levels.

5.2.2 Measurement of Induced *B* and *E*-Field Strength

For ease of measurement and analysis, radiated emissions are assumed to predominate above 30MHz and conducted emissions are assumed to predominate below 30MHz [Wil96, p119]. In the near-field, $d < \lambda/2\pi$ and the wave impedance is determined by the characteristics of the source. Here d is the distance from the radiating source and λ is the wavelength of the radiating wave. Therefore, in the near-field either of the ***E*** or ***B***-field will dominate depending on the source type. A low current, high voltage radiator such as a monopole will generate mainly an ***E***-field of high impedance, while a high current, low voltage radiator such as a current loop will generate mainly a ***B***-field of low impedance. According to [Wil96, p69], measurements of the ***B***-field give better repeatability measurements in the near-field region than measurements of the ***E***-field, which is easily perturbed by nearby objects.

From the above-mentioned assumptions, two basic configurations will be employed for the implementation to assess the induced field strength:

1) For ***B***-field excitation a closed current loop will be used as a magnetic field detector.
2) For ***E***-field excitation a monopole will be used as an electric field detector.

The experiment used measures coupling between two loops, and two monopoles, respectively. One of the loops/monopoles acts as a source while the other acts as a detecting 'sniffer' probe. Besides the above-mentioned assumptions, it is noted that matched circuit terminations are usually desirable for RF circuits but something could go wrong during the deployment or operation of the satellite in orbit, causing a cable to be terminated into an open or short circuit of high or low impedance, respectively.

5.2.3 Home-made Near-Field Probes for Diagnostic Tests

A probe is merely a wire formed into a loop or monopole, which produces a voltage at its terminals proportional to the frequency. Home-made near-field 'sniffer' probes were designed and are shown in Figure 5.2.3. An ***E***-field probe to detect capacitive near-fields is constructed by simply stripping the shielding off the tip of a rigid coaxial cable [Mar98]. The exposed inner conductor that is electrically isolated from the outer conductor acts as a high impedance capacitive pick-up. A ***B***-field probe used to detect inductive near-fields is constructed by a closed rectangular loop from a metallic track on a PCB forming a magnetic pick-up. Probe design is a trade-off between sensitivity and spatial accuracy [Wil96]. The smaller the probe, the more accurately it can locate signals but the less sensitive it will be. Therefore, the area of the loop affects sensitivity.

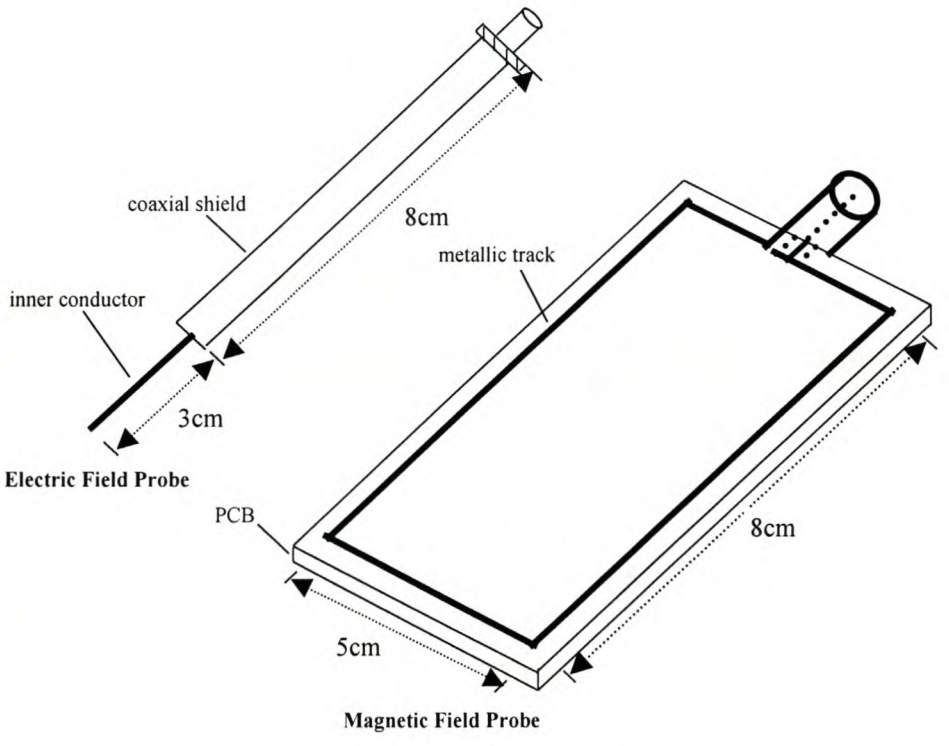

Figure 5.2.3: Home-made near-field probes for diagnostic testing.

One significant requirement for these probes is that their dimensions must be small compared to the length of the CUT acting as an antenna and with the wavelength of the excitation signal. At the highest frequency (1GHz) of interest for the measurements, the wavelength in lossless media is 30cm and the CUT's length is ≈ 25cm while the largest dimensions of the ***B***-field and ***E***-field probes are 8cm and 11cm, respectively. Therefore, the probes are applicable for assessment of the induced field strength.

To anticipate the impact of radiated fields on neighbouring circuitry and characterization of the probes, the ***B*** and ***E***-field probes may be treated as magnetic and electric sensors, respectively. Then, an S_{11} of the ***B***-field probe can be measured outside the EMC ITS well away from any metallic objects. This measurement forms the basis of assigning a value of the loop impedance (Z_{loop}) to the equivalent PCB. The measurement of the internal impedance (Z_{int}) of the electric monopole is not straightforward [Kon99]. A detailed theoretical model of the loop and monopole placed within an enclosure can be found from Konefal *et. al.* In the ***B***-field coupling mechanism, a current flowing in the loop (plus enclosure) under test produces magnetic fields that couple into the ***B***-field detector probe placed in the same vicinity and induces current. Thus, an $EMF_{\boldsymbol{B}probe}$ will develop at the terminals of this probe. The effect is reciprocal, and a current flowing in the ***B***-field loop probe will likewise induce an EMF_{CUT} in the loop formed by the CUT and chassis. Hence, the magnitude of these effects will be the same (i.e. $S_{21} = S_{12}$).

In the ***E***-field coupling mechanism, a voltage on the monopole (plus enclosure) produces electric fields. These fields cause charges to appear on the ***E***-field detector probe placed in the same vicinity. Because of charge flow in and on the probe, a current (I_{source}) will be induced into the probe, and thus, an $EMF_{\boldsymbol{E}probe}$ voltage will develop at the terminals of this probe. Likewise, the effect is reciprocal. Hence, the equivalent magnetic PCB is charaterized by $EMF_{\boldsymbol{B}probe}$ and Z_{loop} while the equivalent electric PCB is charaterized by I_{source} and Z_{int} [Kon99]. It is important to note that the low and high impedances of the ***B*** and ***E***-field probes, respectively, do not match the 50Ω impedance of typical test instrumentation. As these measurements are not absolute, this is not a significant issue.

The probes are best used for tracing and comparing results rather than absolute measurements, particularly in conjunction with a SA or EMI Rx. For RF emissions, measurement probes are regarded as devices that are used to couple the measured variable into the input of the measuring instrumentation. To convert the measured *EMF* voltage at the instrument terminals, V_{SA}, into actual field strength at the probe one has to add the probe's transducer factor, Z_{tt}, and cable attenuation, α_{cable}, (as a function of frequency). Thus, to relate the SA voltage reading to the actual fields the following equations can be applied:

$$\left|\boldsymbol{B}_{actual}\right|_{\mathrm{dB\mu\,V}} = \left|V_{SA}\right|_{\mathrm{dB\mu\,V}} + \left|Z_{tt}\right|_{\mathrm{dB\Omega}} + \left|\alpha_{cable}\right|_{\mathrm{dB\mu\,V}} \qquad (5.2.3.1)$$

$$\left|\boldsymbol{E}_{actual}\right|_{\mathrm{dB\mu\,V}} = \left|V_{SA}\right|_{\mathrm{dB\mu\,V}} + \left|Z_{tt}\right|_{\mathrm{dB\Omega}} + \left|\alpha_{cable}\right|_{\mathrm{dB\mu\,V}} \qquad (5.2.3.2)$$

5.2.4 Experiment 1: Fields Associated with RF Signals

In this experiment the coupling mechanism caused by the ***B*** and ***E***-fields associated with RF signals are addressed. Coaxial cables in satellites are widely used to carry RF, video signals as well as making connections to the Random Access Memory (RAM) trays and other HF signals. To approximate the experiment, the system's *S*-parameters were measured on a calibrated HP8753C ANA with the following settings:

- Frequency range between 300kHz and 1GHz.
- 201 sample points.
- Averaging factor of 8.
- 100Hz IF bandwidth.
- Reference generator output signal of +0dBm.

A coaxial cable of ≈ 0.25m in length was used to interconnect the two sub-enclosures and represents a radiating source. The top sub-enclosure houses the Tx circuit intended to inject a signal via the coaxial lead down to the Rx circuit housed in the sub-enclosure at the bottom, while the chassis (side panel) forms a structural ground. The Tx circuit is emulated by port 1 of the ANA and the Rx circuit can be represented by either a short or open circuit termination. Therefore, an effective radiating loop or monopole above the chassis of the side panel forming a ground return will be realised.

The low to high frequency regime from 300kHz to 1GHz for the measurements includes the Very High Frequency (VHF) and Ultra High Frequency (UHF) bands that are used in the RF communication links of a satellite.

5.2.5 Experiment 2: Measuring Emissions from a Digital Circuit

This section pursues an investigation to address the effects of noise created by the many HF digital circuits in a satellite system, and its crosstalk on neighbouring circuitry.

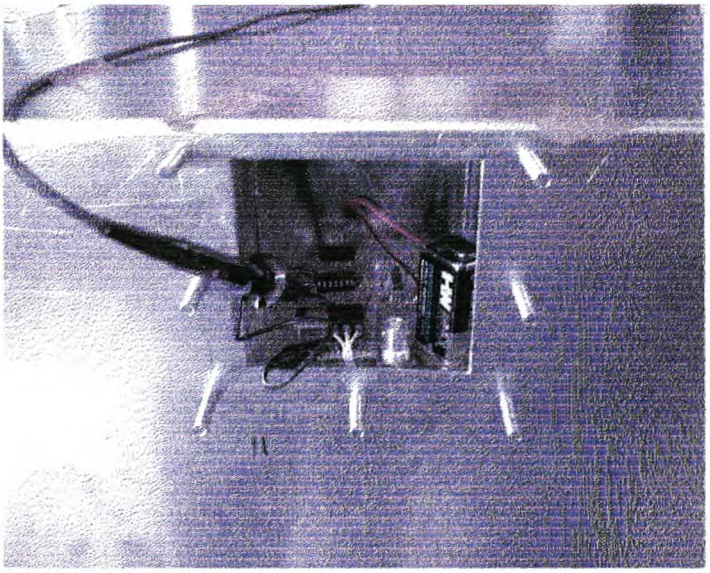

Photograph 5.2.5: Side-view of the Tx sub-enclosure housing the digital circuit.

For demonstration purposes, two boards with modern digital circuits of type 74LS00 chip are used. These circuits are introduced within the sub-enclosures as shown in the Photograph 5.2.5. Measurements will be performed for frequencies between 5MHz and 200MHz.

The objective of the experiment is to assess the importance of CM currents on transmission cables in the total radiated emissions of the cable. It was found important that the experiment configuration setup has to be simple enough, thus it does not represent realistic and a more complicated electronic product. However, this has a benefit of ensuring that additional radiation will not complicate the interpretation of the measured data. The experiment is originally described in [Cla92].

5.2.5.1 General Descriptions

A 10MHz oscillator drive a 74LS00 NAND gate i.e. the oscillator's output is connected to all the inputs of this gate. Then one of the outputs of this gate is connected to all the input of another 74LS00 NAND gate via a 0.25m three-wire ribbon transmission cable as shown in Figure 5.2.5.1. The ribbon cable wires' centre-to-centre separation is ≈ 1mm. The middle wire carried the 10MHz-pulse train output of the driven gate to the gate at the other end, which serves as an active load.

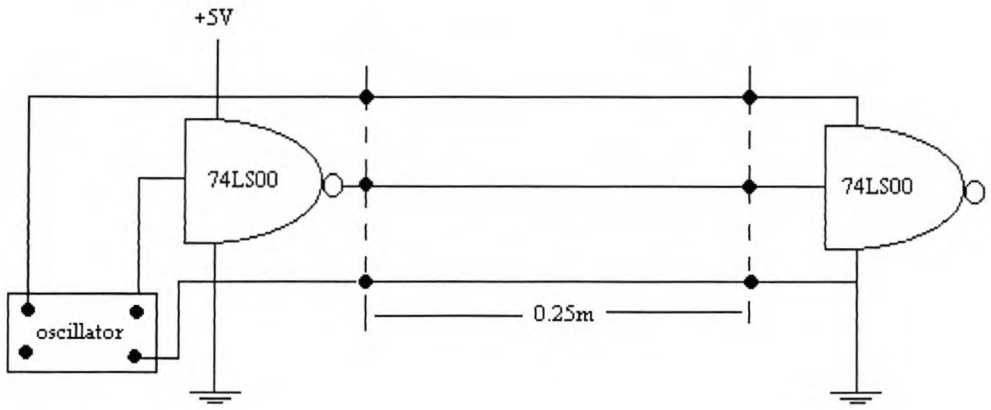

Figure 5.2.5.1: Configuration of the digital circuit used in the experiment.

An outer wire carries the +5V power for the NAND active load and the other outer wire serves as the return for both signals. The +5V power is derived from a +9V battery that powers a L7805CV regulator. This provides a compact source. An external connection to the power mains was avoided. This was intentional so that radiation from the power cord of a power supply would not contaminate the measurements. A picture of the setup is depicted in Photograph 5.2.5.1.

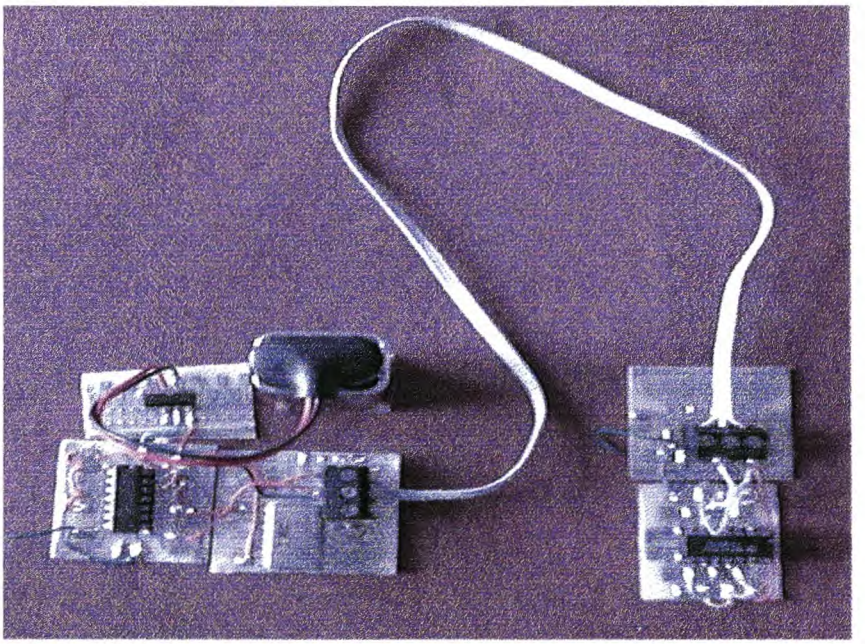

Photograph 5.2.5.1: Digital circuit test setup.

The time-varying current in the signal lead produces a magnetic field around it. The field couples to the detector ***B***-field probe where it induces an *EMF* voltage across its terminals. For the electric coupling, a coupling stray capacitance exists between the signal wire and the detector ***E***-field probe. This capacitance decreases with distance between the two.

5.3 Measurement Procedure

The experiment starts off by looking at the near-field characterization of the screened enclosure in the frequency range from 300kHz to 300MHz, which is below the first resonance of the enclosure. A single-wire transmission was used for the enclosure characterization and was fitted with BNC connectors for ease of interconnecting the external sides of the bottom and top panel of the Tx and Rx sub-enclosures respectively. The single-wire forms a DM loop with the chassis. This type of transmission link is, of course, highly detrimental for EMC and almost never used [Mar01, p36]. It is a single-wire above the chassis or other structural system forming the return. In this case the full signal spectrum is driving the single-wire as an antenna. This worst case measurement will help to characterize the enclosure environment in order to find a point of reference and specify the environment conditions. These measurements are obtained through an S_{21} measurement. Konefal *et. al.* reported that, with the loops/monopoles in positions within an enclosure, the S_{21} of the combined enclosure/loop or enclosure/monopole system can be measured on an ANA. The coupling between the loops emulates magnetic field coupling while the monopoles emulate electric field coupling.

As a precautionary measure the probe must be kept constant during each measurement scan. It should be pointed out that starting from the measurement position P2, P3 and P4, a section of the measuring cable is also exposed to radiated fields inside the enclosure, therefore there is nothing that stops the fields from illuminating the cable as well. To compensate for this, a well-screened cable with very low Z_T such as a semi-rigid coaxial must be used and ferrite chokes must be clamped over this cable. Alternatively, a super-screened cable can also be used, but for rough measurements, an arrangement of this kind is quite satisfactory. A proposed measuring matrix is given in Table 5.3.1 and 5.3.2, which describes the procedure to be followed in undertaking measurements. Note: the CUT termination is made inside the Rx box with an open circuit enhancing ***E***-field, and a short circuit enhancing ***B***-field, characteristics, respectively.

Table 5.3.1: 'Measuring Matrix' procedure for *E*-field detection.

Position of CUT from the Chassis	CUT Termination	Aperture to be Measured	Measuring Device	Instructions
1. CUT against the chassis	Open Circuit	All	***E***-field Probe	Probe discrete positions from the CUT
2. CUT 5cm from chassis	Open Circuit	All	***E***-field Probe	Probe discrete positions from the CUT

Table 5.3.2: 'Measuring Matrix' procedure for *B*-field detection.

Position of CUT from the Chassis	CUT Termination	Aperture to be Measured	Measuring Device	Instructions
1. CUT against the chassis	Short Circuit	All	***B***-field Probe	Measure applicable orientations(φ) at Discrete positions from the CUT
2. CUT 5cm from chassis	Short Circuit	All	***B***-field Probe	Measure applicable orientations(φ) at Discrete positions from the CUT

The investigation proceeds according to the proposed 'measuring matrix' by evaluating the response of the RG 316/U coaxial cable within the EMC ITS. Further measurements were taken on the radiated emissions from digital circuits and their attached transmission cables.

The SA was employed for this measurement. The SA is widely used for "quick look" testing and diagnostics. The instantaneous spectrum display is extremely valuable for confirming the frequency and nature of offending emissions as is the ability to narrow-in on a small part of the spectrum [Wil96].

The following settings, giving a noise floor of ≈ 17dBμV, were used on the SA:

- Resolution bandwidth of 3kHz.
- Frequency range between 5MHz and 200MHz.
- 601 sample points.
- Sweep time of 60seconds i.e. 1minute per scan.

The probes were connected with a low-loss cable to the input of the SA. The measurements were first conducted on a separate test-bench for preliminary tests and within the EMC ITS proposed for use in the development and pre-compliance testing. The preliminary tests were taken at discrete positions of 5cm intervals from the CUT (ribbon). For these measurements the spacing between the two IC's is maximised to avoid direct crosstalk. These are measurement points for the first harmonic (fundamental) of the10MHz digital clock.

The largest dimension of the probe is positioned parallel to the transmission cable in order to obtain the maximum induced field strength from the cable. Care was also taken, to ensure that the setup is kept away from other laboratory equipment that might produce radiation within the frequency band of interest.

5.4 Experimental Results and Discussion

The results presented in this section were obtained through S_{21} measurements for the charaterization as well as the evaluation of the EMC ITS, together with the emission measurements from a digital circuit and their attached transmission cables using a SA. From the observations, the preliminary measurements with the single-wire transmission in the frequency range up to 1GHz have shown that the resonance predicted according to equation (5.2) appears when the enclosure is completely closed. This suggests that the fields within the enclosure add destructively and constructively resulting into a standing wave pattern.

The fields tend to be distorted and absorbed by the metallic walls of the enclosure as the frequency increases. These results were consistent with all measurements, i.e. different positioning and orientation of the pickup probes. It was then observed that the resonance disappeared within the measured response with the lid taken off from the enclosure. Thus, the investigation opted to perform the measurements using the enclosure with the lid off forming a partial enclosure. The difficulty in working with a complete enclosure for this kind of measurement is that, it is strenuous and more time consuming to perform all the measurements through all apertures and the measurement positions with the lid on. For each measurement the probe must be carefully positioned and oriented in an applicable plane and be kept constant during each measurement scan. This would require screwing on/off the lid for each aperture and each measurement position. Several measurements were performed for the induced $\boldsymbol{B}$ and $\boldsymbol{E}$-field strength from various transmission links.

Near-field strength measurements of the $\boldsymbol{B}$-field characterizing the enclosure are shown in Figure 5.4.1 and 5.4.2. These measurements show that the field strength varies by ≈ 5dB to 10dB in an inverse proportion to the measured distance intervals for aperture (a), (b) and (c) in both planes. The magnitude of S_{21} coupling levels are quite high and well above the noise floor of the ANA.

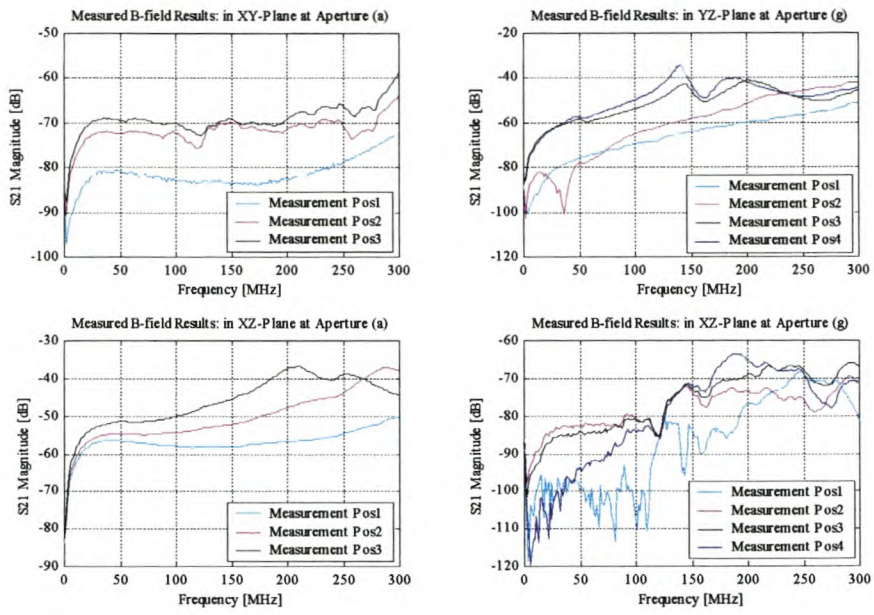

Figure 5.4.1: Measurement of induced *B*-field strength from the single-wire placed against the chassis - detected at aperture (a) and (g).

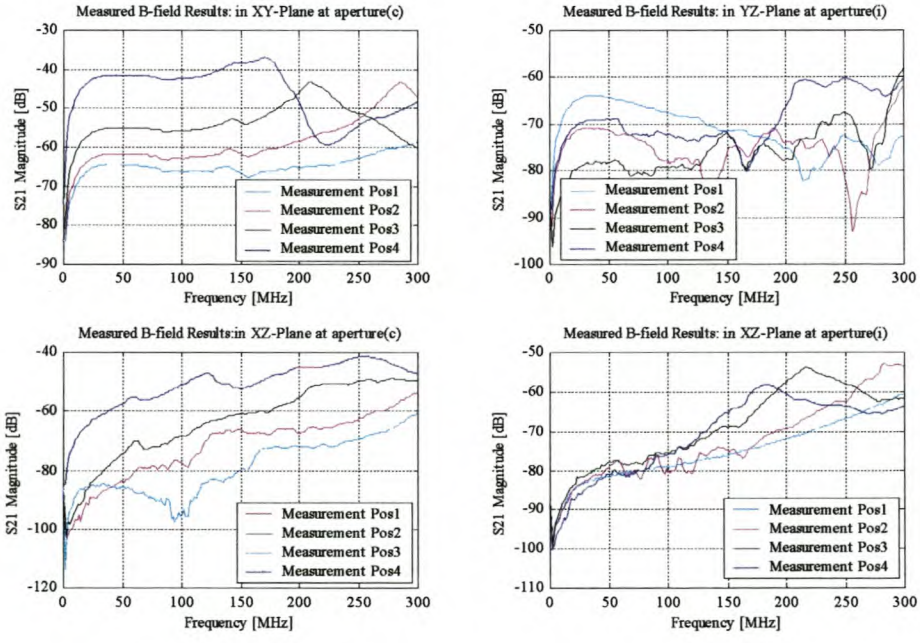

Figure 5.4.2: Measurement of induced *B*-field strength from the single-wire placed against the chassis - detected at aperture (c) and (i).

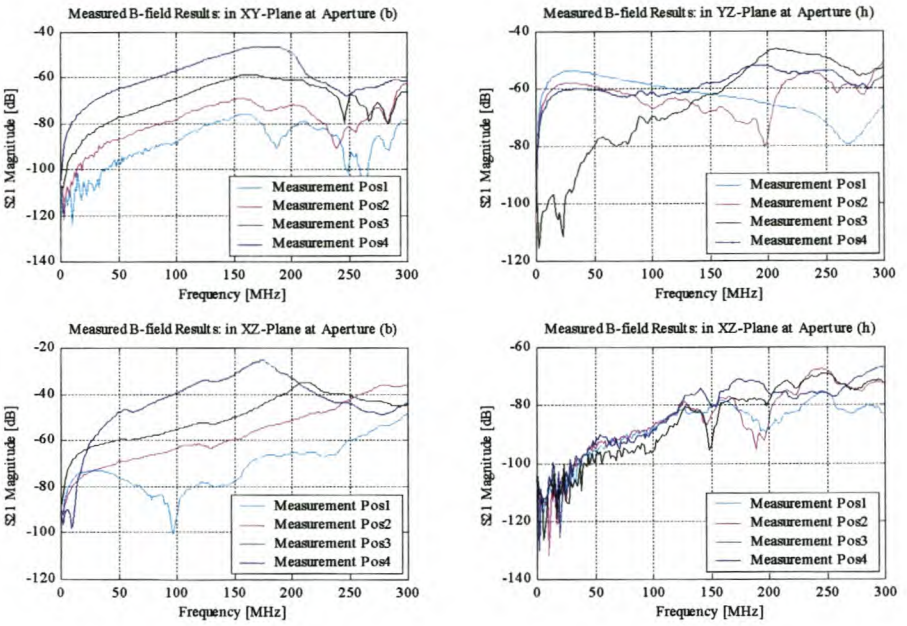

Figure 5.4.3: Measurement of induced *B*-field strength from the single-wire placed against the chassis - detected at aperture (b) and (h).

From the Figures 5.4.1, 5.4.2 and 5.4.3 the results show a noticeable maximum induced ***B***-field strength due to the middle section of the CUT as expected. This is observable for aperture (b), (c), (h) and (i). The middle section of the CUT roughly corresponds to these apertures, while for the top panel apertures it corresponds to measurement positions, P3 and P4 as you probe down the three relevant apertures. More ***B***-field measurements detected at other apertures are shown in appendix D.

The measured response at aperture (a) and (c) is flat below 200MHz for all measurement positions in the XY-plane while in the XZ-plane it increases linearly with an increase in frequency. Above 200MHz the response at aperture (a) increases whereas the response at aperture (c) decreases with an increase in frequency as the detector probe is brought closer to the CUT. But, the response at aperture (b) remains linear with an increase in frequency up to $\approx$ 200MHz in both planes and starts decreasing with increase in frequency for all four-measured positions above 200MHz. This may be due to the way

the fields are distributed within the enclosure. The induced field strength for all three apertures across the band show strong coupling levels of S_{21} measurements.

For aperture (g), (h) and (i), it can be seen that the induced field strength is noisy below 200MHz in the XZ-plane, but the magnitude increases linearly with an increase in frequency. Aperture (g) shows smooth higher induced field strength levels in the YZ-plane than (i) and (h). This gives an indication that the fields may tend to concentrate and follow the metallic wall since aperture (g) is located closer to the top panel. Along these back panel apertures, the response in both planes for each measurement position is not clearly distinguishable as in other aperture because the actual distance from the CUT does not change as one probe through these apertures. The induced field strength detected at apertures on the top panel show smooth coupling levels since the ***B***-field probe is moved parallel to the axis of the CUT. There is higher coupling in both XY and YZ-planes.

Figure 5.4.4 and 5.4.5 present measured results for the induced ***E***-field strength with the CUT placed firmly against the chassis. The ***E***-field probe is moved parallel to the CUT through aperture (d), (e) and (f). The induced ***E***-field strength response crushes the noise floor below 100MHz at ≈ ±90dB for all the measurement positions. From 100MHz to 200MHz the measured response increases linearly with an increase in frequency and above 200MHz the response is flat across the band with reasonable induced ***E***-field strength levels. The near-field response varies ≈ by ±10dB in an inverse proportion to the distance intervals for the apertures in the side and top panel.

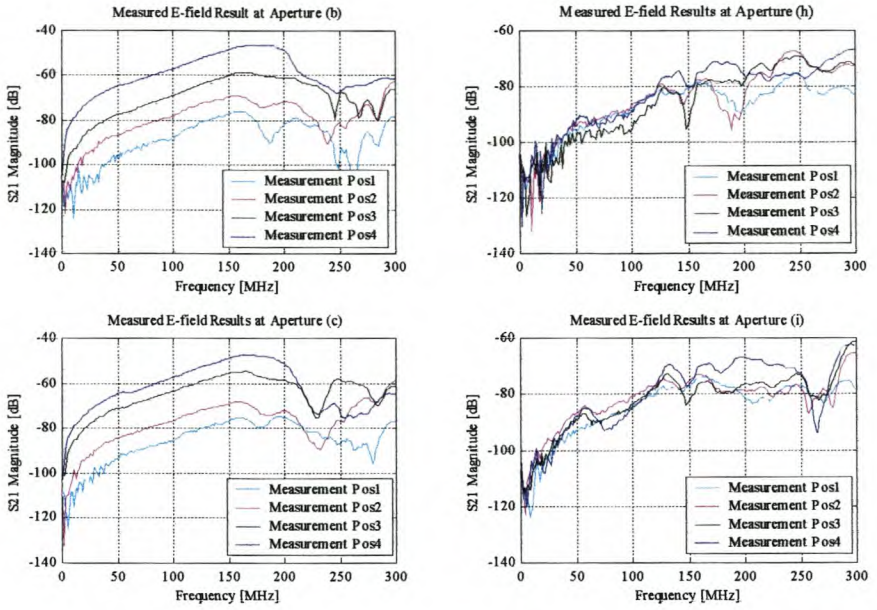

Figure 5.4.4: Measurement of induced *E*-field strength from the single-wire placed against the chassis - detected at aperture (b), (c), (h) and (i).

Comparing the magnitude pickup at each discrete measurement shows that S_{21} measurement has a higher magnitude at (d) than in (e) and (f) since aperture (d) is located closer to the CUT while (f) is located furthest.

At aperture (a), (b) and (c) the ***E***-field probe is oriented perpendicular to the CUT and the S_{21} magnitude levels above 200MHz are lower compared to the top panel apertures. Unlike aperture (d), (e), and (f) the induced ***E***-field strength response at P4 shows a linear increase from low frequencies up to ≈ –55dB above the noise floor at 175MHz. Above this frequency the response drops down to ≈ –60dB.

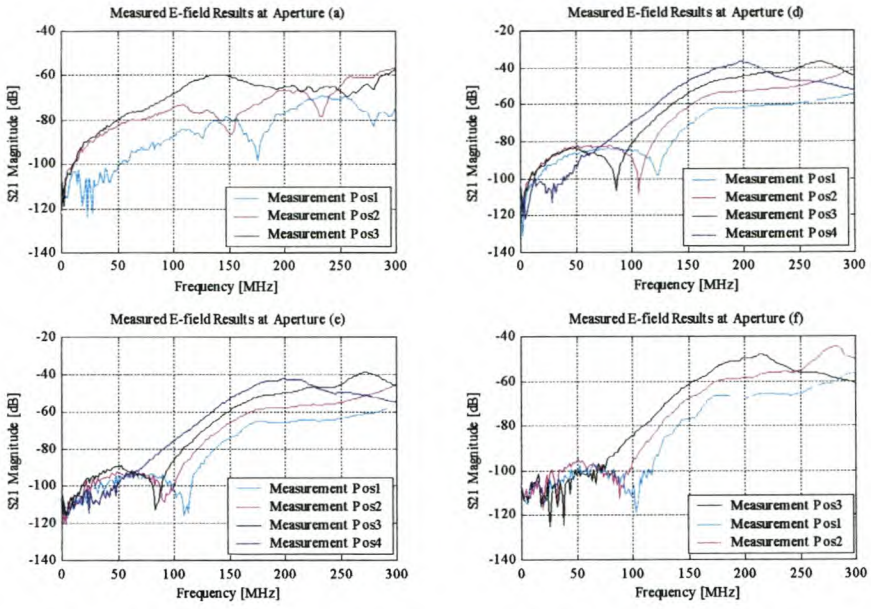

Figure 5.4.5: Measurement of induced *E*-field strength from the single-wire placed against the chassis - detected at aperture (a), (d), (e) and (f).

The induced ***E***-field strength at aperture (g) (not shown), (h) and (i) increases linearly with an increase in frequency, but also noisy below 150MHz. Above 150MHz the closest measurement position to the CUT show an S_{21} magnitude of ≈ –70dB. Through these apertures less induced ***E***-field strength was detected compared to other apertures.

The single-wire transmission was also positioned ≈ 5cm from the chassis formed by the side panel of the enclosure, implying an increase in the DM loop size (results for this are shown in appendix D). The measured applicable positions P1, P2 and P3 showed an increased S_{21} magnitude in the order of ≈ 5dB to 20dB. This suggests that DM excitation may also be effective above 30MHz, if the loop size is large. Since this is a significant change, it is advisable to keep the cables close enough to a structural reference ground or return in order to reduce the loops where the current is flowing.

A dip of ≈ 20dB can be seen for the induced ***E***-field measured response of aperture (h) and (i) with the single-wire placed ≈ 5cm from the chassis in the region from 125MHz to

200MHz. The source of the dip will be related to the modal properties of the open EMC ITS. This dip is not present in the measured results with the CUT positioned against the chassis. The measured results of this case are illustrated in appendix D. The RG 316/U, giving the worst response regarding Z_T, was chosen for tests after the charaterization of the enclosure has been completed. All the measurements depicted in Figure 5.4.6 and 5.4.7 for the induced ***B*** and ***E***-field strength, respectively, showed the following results: The measured results were all lying below the noise floor (≈ -110dB) for frequencies lower than ≈ 400MHz in both measurements.

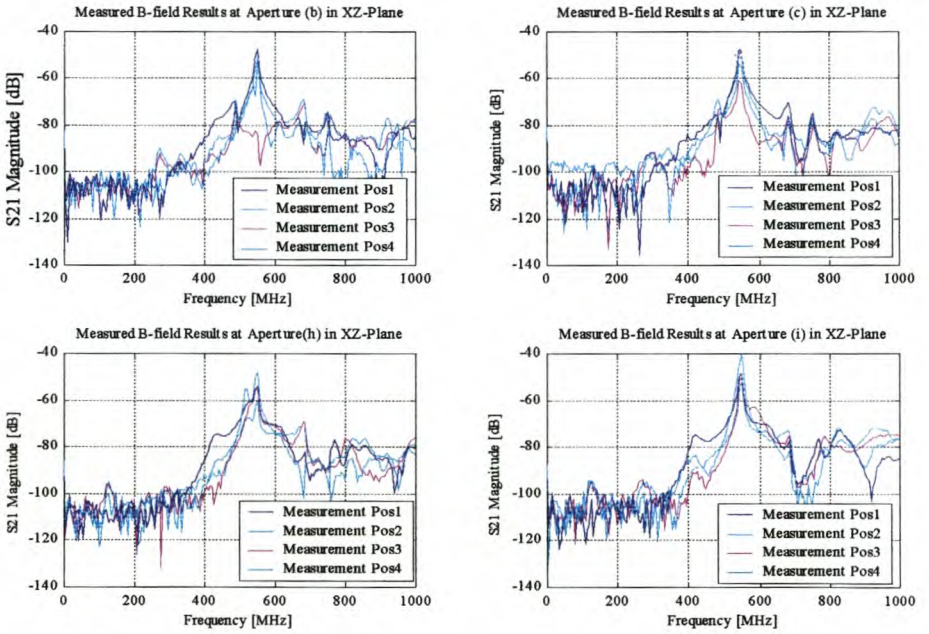

Figure 5.4.6: Measurement of induced *B*-field strength from an RG 316/U coaxial cable placed against the chassis.

The ***B***-field pickup response, then show a linear increase with an increase in frequency, from ≈ 400 – 550MHz up to ≈ -50dB while the ***E***-field pickup response also show a linear increase over the frequency band of ≈ 500 – 630MHz up to ≈ -60dB and then crushes the noise floor for frequencies above 630MHz. Thus, this suggests that the cut-off frequencies for the induced ***B***-field appear before ***E***-field strength at ≈ 400MHz and

500MHz, respectively. This becomes sensible, since the ***E***-field coupling dominates at higher frequencies.

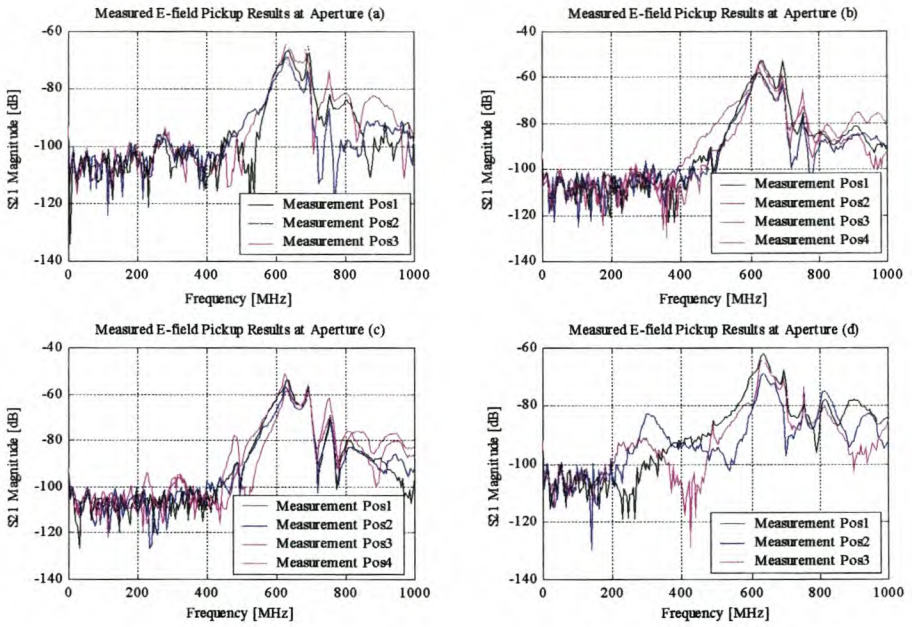

Figure 5.4.7: Measurement of induced *E*-field strength from an RG 316/U coaxial cable placed against the chassis.

The measured response in the discrete measurement positions is almost the same, since the difference between them is not greater than 3dB. This is one major feature that distinguishes the good response of coaxial cables compared to ordinary transmission wires. It can be seen that there are no offending emissions within the VHF band.

The frequency regimes where the induced ***B***-field and ***E***-field strengths are maximum, fall within the UHF band. Therefore, it can be anticipated that these fields will have an impact on other communication links operating in the frequencies between 400MHz and 630MHz. It can be highlighted that the RG 58 cables will provide the best results regarding radiated emission within the enclosure environment, since they have a lower Z_T, hence better screening properties. Both ***B***-field and ***E***-field responses show a dip that

crushes the noise floor nearly at 745MHz. From the observations, closing the enclosure shifts the observed dips (nulls). From the measured results several other findings can be drawn. Distinct peaks at 550MHz and 630MHz can be seen from the induced ***B*** and ***E***-field strength measured results, respectively. The probes relatively pickup almost the same energy in all apertures and applicable orientations. This can be attributed to firstly, the influence of reflections within the enclosure, and secondly, the dimensions of the enclosure that become comparable to the wavelength of the excitation signal above the first resonance of the enclosure.

In experiment 2, the operating clock (or fundamental) frequency of the oscillator is 10MHz and it triggers with a square-waveform, creating harmonics that are multiples of the fundamental. Figure 5.4.8 presents measured results of ***B***-field spectral content due to the coupling associated with high-speed current transients and ***E***-field spectral content due to the coupling associated with high-speed voltage transients. These are preliminary test results including those shown in Figures 5.4.9 and 5.4.10.

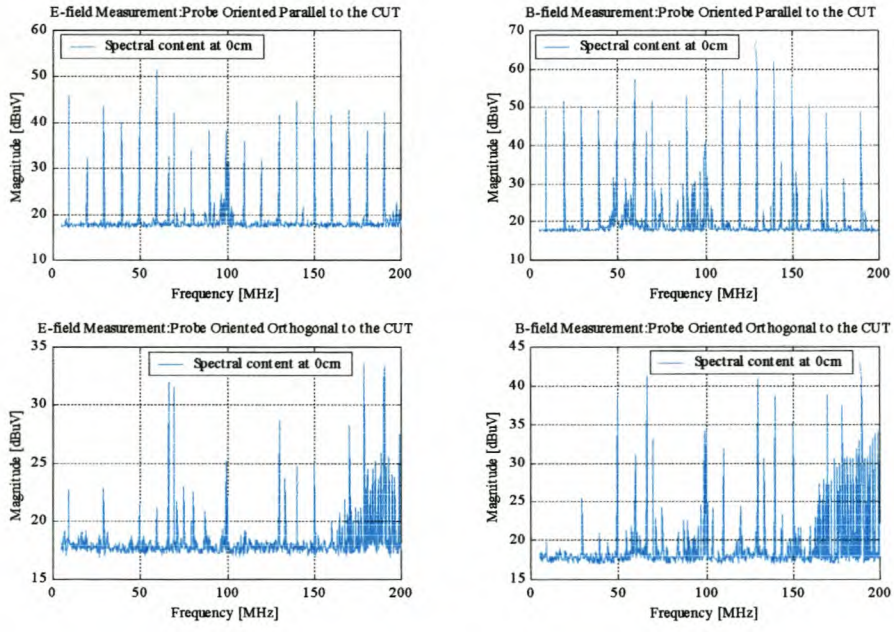

Figure 5.4.8: Spectral content of relative CM current emission detected with the *B* and *E*-field probes placed against the ribbon cable.

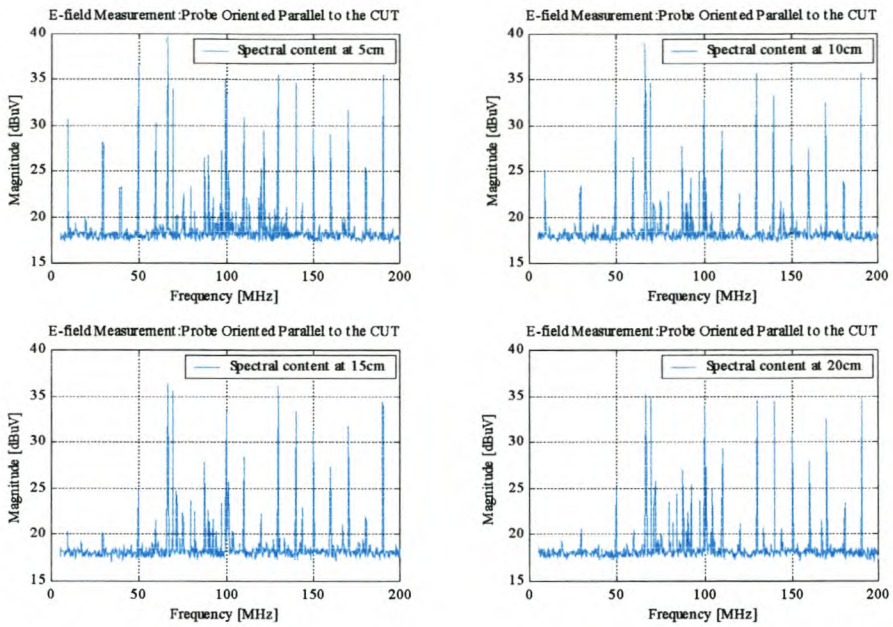

Figure 5.4.9: Spectral content of relative CM current emission detected with an *E*-field probe.

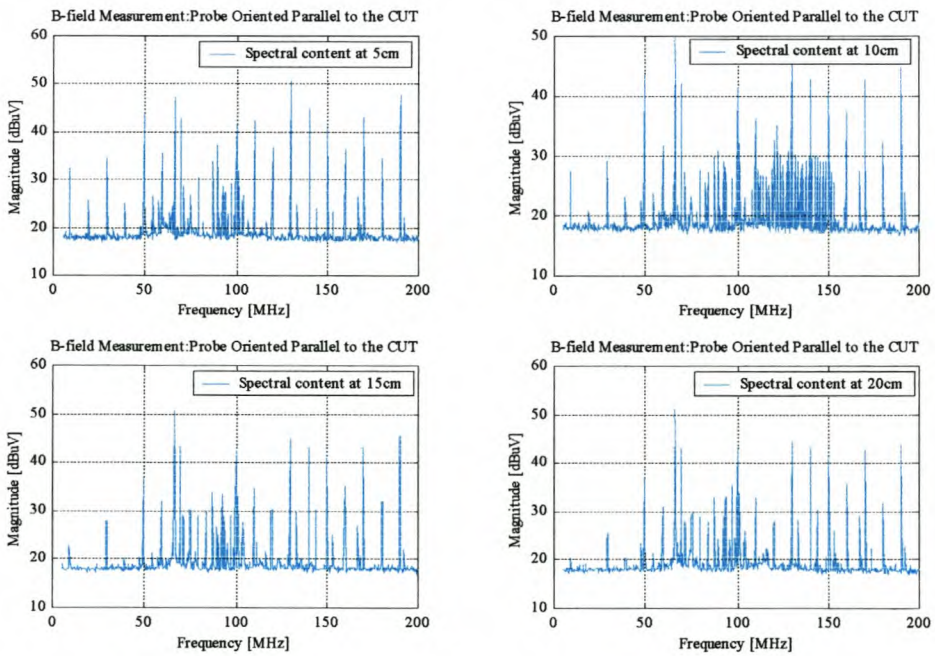

Figure 5.4.10: Spectral content of relative CM current emission detected with a *B*-field probe.

By observation it was found that the detector probes measure maximum induced field strength when placed at the mid-point of the interconnecting CUT as per the theory prediction. As the probe is moved along the axis of the CUT towards the PCB edges, the amplitude of the harmonics decreased.

The results obtained show that a maximum induced field strength is measured when the probes are placed parallel to the test cable carrying a time-varying digital signal, while a minimum induced field strength is detected when the probes are placed at right angles[3] to the CUT.

Figure 5.4.11 and 5.4.12 shows measured results for both the induced ***B*** and ***E***-field strength, respectively, for the test performed within the EMC ITS. In this test, the Tx and Rx digital circuits are electrically isolated from the CUT environment by putting them within the sub-enclosures and are grounded properly while the ribbon cable is exposed to the enclosure environment. This means that within the EMC ITS, the measured response of the induced field strength is due to cable radiated emissions only and any direct contribution from the Tx and Rx PCB's is properly screened or isolated.

From observations, the measurement of induced ***E***-field strength at apertures that are located on the top and back panel showed small harmonic peaks of ≈ 5dB to 20dB above the noise floor of the SA. In measurement positions P1, P2 and P3 the harmonic peaks of less than 6dB were detected at apertures (a), (b) and (c). This is not surprising, because the location of the probe through these apertures is further away from the CUT at (e) and (f) of measurement positions P1, P2, and P3. The ***B***-field probe at apertures (d), (e) and (f) has detected harmonic peaks of ≈ 5dB to 15dB above the noise floor in the XY-plane and nothing was detected in the YZ-plane while at aperture (g), (h) and (i) the harmonic peaks were ≈ 6dB above the noise floor. In the measurement positions P1, P2 and P3, at (g), (h), and (i) the harmonic peaks were less than 10dB.

[3] Appendix D presents results for the other preliminary test with probes placed at right angles to the ribbon cable used.

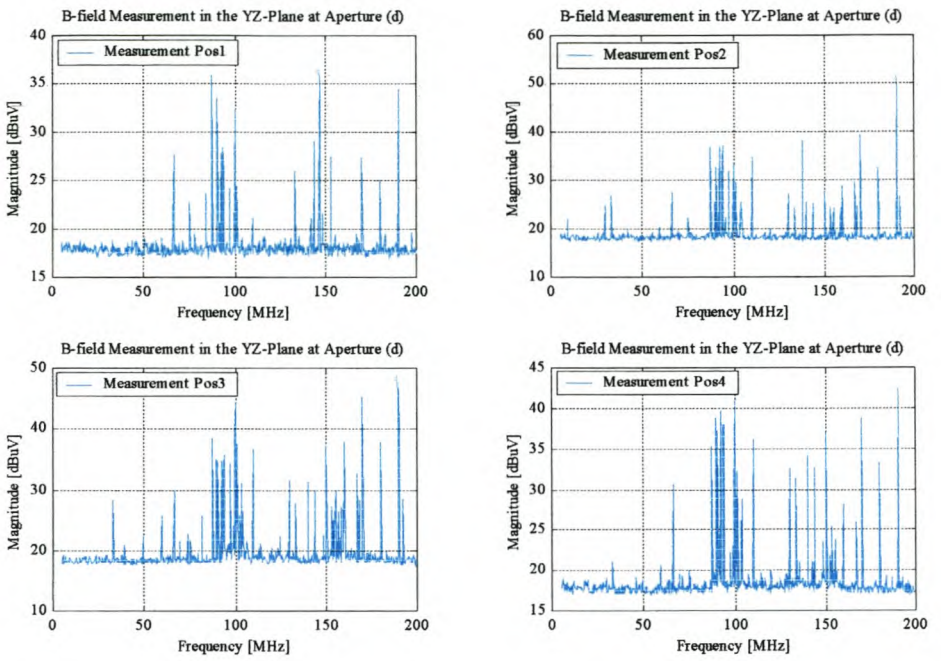

Figure 5.4.11: Spectral content response of relative CM current emissions within the EMC ITS environment: three wire ribbon.

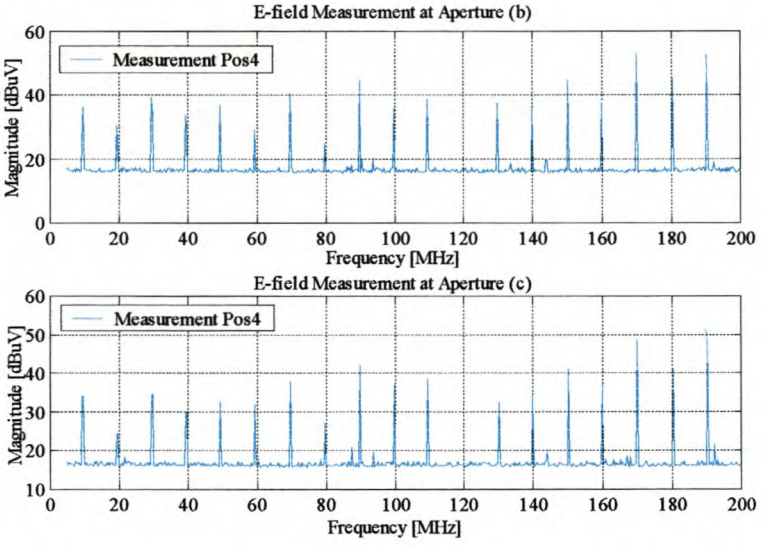

Figure 5.4.12: Spectral content response of relative CM current emissions within the EMC ITS environment - three-wire ribbon.

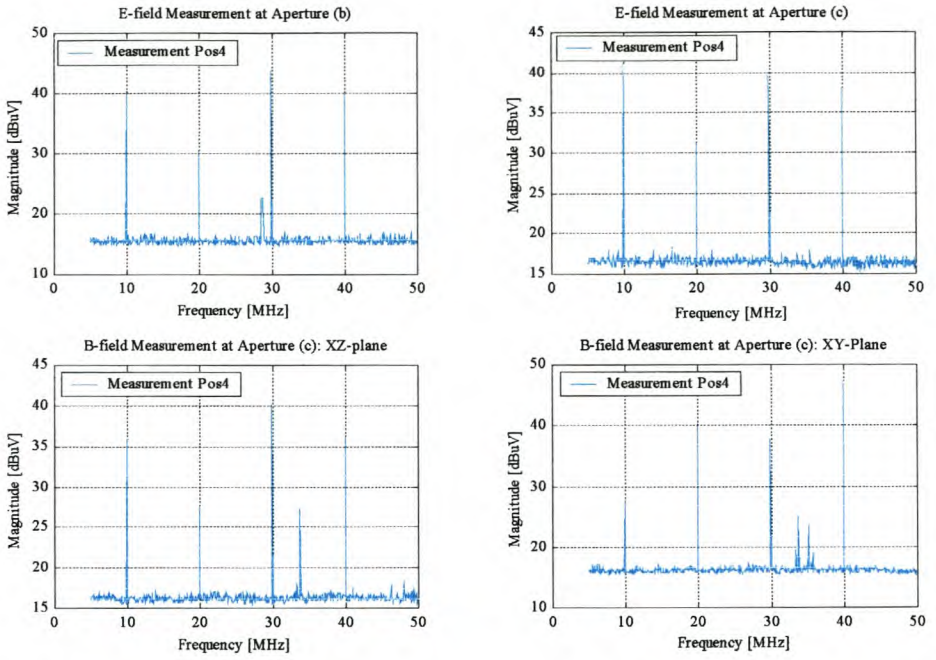

Figure 5.4.13: Spectral content response of relative CM current emissions within the EMC ITS environment – ribbon single-wire against the chassis.

The reasonable peaks shown in Figure 5.4.12 were obtained only for the measurement position 4 while at other measurement positions the induced field strength was not measurable. This gives an indication that the results obtained for the preliminary tests, is a combination of induced field strength that is generated directly from the circuits and their attached transmission cable.

Strongest harmonic amplitude levels are seen at 170MHz and 190MHz. In Figure 5.4.12 and 5.4.13, the ***E***-field measurement is compared to aperture (b) and (c) in measurement position 4. It can be seen that the magnitude of the harmonic peaks detected with no return wire exceed those with a return wire by a value ≈ between 5 to 10dB as shown in Figure 5.4.13.

The significance of the work described here forms the basis for the development of a simple, emission emulation, as well as prediction tool suitable for use early in the design

process where the coupling between major structures on PCB and transmission cables can be measured. This will permit design trade-offs and the placement of devices to be investigated. This is done to minimize EMC related problems that may occur during satellite deployment or satellite operation in orbit. Thus, causing the satellite to malfunction without fulfilling the desired mission.

Exact RFI sources on the VHF and UHF trays of a satellite system can be 'sniffed' out using a monopole probe for electrical field measurement and a small loop probe for magnetic field measurement

5.5 Concluding Remarks

The underlying theory of the EMC ITS was studied and the development of measuring techniques for internal coupling mechanisms involved was then pursued. It was learnt that radiated emission testing requires that the circuits and attached cables be set up within a controlled EM environment under its normal operating conditions. The coaxial cables showed a good EMC performance over the single-wire transmission within the EMC ITS environment. Measurements obtained were checked and found to be repeatable.

Single-wire transmission, including the one used from the ribbon above any metallic structural systems must be avoided. Acceptable levels of S_{21} and harmonic measurement will ensure that circuits and their transmission cables will co-exist in the same environment. Cables must be kept close enough to a structural reference ground or return ground in order to reduce the current loops.

The results are encouraging, though an in-depth theoretical (or mathematical) model of the EMC ITS remains a challenge. The present shortcoming with the emulation tool is the amount of time taken to perform the measurements. With the probes positioned in the axis of the cable a maximum induced field was detected, which is in line with the theory.

The demonstration on logic circuits showed that if care is not taken to keep the probe constant during measurement scans, errors might arise. The noise due to the rise and fall times of voltages and currents can have a significant disturbing effect on neighbouring circuits. Therefore, if it is practical, sensitive circuits must not be coupled to digital circuits. When the digital circuits were placed within the sub-enclosure modules, the amplitude of the harmonics reduced significantly. The measured amplitude levels of the harmonics show that the fast disturbances generated externally by the switching noise of HF digital circuits could cause currents and charges to appear on the shields of interconnecting cables and as the shields are not perfect, these external currents and charges could couple significantly to the internal signal-carrying conductor(s).

Chapter
6

Detailed Discussion of Findings & Exploration of Issues

The primary focus of the chapter is a detailed analysis of results and measurement methods. Before final conclusions can be drawn, a few issues need to be highlighted and explored.

6.1 Coupling to Transmission Cables

The transfer impedance essentially characterizes the coupling via magnetic fields whilst the coupling via the electric fields, the transfer admittance, is mostly neglected. Therefore, a reliable and sensible cable shielding performance parameter is the cable transfer impedance, Z_T. An understanding and proper identification of DM and CM loops, including their associated currents, are important for the correct description of Z_T.

From the literature, DM currents were indicated to be the desired or functional currents of the system and as such can be reliably calculated using TL models. In the case of electrically short lines, lumped-circuit models are also used. CM currents are not necessary for functional performance of the system, but will be present in practical systems. They are difficult to calculate using ideal models as indicated by [Cla92, p415].

6.2 Evaluation of the Current Probe Calibration

The current probe is a useful EMC diagnostic tool through out the design of a product. Since CM currents are difficult to calculate, they can however be measured using current probes.

Results have shown that for a measured probe transfer impedance, Z_{tt}, a $\lambda/4$-resonance effect of the test fixture and CM currents significantly influences the performance of the calibration technique applied particularly at HF. It was found important that the probe be positioned centrally around the source wire and must not be disturbed during measurements otherwise inaccuracies will arise. Parasitic effects that arise at HF are the stray capacitance that exists between the probe's metallic body and the reference plane or GP and between the probe's N-type connector and the metallic structural wall of the screened room.

For the calibration of the current probe, an ANA was used for the detection of the probe voltage in the course of determining Z_{tt}. Therefore, the load impedance at the terminals of the probe is the input impedance to the measurement device, which is usually 50Ω. Thus the calibration curve obtained for the current probe is valid only when the probe is terminated in the same impedance as was in the course of its calibration (usually 50Ω).

It can be highlighted that the models based on S and Z-parameters are able to better account for mismatched situations through the conversion procedure. The mismatch discontinuity is associated with the coaxial inputs of the test fixture and the difference between the probe's input impedance, 50Ω characteristic impedance of the feed cables and that of the source wire, which is different from 50Ω. Also, the internal losses due to the toroid and electrical length of the probe are accounted for through S_{21} and Z_{21}.

6.3 Evaluation of Z_T Measurement Methods

The results obtained from used Z_T measurement techniques showed a linear response with increase in frequency and each cable has depicted a distinct performance regarding Z_T. This parameter was shown to be transposable to parallel conductor pairs over the frequency range of interest.

More time was spent on the wire-loop antenna technique. This was caused mainly by the derivation of the de-embedding procedure. In the practical implementation of the method, it was found important to take care when constructing the 'coax braid', since the inner conductor is not completely removed but electrically isolated from the braid. One must ensure that the inner conductor does not make contact (easy to do) as this causes severe "errors". This common mistake was identified and corrected so as to obtain the final measurements.

The discrepancy in the final measured results is noticeable and may be attributed to the impedance mismatch between the wire-loop antenna and the typical 50Ω impedance of the ANA. If the input impedance of the wire-loop can be improved to match the internal impedance of the measuring equipment, better results can be obtained.

In practice cable shields are mostly grounded or open-ended at the line ends. The measured results obtained with the current-injection approach also proved that the way the cable screen terminates at the connector is critical in maintaining the screening properties of the cable. This is in line with what [Wil96] found. The coupling mechanism employed in the implementation of both test methods showed that the 'poirposing' effect and CM currents that diffuse through the cable shield give rise to a voltage drop on the interior surface of the shield. The voltage drop acts as a voltage source along the cable shield interior. A complete diffusion of current will occur for a shield thickness much less than the skin depth.

In the current-injection method, results are good but not interpretable above 70MHz due to the influence of propagation effects and resonance. The impedance variations in the inner and outer TL's must be taken into account for correct determination of the amplitude of Z_T, as also suggested by [Val97].

The basic idea behind the use of the test-jig implementation actually demonstrates a principle that is often not really understood to be one of the proper ways of solving EMC problems associated with CM currents. The use of jigs demonstrates a way of diverting CM currents on cables before they enter or leave the equipment. This exploration is observable since the jigs have L-shaped upright terminating plates, which divert the injected CM current away from the feed and measuring cables to be within the desired CM path only. This reduces test-jig effects and CM currents from influencing the actual measurement of Z_T.

6.4 Findings on the EMC ITS

In the near-field or induction zone, the fields are strongly dependent on distance. Any move in measurements at positions P1, P2, P3 and P4 toward or away from the radiating source causes a drastic change in the received fields. An increase in cable height above a structural metallic ground results in an increased radiated field. Therefore, current loop sizes should be reduced to give less radiated field. The use of ferrite chokes was necessary in all measurements to limit the CM currents on the measuring cable.

Shielded cables may seem to be the obvious barrier to radiated RFI but application may not be so easy. Putting in shielded cables at the last minute may give disappointing results. The measured results of the RG 316/U suggested that any cable would not necessarily eliminate interference across the entire band. The results up to 1GHz are affected by the reflections within the enclosure and CUT configuration.

Contamination of external cables by internal HF digital circuits was investigated. Cables were found to carry HF harmonics that are not at all part of the desired signal. The ribbon cable carried the10MHz harmonics from the operating clock and their spectrum extends easily to 200MHz. For measurement repeatability, it is important to take into account that the digital signal is time-varying, and that the SA is sweeping the frequency spectrum over a finite time length. When the SA displays the results, it is advisable to always confirm that you get the same results with a lower sweep speed. If the measured results are the same, then the original sweep speed is fine. The EMI receiver takes this into account by dwelling at each frequency according to a CISPR recommendation.

Following the evaluation of various classes of cables within the EMC ITS environment; protocols for the choice of cables could be recommended. Such a document has been published by the International Space Station [ISS]. The work in the EMC ITS has not been sufficiently comprehensive to complete a full protocol recommendation. This could form the basis of future work.

The main deductions made from the EMC ITS evaluation are as follows:

- It is advisable to keep the cables close enough to a structural reference ground or return ground in order to reduce the loops where the current is flowing.
- The difference in the measured response for discrete measurement positions with the CUT being a coaxial cable is negligible small. This is in contrast to when the CUT is a single-wire transmission, where the results show changes of up to approximately 20dB. It can be seen that there are no offending emissions within the VHF band.
- Single-wire transmission cable above any metallic structural systems must be avoided; these were the worst results seen in the previous chapter.

6.5 Concluding Remarks

The literature suggests a sensible evaluation of cable shielding that can be obtained through the measurement of Z_T. The S to Z-parameter modelling in the HF range has been introduced. The availability of this model may be useful during the early design stage to help the designer in predicting the behaviour of the device-under-test. Braid pattern of coaxial cables results in less shielding with an increase in frequency.

Measurements have shown that interference can never be prevented across the band. Current loop sizes must be minimized in order to give less radiation. The time-varying digital signals generate harmonics that can extend to 200MHz and could be detrimental to sensitive devices within close proximity of these circuits.

Chapter 7

Conclusions and Recommendations

The objective of this thesis was to investigate theoretical and metrological techniques that will be used in developing EMC cabling protocols for electronic systems, in particular satellite systems. Measurement test fixtures were designed for the experimental determination of transfer impedance for current probes which are useful in assessing the net CM currents on transmission cables interconnecting modules and the cable transfer impedance of coaxial and parallel conductors. The study also involved a construction of a satellite system hardware emulator for the purposes of obtaining valuable information regarding induced near-field strength and harmonics generated by digital circuits, by means of measurements.

7.1 Conclusions

The cable transfer impedance is a convenient way of characterizing the merit of cable shields as proposed by [Tsa95]. It relates the CM currents flowing on the cable shield's outer surface to the DM voltage developed at the other side of this surface, i.e. between the shield's inner surface and the internal conductor. In the frequency range of interest used, this voltage was due mainly to the diffusion process of CM current through the shield thickness and 'porpoising' effects. Cable transfer impedance is a reciprocal cable parameter as it applies to emission and susceptibility. It can be accurately determined if effects such as CM currents and capacitive coupling are carefully avoided or charaterized

in the test-system. The effects of test-jigs must clearly be distinguished from measured results.

A calibration of a current probe from 300kHz to 1GHz using network analysis techniques was performed successfully. This approach permits the probe's transfer impedance to be corrected for mismatch effects associated with the coaxial input of the calibration fixture and impedance variation from a 50Ω feed cable to a source wire. The applicability of the proposed measurement technique depends on both the frequency range of interest and the detailed geometry of the measurement calibration fixture. Reproducible and sensible measured results for validation were obtained up to 600MHz. At HF care must be taken in positioning the current probe properly, as well as identifying and isolating the influence of parasitic effects from contaminating the desired measurements.

Methods to recover the cable transfer impedance of shielded and unshielded cables were introduced. The current-injection technique is versatile compared to the present wire-loop and other methods, as any type of cable, as well as scalar or vector network analyzer can be employed. The upper frequency limit of the current-injection and wire-loop approach is 80MHz and 50MHz, respectively. This is determined by the factors inherent in each measuring system. Both techniques are economical and straightforward to analyze. Usable results were obtained with a 0.5m cable length between 300kHz and 80MHz for the current-injection method. Satisfactory accuracy and reliability of results was found below 50MHz for the wire-loop approach.

From the measurements it can be deduced that a coaxial cable braid pattern results in less shielding with an increase in frequency. The RG 58A/U coaxial cable depicted lower values of Z_T compared to other cables used. Low values of Z_T imply that the cable has a good performance and therefore it will have a higher degree of maintaining signal integrity in information carrying cables. Thus, cable transfer impedance is a practical tool for shielding performance evaluation and testing of cable philosophy and its result is usable in classifying cables for verification and signal usage.

Considerable attention was given to theoretical and experimental proposals for the measurement techniques to assist electronic integration engineers in the satellite research and development to cope with EMC requirements. Measurements done in the EMC ITS have shown that it is important to ground coaxial cable connections properly on both ends and they must be kept close to the GP or chassis when used to connect different modules. This is in line with [Mil98] and allows the intentional signal to return via a desired path.

The coaxial cables showed a better EMC performance over the single transmission wires within the EMC ITS environment for frequencies below the first resonance (≈ 470MHz) of the enclosure. This suggest that, if the cabling layout protocol is good, the transmission cable(s) interconnecting sub-systems will give less radiated fields. These measurements were consistent with all measured positions and orientations of the probes.

The rapid disturbances produced externally by the switching noise of HF digital circuits could cause currents and charges to appear on the shields of interconnecting cables and, as shields are not perfect, these external currents and charges could couple significantly to the internal signal-carrying conductor(s) and corrupt data. Results have demonstrated that the 10MHz operating clock harmonics can easily extent up to 200MHz. Thus, the source of radiation in logic circuits is the operating clock and its harmonics. A significant reduction in emission levels was observable when the 'sniffer' probes were positioned in an orthogonal direction to the ribbon cable. The EMC ITS has set a point of departure for the investigations of an early design analysis of internal field coupling mechanisms, i.e. near-fields can be measured to see if they are within acceptable levels.

7.2 Recommendations and Future Work

It was shown that the transfer impedance of current probes could be determined with the employment of a low cost test fixture. Test measurement of the net CM currents on all peripheral cables of a design, or a prototype of the design, can be performed in the development laboratory using a current probe with known transfer impedance in conjunction with a SA. It is a simple method for determining whether a particular peripheral cable will create serious radiated emission problems. Therefore, it will be used to determine whether an anticipated "fix" such as adding a ferrite bead, choke, etc, on a peripheral cable to reduce the CM currents has, in fact, reduced the CM current. Transmission cable's CM current can be measured simply with the probe before and after the implementation of the "fix".

For the achievement of EMC, transmission cables and connectors must be carefully specified. Test-jigs must be designed to keep the test-system stable, regarding the distribution of current on the CUT shield. The CUT shield, or a return conductor in unshielded cables, should form a two wire TL over the GP so that the EM environment is well defined. The idea behind L-shaped plates that are similar to the upright terminating plates of the jig can serve as a useful application. In principle, they can be placed as barriers if suitable for the environment and route currents such that incoming disturbance current is diverted before entering the circuit and outgoing disturbance current is diverted before it leaves the circuit. Also, ferrite chokes can be clamped over the cables interconnecting circuits at the entry or exit interface points to absorb these disturbance currents. This is in line with what [Wil96] found.

The information on measured cable transfer impedance suggests the importance of cable choice and connections in electronic systems. A common cabling protocol that is usually followed, is to group cables in a harness. This can be facilitated by the knowledge of the cable transfer impedance data of various cables. Cables of different categories regarding Z_T must never be in the same harness, e.g. a cable that has a very high Z_T, thus carry HF

interfering currents, must not be grouped together with cables that transport low speed signals for audio, video, etc. Specifically in devising the interconnection links between the RAM trays and cameras of a satellite. The selection of appropriate cables and connectors according to the cable property Z_T will provide TL data-links with a high level of shielding against interference. Thus, the use of low Z_T cables in a design is recommended. The optical link can be chosen, if affordable, for a harsh environment or to transfer HF signals since they can neither emit nor pick up EM fields.

High-speed digital circuits and their attached cables should be placed far away from any sensitive devices. If the proximity between sub-systems allows it, the attached cables can be positioned at right angles to the sensitive device receiving the interfering signals. This will reduce crosstalk between the sensitive device and the cable carrying a high-speed signal. Reduction in the current loop size is also useful in giving less radiated fields in the proximity of sensitive devices. The application of a single wire transmission next to the chassis or other structural ground reference must be avoided, as proposed by [Mar01].

The wire-loop and current-injection methods call for further investigation regarding their upper frequency limits. An improved bandwidth for each method will contribute significantly to cable verification and evaluation. The de-embedding procedure of the wire-loop approach requires an in-depth analysis as to finding the source of error causing it not to work satisfactorily.

The EMC ITS serves as a starting point for other experimental techniques that can be developed further to evaluate the performance of electronic systems before hand, and to avoid expensive re-designs after prototyping. New improvements on the EMC ITS can be taken to a greater extend of giving a description model to derive coupling parameters for a PCB. This can then be used in a large-scale system (enclosure and cables), of which the PCB is a part, to theoretically predict the CM emissions. A software prediction tool such as Feko can be used to model certain radiating cables or PCBs represented by a loop or monopole antenna within the EMC ITS.

References

[Atk84] D.M. Atkinson, "A Current Transformer Method for the Surface Transfer Impedance Measurement of Braided Coaxial Cables", *Project Report*, Department of Electronic and Electrical Engineering, University of Sheffield, United Kingdom, 1984.
http://www.eng.dmu.ac.uk/aeg/alyse/Intro_to_C_P_Method.html

[Bel99] M. Bemmelmans, Issues and Sensors in EMC, Project Report for the Ir – degree, Eindhoven University of Technology and University of Stellenbosch, Stellenbosch, Republic of South Africa, 1999.

[Ben97] T.M. Benson, A.P. Duffy and C.F. Cheng, "Assessing the Performance of a Current Probe Based Method for Determining Surface Transfer Impedance", *IEE 10th International Conference on Electromagn. Compat.*, Conference Publication NO. 455, September 1997, pp. 137-141.

[Ben96] T.M. Benson and C.F. Cheng, "Rapid Method for Measurement of Cable Surface Transfer Impedance", *Microwave and Optical Technology Letters*, vol. 12, NO. 4, July 1996, pp. 187-189.

[Cer01] G. Cerri, R. De Leo, and V. Mariani Primiani, "A High Frequency Model of Current Probes for Injection Purposes", *14th European Zurich Conference on Electromagn. Compat.*, Dipartimento di Electronica and Automatica, Università di Ancona, Italy, March 2001.

[Che95] C.F. Cheng, "To Develop Simple Methods to Measure Surface Transfer Impedance, Z_T", *Project Report*, Department of Electrical and Electronic Engineering, University of Nottingham, United Kingdom, 1995. *http://www.eng.dmu.ac.uk/aeg/alyse/Intro_to_C_P_Method.html*

[Cla92] Clayton R. Paul, Introduction to Electromagnetic Compatibility, John Wiley & Sons, Inc., New York, 1992.

[Clo99] J.H. Cloete, Engineering Electromagnetics for Postgraduate Diploma in Satellite Communications Engineering, Course Notes, University of Stellenbosch, Stellenbosch, Republic of South Africa, 1999.

[Coa96] A.R. Coates, "The Development of a Simple Method for the Evaluation of the Surface Transfer Impedance of Coaxial Cables", Project Report, Department of Electrical and Electronic Engineering, University of Nottingham, United Kingdom, 1996. *http://www.eng.dmu.ac.uk/aeg/alyse/Convolutional_Methods_for_Measuring_Z_t_and_SE.html*

[Deu93] A.P.J. van Deursen, Electromagnetic Compatibility. Part 5, Installation and Mitigation Guidelines. Section 3, Cabling and Wiring, Research Report, Eindhoven University of Technology, Eindhoven, Netherlands, July 1993.

[Fou98] A.P.C. Fourie, O. Givati and A.R. Clark, "Simple Technique for the Measurement of the Transfer Impedance of Variable Length Coaxial Interconnecting Leads", *IEEE Trans. Electrmagn. Compat.*, vol. 40, NO. 2, May 1998, pp. 163-166.

[Hau89] Hermann A. Haus and James R. Melcher, Electromagnetic Fields and Energy, Prentice-Hall, Inc, Mexico, 1989, pp. 1-3 and 71.

[Hel95] M.J.A.M. van Helvoort, Grounding Structures for the EMC-Protection of Cabling and Wiring, Ph.D. Thesis, Eindhoven University of Technology, Eindhoven, Netherlands, 1995.

[Hor98] Frank B.M. van Horck, Electromagnetic Compatibility and Printed Circuit Boards, Ph.D. Thesis, Eindhoven University of Technology, Nertherlands, 1998.

[IEC] IEC document 50(161), "IEC: Electromagnetic Compatibility" specification series, over-printed in South Africa by the South African Bureau of Standards as the SABS IEC 61000 series.

[ISS] International Space Station, "Space Station Cable/Wire Design and Control Requirements for Electromagnetic Compatibility", SSP 30242 Revision D, 3 April 1996.

[Kle93] Thomas Kley, "Optimized Single-Braided Cable Shields", *IEEE Trans. Electrmagn. Compat.*, vol. 35, NO. 1, February 1993, pp. 1-9.

[Kle93] Thomas Kley, "Measuring the Coupling Parameters of Shielded Cables", *IEEE Trans. Electrmagn. Compat.*, vol. 35, NO. 1, February 1993, pp. 10-20.

[Kle93] Thomas Kley, "Electromagnetic Coupling to and from Shielded Cables – Optimizing Factors", *IEEE Trans. Electrmagn. Compat.*, vol. 34, NO. 1, February 1993, pp. 39-46.

[Kon99] T. Konefal, J.F. Dawson, A. Denton, T.M. Benson, C. Christopoulos, A.C. Marvin, S.J. Porter and D.W.P. Thomas, "Electromagnetic Field Predictions Inside Screened Enclosures Containing Radiators", *IEE International Conference on Electromagn. Compat.,* Conference Publication NO. 464, EMC York, 1999, pp. 95-100.

[Laa98] P.C.T. van der Laan and A.P.J. van Deursen, "Reliable Protection of Electronics Against Lightning: Some Practical Applications", *IEEE Trans. Electrmagn. Compat.*, vol. 40, NO. 4, November 1998, pp. 513-520.

[Mar01] Michel Mardiguian, Controlling Radiated Emissions by Design, Second Edition, Kluwer Academic Publishers, Inc., Boston, 2001, p. 33.

[Mar98] Johan B. Maree, An Electromagnetic Compatibility Philosophy and Appropriate Techniques – A Low Cost Approach, Masters Thesis, University of Stellenbosch, Stellenbosch, Republic of South Africa, 1998.

[Mil98] Garth W. Milne, "Ground Voltage and Current Cancellation by Co-axial Cable", *COMSIG Proceedings,* September 1998, pp. 327 – 332.

[Mil98] Garth W. Milne, E. Jansen, Jacques J. Roux, Jan-Albert Koekemoer and Pieter P.A. Kotzé, "EMC and RFI Problems and Solutions on the SUNSAT Micro-satellite", *COMSIG Proceedings,* September 1998, pp. 293–298.

[Mil93] Garth W. Milne, P.J. Bakkes, A Schoonwinkel, J.J. du Plessis, J.H.R. Enslin, W.H. Steyn, S. Mostert, K. D. Palmer and D.M. Weber, "SUNSAT, Stellenbosch University and SA-AMSAT's Remote Sensing and Packet Communications Microsatellite", *Proceedings of the Conference on Small Satellites* NO.7. Utah, USA, September 1993, pp.1-20.

[Mor97] A. Morriello, T.M. Benson, A.P. Duffy, and C.F. Cheng, "Surface Transfer Impedance Measurement: A Comparison Between Current Probe and Pull-On Braid Methods for Coaxial Cables", *IEEE Trans. Electrmagn. Compat.*, vol. 40, NO.1, February 1998, pp. 69-76.

[Oly99] F. Olyslager, E. Laermans, D. De Zutter, S. Criel, R. De Smedt, N. Lietaert, and A. De Clercq, "Numerical and Experimental Study of the Shielding Effectiveness of a Metallic Enclosure", *IEEE Trans. Electrmagn. Compat.*, vol. 41, NO.3, August 1999, pp. 202-213.

[Poz98] David M. Pozar, Microwave Engineering, Second Edition, John Wiley & Sons, Inc., New York, 1998, p. 187-199.

[Ram94] Simon Ramo, John R. Whinnery and Theodore Van Duzer, Fields and Waves in Communication Electronics, John Wiley & Sons, Inc., New York, 1994, pp. 171-175.

[Rüt99] M. Rütschlin and H.C. Reader, "Thoughts on Transfer Impedance", *Internal Report*, University of Stellenbosch, Stellenbosch, Republic of South Africa, 1999.

[Tes97] Frederick M. Tesche, Michel V. Ianoz and Torbjörn Karlsson, EMC Analysis Methods and Computational Models, John Wiley & Sons, Inc., New York, 1997.

[Tsa95] Anatoly Tsaliovich, Cable Shielding for Electromagnetic Compatibility, Van Nostrand Reinhold, Inc., New York, 1995, pp. 131-143.

[Val97] B. Vanlandschoot and L. Martens, "New Method for Measuring Transfer Impedance and Transfer Admittance of Shields Using a Trixial Cell", *IEEE Trans. Electrmagn. Compat.*, vol. 39, NO.2, May 1997, pp. 180-185.

[Van78] Edward F. Vance, Coupling to Shielded Cables, John Wiley & Sons, Inc., New York, 1978, pp. 130-138.

[Wal99] Craig Walliser, "EMC in the Control Environment", *Elektron Journal of the SAIEE*, Adroit Technologies, 1999, pp. 41-42.

[Wil96] Tim Williams, EMC for Product Designers, Second Edition, Newnes, Butterworth-Heinemann, Inc., Oxford, 1996, pp. 143-148 and 208.

Appendix A

A Flow Diagram for Evaluating Cable Shielding

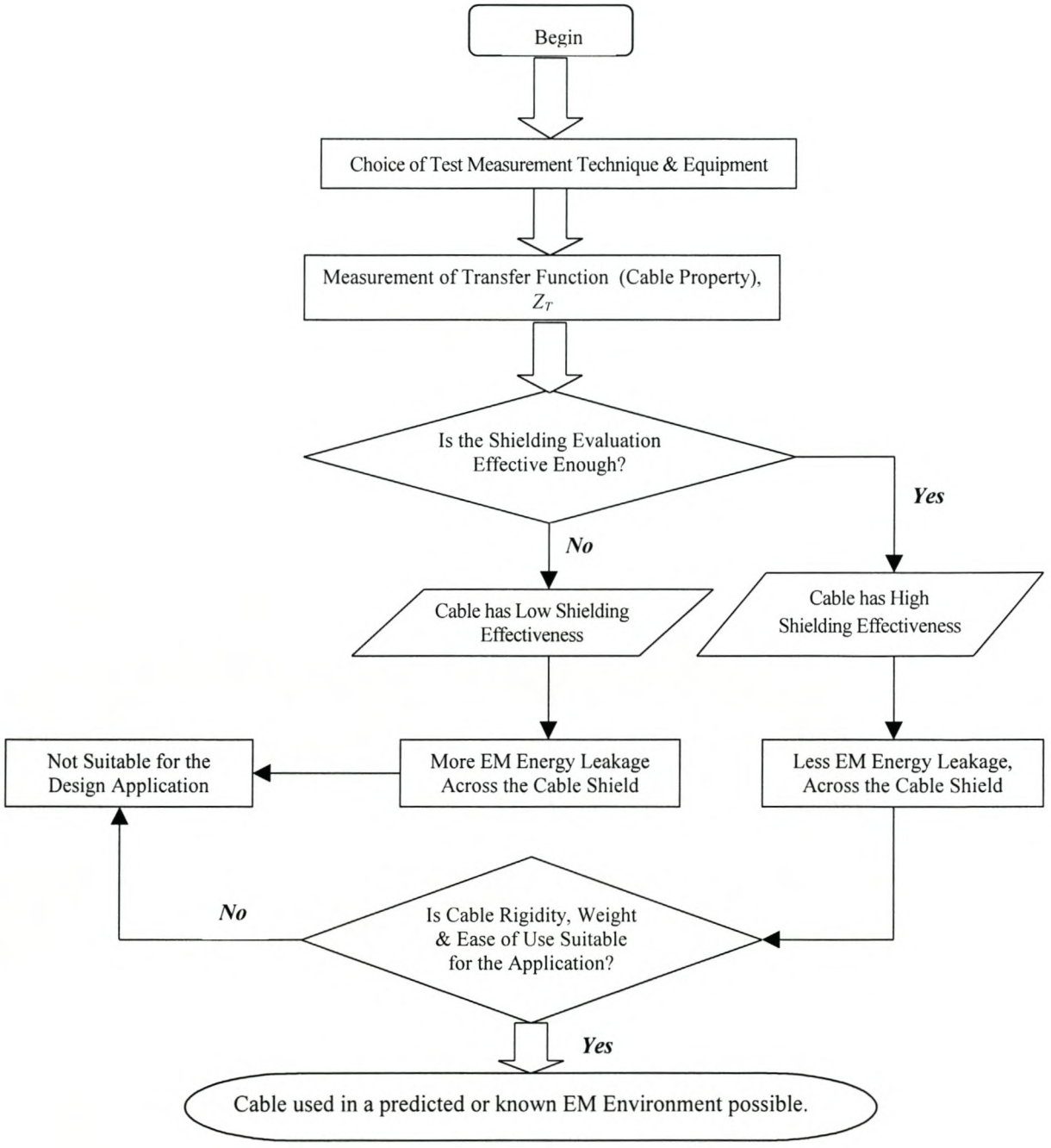

Appendix

B

Technical Specifications & Description of the EMCO[2] Probe

B.1 Technical Specifications

At lower frequencies, the input signal's current level can be no greater than the specified maximum power current. When both signal and power currents are high, their sum should not exceed the limits given.

Table B.1: Physical and electrical specifications for the Inductive Current Clamp.

ELECTRICAL		PHYSICAL	
Frequency Range (L-Model 20Hz)	1-1000 MHz	Window Size	1.25" diameter
Transfer Impedance	1-10 Ω (+/-2.0 dB)	Assembled Dimensions	3.5" long, 1.4" thick
RF Current Range (RF CW)	20.0 Amps	Weight	15 oz.
RF Current Range (Pulse)	50 Amps for duty cycle less than 0.4	Output Connector	Type N
Maximum Power Current (DC-400Hz)	200 Amps		
Maximum Power Voltage	No limitation, subject to adequate conductor insulation		
Internal Loading	No		
Rated Output Load Impedance	50 Ω		
Sensitivity Under Rated Load	0.2 microamperes with one microvolt sensitivity receiver and 5 Ω transfer impedance		

[2] For more information about the probe, refer to the Equipment Manual, EMCO Model 94111 Series Current Probe, EMC Test Systems, Texas, 1997.

Great care must be taken to prevent the uninsulated current probe connector and cable connectors coming in contact with the GP or other nearby conductors. This will prohibit possible measurement errors due to ground loops, and will avoid danger from high voltages.

Table B.1 gives the physical and electrical specifications for the inductive current clamp as supplied by the manufacturer and must be clearly understood before a test-technique is planned and undertaken.

B.2 General Description of the Current Probe

EMCO [EMCO, 97], the 94111 series current probe manufacturer, has reported that the EMC test system's RF current probe is a clamp-on RF current transformer. It is designed for use with EMI test receivers such as spectrum or network analyzers, or with any similar instruments having 50Ω input impedances. The 94111 series current probe is simply clamped around the test conductor, which then becomes a one-turn primary winding of a current transformer. Measurements can be made on single or multi-conductor cables, grounding and bonding straps, outer conductors of shielding conduits, coaxial cables, etc.

Appendix

C

Listings of Matlab Routines

C.1 Determining Z_{tt} from Measured S-parameters

```
%%%%%%%%%%%%%%%%%%%%%%%%%%%%%%%%%%%%%%%%%%%%%%%%%%%%%%%%%%%%%%%%%%%%%%%%
%*    Determination of Ztt from Measured S-parameters                  %
%*    This Program Computes the Transducer Factor, Ztt of a Current Clamp  %
%*    Frequency ranges: 300kHz-200MHz and 300kHz-1GHz                  %

clear all;
cd c:\MEPrject\Chapt3\new
%                 Reflection & Transmission Coefficients              %
% Loading Raw-Data                                                    %
      load AS11.txt
      load AS21.txt
      load AS12.txt
      load AS22.txt
      as11 = AS11(1:51,1) + i*AS11(1:51,2);
      as21 = AS21(1:51,1) + i*AS21(1:51,2);
      as12 = AS12(1:51,1) + i*AS12(1:51,2);
      as22 = AS22(1:51,1) + i*AS22(1:51,2);
      load npldons11.txt;    % lid on
      load npldoffs11.txt;   % lid off

% Measurements Outside the Screened Room                              %
      load wpnps11.txt % s11 response with probe not present.
      load BS11.txt
      load BS21.txt
      load BS12.txt
      load BS22.txt
      npldons11 = npldons11(1:51,1) + i*npldons11(1:51,2);
      npldoffs11 = npldoffs11(1:51,1) + i*npldoffs11(1:51,2);
```

```
nps11 = wpnps11(1:51,1) + i*wpnps11(1:51,2);
bs11 = BS11(1:51,1) + i*BS11(1:51,2);
bs21 = BS21(1:51,1) + i*BS21(1:51,2);
bs12 = BS12(1:51,1) + i*BS12(1:51,2);
bs22 = BS22(1:51,1) + i*BS22(1:51,2);

% Addition of Ferrites Chokes:
load BfcS11.txt
load BfcS21.txt
load BfcS12.txt
load BfcS22.txt
cs11 = BfcS11(1:51,1) + i*BfcS11(1:51,2);
cs21 = BfcS21(1:51,1) + i*BfcS21(1:51,2);
cs12 = BfcS12(1:51,1) + i*BfcS12(1:51,2);
cs22 = BfcS22(1:51,1) + i*BfcS22(1:51,2);

%-----------------------------------------------------------------------------------------------------%

%                    Conversion from S to Z Parameters                    %

% S to Z conversion procedure using a matrix

Zo = 50; % Matched finite termination
U = [1 0;0 1];

for X = 1:51
  S = [as11(X) as12(X);as21(X) as22(X)];
  Z = inv(U - S)*(U + S);
  aZ11(X,1) = Zo*Z(1,1);
  aZ12(X,1) = Zo*Z(1,2);
  aZ21(X,1) = Zo*Z(2,1);
  aZ22(X,1) = Zo*Z(2,2);
end

for X = 1:51
  S = [bs11(X) bs12(X);bs21(X) bs22(X)];
  Z = inv(U - S)*(U + S);
  bZ11(X,1) = Zo*Z(1,1);
  bZ12(X,1) = Zo*Z(1,2);
  bZ21(X,1) = Zo*Z(2,1);
  bZ22(X,1) = Zo*Z(2,2);
end


% Test with Addition of Ferrite Chokes
```

```
for X = 1:51
  S = [cs11(X) cs12(X);cs21(X) cs22(X)];
  Z = inv(U - S)*(U + S);
  bfZ11(X,1) = Zo*Z(1,1);
  bfZ12(X,1) = Zo*Z(1,2);
  bfZ21(X,1) = Zo*Z(2,1);
  bfZ22(X,1) = Zo*Z(2,2);
end
```

% EMCO Current Probe Transducer Factor from 0.3MHz to 1000MHz:

Z_{tt} = [0.300000,0.5047773
0.400000,0.6114288
0.500000,0.7002804
0.600000,0.7764071
0.700000,0.8433412
0.800000,0.9033793
0.900000,0.9577489
1,0.9964087
2,1.3613117
3,1.5985767
4,1.7750313
5,1.9134753
6,2.0257402
7,2.1198730
8,2.2040155
9,2.2818236
10,2.3552307
20,2.8924347
30,3.2164458
40,3.4867042
50,3.7370590
60,3.9790490
70,4.1799193
80,4.2940558
90,4.3118313
100,4.3026890
110,4.3294600
120,4.4318331
130,4.5931735
140,4.7691951
150,4.8754090
160,4.8823842
170,4.8476837
180,4.8311196

```
190,4.8529031
200,4.9470493
225,5.2710202
250,5.2765945
275,5.3527556
300,5.5394991
325,5.5214467
350,5.6571716
375,5.7833034
400,5.8065877
425,6.0651690
450,6.0760971
475,6.0626131
500,6.4396038
525,6.4110814
550,6.3363266
575,6.7706090
600,6.7863770
625,6.5663108
650,6.7908633
675,6.8992115
700,6.6137633
725,6.6820062
750,6.9055752
775,6.5880170
800,6.4231503
825,6.7451941
850,6.5275018
875,6.5351606
900,6.8403869
925,6.7626953
950,6.7309443
975,6.9328819
1000,7.0081836];


 f1 = linspace(0.3,200,51);
 f1 = f1';
 nuweZtt = spline(Ztt(:,1),Ztt(:,2),f1);
 f = linspace(0.3,1000,51);
 f = f';
 newZtt = spline(Ztt(:,1),Ztt(:,2),f);
```

```
% S-Parameter versus Frequency Plots:

figure
plot(f,20*log10(abs(bs11)),'m-.',f,20*log10(abs(cs11)),'k--',...
  f,20*log10(abs(npldons11)),'g',f,20*log10(abs(npldoffs11)),'r')
grid
title('Reflection Coefficient Response of the Current Probe Test-System')
ylabel(' s11 Magnitude [dB]')
xlabel('Frequency [MHz]')
axes(legend('case 4','case 3','case 2','case 1'))

figure
plot(f,20*log10(abs(bs21)),'m-.',f,20*log10(abs(cs21)),'k--')
grid
title('Transmission Coefficient Response of the EMCO Inductive Current Clamp
Test System')
ylabel('Magnitude [dB]')
xlabel('Frequency [MHz]')
axes(legend('S21 response without ferrite chokes','S21 response with ferrite
chokes'))

% Z-Parameter versus Frequency Plots:

figure
subplot(2,2,1)
plot(f,real(bZ11),'r',f,imag(bZ11),'m-.')
grid
title('Input Impedance Looking into Port 1')
ylabel('z11[Ohm]')
xlabel('Frequency [MHz]')
axes(legend('real','imag'))
subplot(2,2,2)
plot(f,real(bZ12),'r',f,imag(bZ12),'m-.')
grid
title('Transfer Impedance of the Test System')
ylabel('z12[Ohm]')
xlabel('Frequency [MHz]')
axes(legend('real','imag'))
subplot(2,2,3)
plot(f,real(bZ21),'r',f,imag(bZ21),'m-.')
grid
title('Transfer Impedance of the Test System')
ylabel('z21[Ohm]')
xlabel('Frequency [MHz]')
axes(legend('real','imag'))
subplot(2,2,4)
```

```
plot(f,real(bZ22),'r',f,imag(bZ22),'m-.')
grid
title('Input Impedance Looking into Port 2')
ylabel('z22[Ohm]')
xlabel('Frequency [MHz]')
axes(legend('real','imag'))

Zin_probe = Zo*(1 + bs11)./(1 - bs11);

aZt = aZ21./(1 + aZ22/Zo);

% Ztt Curves:

figure
semilogx(f1,20*log10(abs(aZt)),'m-.',f1,20*log10(abs(nuweZtt)),'g')
grid
title('Transfer Impedance for EMCO Inductive Current Clamp')
ylabel('Ztt Magnitude [dBOhm]')
xlabel('Frequency [MHz]')
axes(legend('Manufacturer-Response','Present Technique Response'))

bZt = bZ21./(1 + bZ22/Zo);
bfZt = bfZ21./(1 + bfZ22/Zo);
figure
semilogx(f,20*log10(abs(bZt)),'r',f,20*log10(abs(bfZt)),'m-.',f,...
  20*log10(abs(newZtt)),'k--')
grid
title('Transfer Impedance for EMCO Inductive Current Clamp')
ylabel('Ztt Magnitude [dBOhm]')
xlabel('Frequency [MHz]')
axes(legend('Response without Ferrites Chokes',...
  'Response with Ferrites Chokes','Manufacturer-Response'))

%----------------------------------------End of Code---------------------------------------- %
```

C.2 Computation of Z_T

C.2.1 Wire-Loop Method Routine

```
%%%%%%%%%%%%%%%%%%%%%%%%%%%%%%%%%%%%%%%%%%%%%%%%%%%%%%%%%
%*      Wire-Loop Antenna Method                                     %
%*      The program computes ZT parameter of various cables          %
%*      An ANA was used. Port-1 connected to the CUT & Port-2 to Wire-Loop   %
     clear all;

     f = linspace(0.3,200,401);  % frequency range
     f = f';

%       'Coax Braid' Measurement for De-embedding                    %

        load c:\MEPrject\Chapt3\srmeas\coaxbS11.txt
                S11 = coaxbS11(1:401,1) + i*coaxbS11(1:401,2);
        load c:\MEPrject\Chapt3\srmeas\coaxbS22.txt
                S22 = coaxbS22(1:401,1) + i*coaxbS22(1:401,2);
        load c:\MEPrject\Chapt3\srmeas\coaxbS21.txt
                S21 = coaxbS21(1:401,1) + i*coaxbS21(1:401,2);
        load c:\MEPrject\Chapt3\srmeas\coaxbS12.txt
          S12 = coaxbS12(1:401,1) + i*coaxbS12(1:401,2);

%       RG 58 A/U
        load c:\MEPrject\Chapt3\srmeas\meauS11.txt
                auwS11 = meauS11(1:401,1) + i*meauS11(1:401,2);
        load c:\MEPrject\Chapt3\srmeas\meauS22.txt
                auwS22 = meauS22(1:401,1) + i*meauS22(1:401,2);
        load c:\MEPrject\Chapt3\srmeas\meauS21.txt
                auwS21 = meauS21(1:401,1) + i*meauS21(1:401,2);
        load c:\MEPrject\Chapt3\srmeas\meauS12.txt
                auwS12 = meauS12(1:401,1) + i*meauS12(1:401,2);

%       RG 58 C/U-MIL
        load c:\MEPrject\Chapt3\srmeas\mecuS11.txt
                cuwS11 = mecuS11(1:401,1) + i*mecuS11(1:401,2);
        load c:\MEPrject\Chapt3\srmeas\mecuS22.txt
                cuwS22 = mecuS22(1:401,1) + i*mecuS22(1:401,2);
        load c:\MEPrject\Chapt3\srmeas\mecuS21.txt
                cuwS21 = mecuS21(1:401,1) + i*mecuS21(1:401,2);
        load c:\MEPrject\Chapt3\srmeas\mecuS12.txt
```

```
cuwS12 = mecuS12(1:401,1) + i*mecuS12(1:401,2);
%                S to Z Conversion Using a Matrix:                %

Zo = 50; % internal impedance of the detector;
U = [1 0;0 1];
        %       'Coax Braid'
        for X = 1:401
          S = [S11(X) S12(X);S21(X) S22(X)];
          Z = inv(U - S)*(U + S);
          BZ11(X,1) = Zo*Z(1,1);
          BZ12(X,1) = Zo*Z(1,2);
          BZ21(X,1) = Zo*Z(2,1);
          BZ22(X,1) = Zo*Z(2,2);
        end
        %       RG58 A/U
        for X = 1:401
          S = [auwS11(X) auwS12(X);auwS21(X) auwS22(X)];
          Z = inv(U - S)*(U + S);
          auwZ11(X,1) = Zo*Z(1,1);
          auwZ12(X,1) = Zo*Z(1,2);
          auwZ21(X,1) = Zo*Z(2,1);
          auwZ22(X,1) = Zo*Z(2,2);
        end
        %       RG58 C/U
        Zo = 50;
        U = [1 0;0 1];
        for X = 1:401
          S = [cuwS11(X) cuwS12(X);cuwS21(X) cuwS22(X)];
          Z = inv(U - S)*(U + S);
          cuwZ11(X,1) = Zo*Z(1,1);
          cuwZ12(X,1) = Zo*Z(1,2);
          cuwZ21(X,1) = Zo*Z(2,1);
          cuwZ22(X,1) = Zo*Z(2,2);
        end

        CUTZin = Zo*(1 + S11)./(1 - S11); % computing test-cable's input impedance
        CUTZin1 = Zo*(1 + auwS11)./(1 - auwS11);

% System Transfer Impedance Z't - with 'Coax Braid' in Place        %

        Z't = BZ12./(1 + BZ11/Zo);

% System Transfer Impedance Zt – with Cable-Under-Test in Place     %
        auZt = auwZ12./(1 + auwZ11/Zo);
        cuZt = cuwZ12./(1 + cuwZ11/Zo);
```

% <u>Cable Transfer Impedance Plots:</u> %

$auZ_T = 2*auZ_t.*CUTZin ./ Z_t'$;
$cuZ_T = 2*cuZ_t.*CUTZin./ Z_t'$;

```
figure(1)
plot(f,abs(auZt),'m:',f,abs(cuZt),'b-.')
grid
axis([0 60 0 0.75])
title('Cable Transfer Impedance of RG 58 Coaxial Cables')
ylabel('Magnitude [Ohm/m]')
xlabel('Frequency [MHz]')
axes(legend('RG 58A/U','RG 58C/U'))
```

%--End of Code-------------------------------------%

C.2.2 Solving for Z_T – ANA Method

```
%%%%%%%%%%%%%%%%%%%%%%%%%%%%%%%%%%%%%%%%%%%%%%%%%%%%%%%%%%%%
%*    Current-Injection Method                                              %
%*    CUT end with internal short circuit on port-1 and the open end to port-2   %

        clear all;
        f = linspace(0.3,100,51);
        f = f';

% --------------------Measured S-Parameter Data for - Co-axial Cables----------------------;

% RG 316/U: // also used in SUNSAT for RF Signals

        load c:\MScEngSci2001\Chapt4\Winjmethod\test1RGuS11.txt
            uS11 = test1RGuS11(1:51,1) + i*test1RGuS11(1:51,2);
        load c:\MScEngSci2001\Chapt4\Winjmethod\test1RGuS12.txt
            uS12 = test1RGuS12(1:51,1) + i*test1RGuS12(1:51,2);
        load c:\MScEngSci2001\Chapt4\Winjmethod\test1RGuS21.txt
            uS21 = test1RGuS21(1:51,1) + i*test1RGuS21(1:51,2);
        load c:\MScEngSci2001\Chapt4\Winjmethod\test1RGuS22.txt
            uS22 = test1RGuS22(1:51,1) + i*test1RGuS22(1:51,2);

% RG 316/U: (1st Measurement) with different SMA connector pins
```

```
load c:\MScEngSci2001\Chapt4\Winjmethod\uanaS11.txt
    puS11 = uanaS11(1:51,1) + i*uanaS11(1:51,2);
load c:\MScEngSci2001\Chapt4\Winjmethod\uanaS12.txt
    puS12 = uanaS12(1:51,1) + i*uanaS12(1:51,2);
load c:\MScEngSci2001\Chapt4\Winjmethod\uanaS21.txt
    puS21 = uanaS21(1:51,1) + i*uanaS21(1:51,2);
load c:\MScEngSci2001\Chapt4\Winjmethod\uanaS22.txt
    puS22 = uanaS22(1:51,1) + i*uanaS22(1:51,2);

%  RG 316/U: (2nd Measurement) with different SMA connector pins
        load c:\MScEngSci2001\Chapt4\Winjmethod\uana1S11.txt
            pu1S11 = uana1S11(1:51,1) + i*uana1S11(1:51,2);
        load c:\MScEngSci2001\Chapt4\Winjmethod\uana1S12.txt
            pu1S12 = uana1S12(1:51,1) + i*uana1S12(1:51,2);
        load c:\MScEngSci2001\Chapt4\Winjmethod\uana1S21.txt
            pu1S21 = uana1S21(1:51,1) + i*uana1S21(1:51,2);
        load c:\MScEngSci2001\Chapt4\Winjmethod\uana1S22.txt
            pu1S22 = uana1S22(1:51,1) + i*uana1S22(1:51,2);

%----RG58C/U
%_SetupB
        load c:\MScEngSci2001\Chapt4\Winjmethod\tBRGcuS11.txt
            BcuS11 = tBRGcuS11(1:51,1) + i*tBRGcuS11(1:51,2);
        load c:\MScEngSci2001\Chapt4\Winjmethod\tBRGcuS12.txt
            BcuS12 = tBRGcuS12(1:51,1) + i*tBRGcuS12(1:51,2);
        load c:\MScEngSci2001\Chapt4\Winjmethod\tBRGcuS21.txt
            BcuS21 = tBRGcuS21(1:51,1) + i*tBRGcuS21(1:51,2);
        load c:\MScEngSci2001\Chapt4\Winjmethod\tBRGcuS22.txt
            BcuS22 = tBRGcuS22(1:51,1) + i*tBRGcuS22(1:51,2);
%_SetupA
        load c:\MScEngSci2001\Chapt4\Winjmethod\AcuS11.txt
            AcuS11 = AcuS11(1:51,1) + i*AcuS11(1:51,2);
        load c:\MScEngSci2001\Chapt4\Winjmethod\AcuS12.txt
            AcuS12 = AcuS12(1:51,1) + i*AcuS12(1:51,2);
        load c:\MScEngSci2001\Chapt4\Winjmethod\AcuS21.txt
            AcuS21 = AcuS21(1:51,1) + i*AcuS21(1:51,2);
        load c:\MScEngSci2001\Chapt4\Winjmethod\AcuS22.txt
            AcuS22 = AcuS22(1:51,1) + i*AcuS22(1:51,2);

%----RG 58A/U
%_SetupB
        load c:\MScEngSci2001\Chapt4\Winjmethod\tBRGauS11.txt
            BauS11 = tBRGauS11(1:51,1) + i*tBRGauS11(1:51,2);
        load c:\MScEngSci2001\Chapt4\Winjmethod\tBRGauS12.txt
            BauS12 = tBRGauS12(1:51,1) + i*tBRGauS12(1:51,2);
        load c:\MScEngSci2001\Chapt4\Winjmethod\tBRGauS21.txt
```

```
        BauS21 = tBRGauS21(1:51,1) + i*tBRGauS21(1:51,2);
    load c:\MScEngSci2001\Chapt4\Winjmethod\tBRGauS22.txt
        BauS22 = tBRGauS22(1:51,1) + i*tBRGauS22(1:51,2);

%_SetupA
    load c:\MScEngSci2001\Chapt4\Winjmethod\tARGauS11.txt
        AauS11 = tARGauS11(1:51,1) + i*tARGauS11(1:51,2);
    load c:\MScEngSci2001\Chapt4\Winjmethod\tARGauS12.txt
        AauS12 = tARGauS12(1:51,1) + i*tARGauS12(1:51,2);
    load c:\MScEngSci2001\Chapt4\Winjmethod\tARGauS21.txt
        AauS21 = tARGauS21(1:51,1) + i*tARGauS21(1:51,2);
    load c:\MScEngSci2001\Chapt4\Winjmethod\tARGauS22.txt
        AauS22 = tARGauS22(1:51,1) + i*tARGauS22(1:51,2);

% Use of Ferrite Chokes to suppress CM current;
    load c:\MScEngSci2001\Chapt4\Winjmethod\tBfcRGcuS11.txt
        fcBcuS11 = tBfcRGcuS11(1:51,1) + i*tBfcRGcuS11(1:51,2);
    load c:\MScEngSci2001\Chapt4\Winjmethod\tBfcRGcuS21.txt
        fcBcuS21 = tBfcRGcuS21(1:51,1) + i*tBfcRGcuS21(1:51,2);
    load c:\MScEngSci2001\Chapt4\Winjmethod\tBfcRGcuS12.txt
        fcBcuS12 = tBfcRGcuS12(1:51,1) + i*tBfcRGcuS12(1:51,2);
    load c:\MScEngSci2001\Chapt4\Winjmethod\tBfcRGcuS22.txt
        fcBcuS22 = tBfcRGcuS22(1:51,1) + i*tBfcRGcuS22(1:51,2);

    load c:\MScEngSci2001\Chapt4\Winjmethod\tBfcRGauS11.txt
        fcBauS11 = tBfcRGauS11(1:51,1) + i*tBfcRGauS11(1:51,2);
    load c:\MScEngSci2001\Chapt4\Winjmethod\tBfcRGauS21.txt
        fcBauS21 = tBfcRGauS21(1:51,1) + i*tBfcRGauS21(1:51,2);
    load c:\MScEngSci2001\Chapt4\Winjmethod\tBfcRGauS12.txt
        fcBauS12 = tBfcRGcuS12(1:51,1) + i*tBfcRGauS12(1:51,2);
    load c:\MScEngSci2001\Chapt4\Winjmethod\tBfcRGauS22.txt
        fcBauS22 = tBfcRGauS22(1:51,1) + i*tBfcRGauS22(1:51,2);

%---------------------------------- End of Measured Data---------------------- ----------;


% ---------------------------- Finding Impedance [Z] Parameters-----------------------------;

Zo = 50;
U = [1 0;0 1];
%_(Test 1)
    for X = 1:51
      S = [uS11(X) uS12(X);uS21(X) uS22(X)];
      Z = inv(U - S)*(U + S); % To find Z in-terms of S
      uZ11(X,1) = Zo*Z(1,1);
      uZ12(X,1) = Zo*Z(1,2);
```

```
        uZ21(X,1) = Zo*Z(2,1);
        uZ22(X,1) = Zo*Z(2,2);
      end

%_(Test 2)
      for X = 1:51
        S = [BcuS11(X) BcuS12(X);BcuS21(X) BcuS22(X)];
        Z = inv(U - S)*(U + S); % To find Z in-terms of S
        BcuZ11(X,1) = Zo*Z(1,1);
        BcuZ12(X,1) = Zo*Z(1,2);
        BcuZ21(X,1) = Zo*Z(2,1);
        BcuZ22(X,1) = Zo*Z(2,2);
      end
%_(Test 3)
      for X = 1:51
        S = [BauS11(X) BauS12(X);BauS21(X) BauS22(X)];
        Z = inv(U - S)*(U + S); % To find Z in-terms of S
        BauZ11(X,1) = Zo*Z(1,1);
        BauZ12(X,1) = Zo*Z(1,2);
        BauZ21(X,1) = Zo*Z(2,1);
        BauZ22(X,1) = Zo*Z(2,2);
      end
%_(Test 4)
      for X = 1:51
        S = [AcuS11(X) AcuS12(X);AcuS21(X) AcuS22(X)];
        Z = inv(U - S)*(U + S); % To find Z in-terms of S
        AcuZ11(X,1) = Zo*Z(1,1);
        AcuZ12(X,1) = Zo*Z(1,2);
        AcuZ21(X,1) = Zo*Z(2,1);
        AcuZ22(X,1) = Zo*Z(2,2);
      end
%_(Test 5)
      for X = 1:51
        S = [AauS11(X) AauS12(X);AauS21(X) AauS22(X)];
        Z = inv(U - S)*(U + S); % To find Z in-terms of S
        AauZ11(X,1) = Zo*Z(1,1);
        AauZ12(X,1) = Zo*Z(1,2);
        AauZ21(X,1) = Zo*Z(2,1);
        AauZ22(X,1) = Zo*Z(2,2);
      end
%_(Test 6)
      for X = 1:51
        S = [fcBcuS11(X) fcBcuS12(X);fcBcuS21(X) fcBcuS22(X)];
        Z = inv(U - S)*(U + S); % To find Z in-terms of S
        fcBcuZ11(X,1) = Zo*Z(1,1);
        fcBcuZ12(X,1) = Zo*Z(1,2);
```

```
        fcBcuZ21(X,1) = Zo*Z(2,1);
        fcBcuZ22(X,1) = Zo*Z(2,2);
      end
%_(Test 7)
      for X = 1:51
        S = [fcBauS11(X) fcBauS12(X);fcBauS21(X) fcBauS22(X)];
        Z = inv(U - S)*(U + S); % To find Z in-terms of S
        fcBauZ11(X,1) = Zo*Z(1,1);
        fcBauZ12(X,1) = Zo*Z(1,2);
        fcBauZ21(X,1) = Zo*Z(2,1);
        fcBauZ22(X,1) = Zo*Z(2,2);
      end
%_(Test 8)
      for X = 1:51
        S = [pu1S11(X) pu1S12(X);pu1S21(X) pu1S22(X)];
        Z = inv(U - S)*(U + S); % To find Z in-terms of S
        pu1Z11(X,1) = Zo*Z(1,1);
        pu1Z12(X,1) = Zo*Z(1,2);
        pu1Z21(X,1) = Zo*Z(2,1);
        pu1Z22(X,1) = Zo*Z(2,2);
      end
%_(Test 9)
      for X = 1:51
        S = [puS11(X) puS12(X);puS21(X) puS22(X)];
        Z = inv(U - S)*(U + S); % To find Z in-terms of S
        puZ11(X,1) = Zo*Z(1,1);
        puZ12(X,1) = Zo*Z(1,2);
        puZ21(X,1) = Zo*Z(2,1);
        puZ22(X,1) = Zo*Z(2,2);
      end
%*-------------------------------------------------------------------------------------------------------------;

s = 0.5;  % cable lead length in meters

      Zt1 = uZ21./(1 + uZ22/Zo);
      Zt1 = Zt1/(s);
      Zt2 = BcuZ21./(1 + BcuZ22/Zo);
      Zt2 = Zt2/(s);
      Zt3 = BauZ21./(1 + BauZ22/Zo);
      Zt3 = Zt3/(s);
      Zt4 = AcuZ21./(1 + AcuZ22/Zo);
      Zt4 = Zt4/(s);
      Zt5 = AauZ21./(1 + AauZ22/Zo);
      Zt5 = Zt5/(s);
      Zt6 = fcBcuZ21./(1 + fcBcuZ22/Zo);
      Zt6 = Zt6/(s);
```

```
        Zt7 = fcBauZ21./(1 + fcBauZ22/Zo);
        Zt7 = Zt7/(s);
figure(1)
plot(f,abs(Zt4),'g',f,abs(Zt1),'r',f,abs(Zt5),'b')
grid
axis([0 60 0 0.75])
title('Measured Cable Transfer Impedance Response')
ylabel('Magnitude [Ohm/m]')
xlabel('Frequency [MHz]')
axes(legend('RG 316/U','RG 58C/U','RG 58A/U'))
%*------------------------- ---------------------- END--------------------------------------------;
```

C.2.3 Solving for Z_T – SA Method

```
%%%%%%%%%%%%%%%%%%%%%%%%%%%%%%%%%%%%%%%%%%%%%%%%%%%%%%%%%%%%%%%%%%%%%%%%%%%
%*      This program computes ZT of various cables.                                              %
%*      SA (HP8562A [1kHz-22GHz]) & SG (R&S SML03 [9kHz-3.3GHz]).                    %
%*      Frequency Range of 10kHz-100MHz.                                                          %

clear all;

% -------------------- ---------------------Importing Data---------------------------------------;
% The Reference Signal-----------------------------------------------------;
        load c:\MScEngSci2001\Chapt4\Winjmethod\refsigl.txt

% Vcable--------------------------------------------------------------------;
        load c:\MScEngSci2001\Chapt4\Winjmethod\STOVcable.txt
        load c:\MScEngSci2001\Chapt4\Winjmethod\UVcable.txt
        load c:\MScEngSci2001\Chapt4\Winjmethod\CUVcable.txt
        load c:\MScEngSci2001\Chapt4\Winjmethod\AUVcable.txt

% Vmprobe-------------------------------------------------------------------;
        load c:\MScEngSci2001\Chapt4\Winjmethod\STPVmprobe.txt
        load c:\MScEngSci2001\Chapt4\Winjmethod\UVmprobe.txt
        load c:\MScEngSci2001\Chapt4\Winjmethod\CUVmprobe.txt
        load c:\MScEngSci2001\Chapt4\Winjmethod\AUVmprobe.txt

% RG 316/U added data
        load c:\MScEngSci2001\Chapt4\Winjmethod\Vmpmeas_nt.txt
        load c:\MScEngSci2001\Chapt4\Winjmethod\Vsameas_nt.txt
```

```
% From the following ANA data, S11 is used to extract Zin:

load c:\MScEngSci2001\Chapt4\Winjmethod\ShieldedtprS11.txt
    st_prS11 = ShieldedtprS11(1:51,1) + i*ShieldedtprS11(1:51,2);
load c:\MScEngSci2001\Chapt4\Winjmethod\ShieldedtprS12.txt
    st_prS12 = ShieldedtprS12(1:51,1) + i*ShieldedtprS12(1:51,2);
load c:\MScEngSci2001\Chapt4\Winjmethod\ShieldedtprS21.txt
    st_prS21 = ShieldedtprS21(1:51,1) + i*ShieldedtprS21(1:51,2);
load c:\MScEngSci2001\Chapt4\Winjmethod\ShieldedtprS22.txt
    st_prS22 = ShieldedtprS22(1:51,1) + i*ShieldedtprS22(1:51,2);

load c:\MScEngSci2001\Chapt4\Winjmethod\AcuS11.txt
    AcuS11 = AcuS11(1:51,1) + i*AcuS11(1:51,2);
load c:\MScEngSci2001\Chapt4\Winjmethod\AcuS12.txt
    AcuS12 = AcuS12(1:51,1) + i*AcuS12(1:51,2);
load c:\MScEngSci2001\Chapt4\Winjmethod\AcuS21.txt
    AcuS21 = AcuS21(1:51,1) + i*AcuS21(1:51,2);
load c:\MScEngSci2001\Chapt4\Winjmethod\AcuS22.txt
    AcuS22 = AcuS22(1:51,1) + i*AcuS22(1:51,2);

load c:\MScEngSci2001\Chapt4\Winjmethod\tARGauS11.txt
    AauS11 = tARGauS11(1:51,1) + i*tARGauS11(1:51,2);
load c:\MScEngSci2001\Chapt4\Winjmethod\tARGauS12.txt
    AauS12 = tARGauS12(1:51,1) + i*tARGauS12(1:51,2);
load c:\MScEngSci2001\Chapt4\Winjmethod\tARGauS21.txt
    AauS21 = tARGauS21(1:51,1) + i*tARGauS21(1:51,2);
load c:\MScEngSci2001\Chapt4\Winjmethod\tARGauS22.txt
    AauS22 = tARGauS22(1:51,1) + i*tARGauS22(1:51,2);


load c:\MScEngSci2001\Chapt4\Winjmethod\test1RGuS11.txt  % (first Meas)
    uS11 = test1RGuS11(1:51,1) + i*test1RGuS11(1:51,2);
load c:\MScEngSci2001\Chapt4\Winjmethod\test1RGuS12.txt
    uS12 = test1RGuS12(1:51,1) + i*test1RGuS12(1:51,2);
load c:\MScEngSci2001\Chapt4\Winjmethod\test1RGuS21.txt
    uS21 = test1RGuS21(1:51,1) + i*test1RGuS21(1:51,2);
load c:\MScEngSci2001\Chapt4\Winjmethod\test1RGuS22.txt
    uS22 = test1RGuS22(1:51,1) + i*test1RGuS22(1:51,2);

% RG 316/U: (2nd Meas) With different SMA connector pins
load c:\MScEngSci2001\Chapt4\Winjmethod\uana1S11.txt
    uS11 = uana1S11(1:51,1) + i*uana1S11(1:51,2);
load c:\MScEngSci2001\Chapt4\Winjmethod\uana1S12.txt
```

```
        uS12 = uana1S12(1:51,1) + i*uana1S12(1:51,2);
    load c:\MScEngSci2001\Chapt4\Winjmethod\uana1S21.txt
        uS21 = uana1S21(1:51,1) + i*uana1S21(1:51,2);
    load c:\MScEngSci2001\Chapt4\Winjmethod\uana1S22.txt
        uS22 = uana1S22(1:51,1) + i*uana1S22(1:51,2);

%============================================================
;

f = linspace(0.3,100,51);
f = f';
newf = linspace(0.01,100,601);
newf = newf';

% EMCO Probe Transducer Factor [Ohms] v/s Frequency(MHz)
Ztt =[  0.010000,0.0193752
      0.020000,0.0430953
      0.030000,0.0647381
      0.040000,0.0858285
      0.050000,0.1065475
      0.060000,0.1270061
      0.070000,0.1469749
      0.080000,0.1665739
      0.090000,0.1861319
      0.100000,0.2050883
      0.200000,0.3725530
      0.300000,0.5047773
      0.400000,0.6114288
        0.500000,0.7002804
      0.600000,0.7764071
      0.700000,0.8433412
      0.800000,0.9033793
      0.900000,0.9577489
         1,0.9964087
         2,1.3613117
         3,1.5985767
         4,1.7750313
         5,1.9134753
         6,2.0257402
         7,2.1198730
         8,2.2040155
         9,2.2818236
        10,2.3552307
        20,2.8924347
        30,3.2164458
        40,3.4867042
        50,3.7370590
```

```
        60,3.9790490
        70,4.1799193
        80,4.2940558
        90,4.3118313
        100,4.3026890];

%       Impedance [Z] Parameters:
% Z-parameter Conversion Procedure:
Zo = 50;
U = [1 0;0 1];
%_(Test 1)
        for X = 1:51
          S = [uS11(X) uS12(X);uS21(X) uS22(X)];
          Z = inv(U - S)*(U + S); % To find Z in-terms of S
          uZ11(X,1) = Zo*Z(1,1);
          uZ12(X,1) = Zo*Z(1,2);
          uZ21(X,1) = Zo*Z(2,1);
          uZ22(X,1) = Zo*Z(2,2);
        end
%_(Test 2)
        for X = 1:51
          S = [AcuS11(X) AcuS12(X);AcuS21(X) AcuS22(X)];
          Z = inv(U - S)*(U + S); % To find Z in-terms of S
          AcuZ11(X,1) = Zo*Z(1,1);
          AcuZ12(X,1) = Zo*Z(1,2);
          AcuZ21(X,1) = Zo*Z(2,1);
          AcuZ22(X,1) = Zo*Z(2,2);
        end
%_(Test 3)
        for X = 1:51
          S = [AauS11(X) AauS12(X);AauS21(X) AauS22(X)];
          Z = inv(U - S)*(U + S); % To find Z in-terms of S
          AauZ11(X,1) = Zo*Z(1,1);
          AauZ12(X,1) = Zo*Z(1,2);
          AauZ21(X,1) = Zo*Z(2,1);
          AauZ22(X,1) = Zo*Z(2,2);
        end
%_(Test 6)
        for X = 1:51
          S = [st_prS11(X) st_prS12(X);st_prS21(X) st_prS22(X)];
          Z = inv(U - S)*(U + S); % To find Z in-terms of S
          st_prZ11(X,1) = Zo*Z(1,1);
          st_prZ12(X,1) = Zo*Z(1,2);
          st_prZ21(X,1) = Zo*Z(2,1);
          st_prZ22(X,1) = Zo*Z(2,2);
        end
```

```
Zo2 = 50; % finite termination of the measuring instrument
%*      Interpolation Process the available Probe Transducer Factor to Measured Data;


        newZtt = spline(Ztt(:,1),Ztt(:,2),newf);

        newcuZ22 = spline(f,AcuZ22(:,1),newf); % Impedance Looking into Port-2
        newauZ22 = spline(f,AauZ22(:,1),newf);
        newuZ22 = spline(f,uZ22(:,1),newf);
        newstpZ22 = spline(f,st_prZ22(:,1),newf);

        cuZin2 = Zo*(1 + AcuS22)./(1 - AcuS22);
        auZin2 = Zo*(1 + AauS22)./(1 - AauS22);
        uZin2 = Zo*(1 + uS22)./(1 - uS22);
        stpZin2 = Zo*(1 + st_prS22)./(1 - st_prS22);

        ncuZin2 = spline(f,cuZin2(:,1),newf);
        nauZin2 = spline(f,auZin2(:,1),newf);
        nuZin2 = spline(f,uZin2(:,1),newf);
        nstpZin2 = spline(f,stpZin2(:,1),newf);

        cuP = 10.^(CUVmprobe/10)*1e-3;
        cuV = sqrt(cuP*Zo);
        cuIcm = cuV./newZtt; % RG 58C/U CM-Current

        auP = 10.^(AUVmprobe/10)*1e-3;
        auV = sqrt(auP*Zo);
        auIcm = auV./newZtt; % RG 58 A/U CM-Current

        uP = 10.^(UVmprobe/10)*1e-3;
        uV = sqrt(uP*Zo);
        uIcm = uV./newZtt; % RG 316/U CM-Current (first measurement)

        newuP = 10.^(Vmpmeas_nt/10)*1e-3;
        newuV = sqrt(newuP*Zo);
        newuIcm = newuV./newZtt; % RG 316/U CM-Current (second measurement)

        sP = 10.^(STPVmprobe/10)*1e-3;
        sV = sqrt(sP*Zo);
        sIcm = sV./newZtt; % STP CM-Current

        % RG 58C/U
```

```
P1 = 10.^(CUVcable/10)*1e-3;
V1 = sqrt(P1*Zo); % CUT-Output
V1 = V1.*(ncuZin2 + Zo2)./Zo2;
cuZt = 2*V1./cuIcm;
% RG 58A/U
P2 = 10.^(AUVcable/10)*1e-3;
V2 = sqrt(P2*Zo); % CUT-Output
V2 = V2.*(nauZin2 + Zo2)./Zo2;
auZt = 2*V2./auIcm;

% RG 316/U
P3 = 10.^(UVcable/10)*1e-3;
V3 = sqrt(P3*Zo); % CUT-Output
V3 = V3.*(nuZin2 + Zo2)./Zo2;
uZt = 2*V3./uIcm;
newP3 = 10.^(Vsameas_nt/10)*1e-3;
newV3 = sqrt(newP3*Zo); % CUT-Output
newV3 = newV3.*(nuZin2 + Zo2)./Zo2;
newuZt = 2*newV3./newuIcm;

% Shielded Twisted-Pair
P4 = 10.^(STOVcable/10)*1e-3;
V4 = sqrt(P4*Zo); % CUT-Output
V4 = V4.*(nstpZin2 + Zo2)./Zo2;
sZt = 2*V4./sIcm;

figure(1)
plot(newf,abs(cuZt),'b-.',newf,abs(auZt),'r-.',newf,abs(uZt),'g-.')
grid
hold
axis([0 60 0 0.75])
title('Measured Cable Transfer Impedance Response of RG Coaxial Cables')
ylabel('Magnitude [Ohm/m]')
xlabel('Frequency [MHz]')
axes(legend('RG 58C/U','RG 58A/U','RG 316/U'))


% Using a Spectrum Analyzer + Signal Generator
figure(2)
plot(newf,abs(sZt),'m-.')
grid
title('Measured Cable Transfer Impedance a Shielded Twisted-Pair Cable')
ylabel('Magnitude [Ohm/m]')
xlabel('Frequency [MHz]')
axes(legend('Shielded Twisted Pair'))
```

%*-- End ---;

C.3 Processing the EMC ITS Measured Data

```
%%%%%%%%%%%%%%%%%%%%%%%%%%%%%%%%%%%%%%%%%%%%%%%%%%%%%%%%%%%%
%
% StoreM.m

% Written by Wessel van Brakel.  Program takes matrices of
measured data
% and store it in the appropriate place within the Data
Matrix "MDataM"
% (MDataM gets saved in the file MDataM.dat) to make the
post-processing
% and plotting of the different configurations (seperate
programmes still
% to be written for these functions - Silulami Doyi) for
the Magnetic
% Pick-Up Loop Measurements easier.

% Measured data have to be saved in real and imaginary
format in the first two
% columns of a matrix called "MData" before running
"StoreM.m" !

% Nine apertures (labeled a - i) to measure through
% Four discrete measuring positions (P2, P4, P6, P8 - each
10 cm interval from cable connector)
% Only two different orientations at each position through
different apertures:
%     [a,b,c - xy & xz] [d,e,f - xy & yz] [g,h,i - xz & yz]


%%%START%%%

% Fixed Variables:
NumfPoints = 201;  % "Number of Frequency Points" setting
on ANA during measurements

% Initialize!!
   A=0;
   B=0;
```

```
   C=0;
   Term = 0;

%Input Variable:
   ApUsed = input('What aperture was measured through ? (a -
   i)','s');

if ApUsed=='a'    % if a is the apreture used, then assign
to variable ApUsed.
   A = 1;         % set variable A to 1
elseif ApUsed=='b'
   A = 2;
elseif ApUsed=='c'
   A = 3;
elseif ApUsed=='d'
   A = 4;
elseif ApUsed=='e'
   A = 5;
elseif ApUsed=='f'
   A = 6;
elseif ApUsed=='g'
   A = 7;
elseif ApUsed=='h'
   A = 8;
elseif ApUsed=='i'
   A = 9;
else
   input('No such Aperture !!!')
   Term = 1;
end


if Term==0

Pos = input('At what position was the measurement performed
at ? (P2, P4, P6, P8)','s');

if Pos=='P2'
   B = 1;
 elseif Pos=='P4'
   B = 2;
 elseif Pos=='P6'
   B = 3;
 elseif Pos=='P8'
   B = 4;
 else
   input('No such Position !!!')
```

```
   Term = 1;
 end

end


if Term==0

if A==1|A==2|A==3
   Or = input('With what orientation was the measurement
performed ? (xy, xz)','s');
   if Or == 'xy'
      C =1;
   elseif Or=='xz'
      C = 2;
   else
      input('No such orientation !!!')
      Term = 1;
   end
elseif A==4|A==5|A==6
       Or = input('With what orientation was the
measurement performed ? (xy, yz)','s');
       if Or == 'xy'
          C =1;
       elseif Or=='yz'
          C = 2;
       else
          input('No such orientation !!!')
          Term =1;
       end
elseif A==7|A==8|A==9
       Or = input('With what orientation was the
measurement performed ? (xz, yz)','s');
       if Or == 'xz'
          C =1;
       elseif Or=='yz'
          C = 2;
       else
          input('No such orientation !!!')
          Term = 1;
       end
end

end
```

```
%Main Procedure to write data to Data Matrix if all the
inputs are satisfactory:
if Term == 0
   Realcol = (A*2)-1;
   Imagcol = (A*2);
   rowb = ((((B-1)*2)+(C-1))*NumfPoints)+1;
   rowe = rowb+NumfPoints-1;

   load MDataM.dat -ascii
   MDataM(rowb:rowe,Realcol) = MData(:,1);
   MDataM(rowb:rowe,Imagcol) = MData(:,2);
   save MDataM.dat MDataM -ascii
end

% a,xy: matrices of measured data of aperture a & orientatin
xy.
% a1 = Mdata1;
% a2 = Mdata2;
% a3 = Mdata3;
% a4 = Mdata4;

%clear all
%clc
```

Appendix D

Measurement of Induced Near-Field Strength

D.1 Measurement of *B*-field with the Single-Wire Transmission Placed against the Chassis

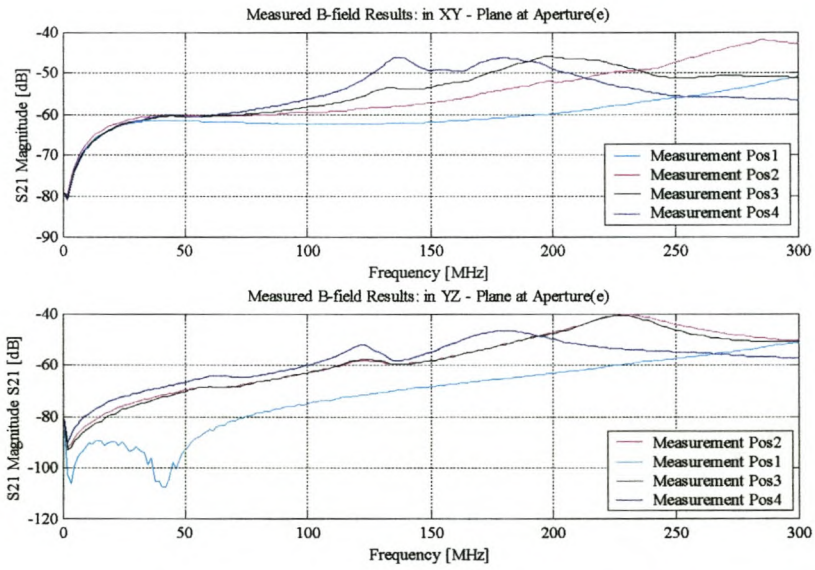

Figure D.1.1: Measured induced *B*-field strength from a current-driven single-wire loop at aperture (e).

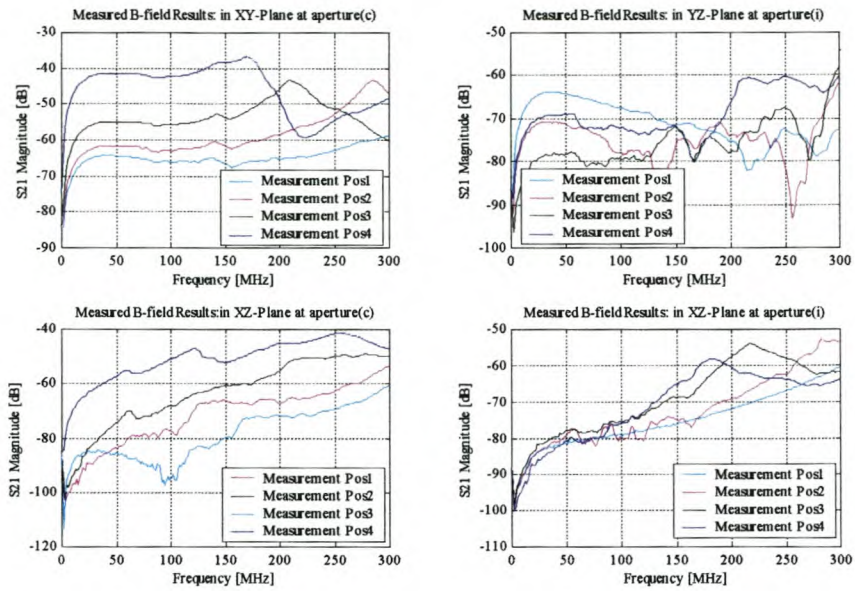

Figure D.1.2: Measured induced *B*-field strength from a current-driven single-wire loop at aperture (c) and (i).

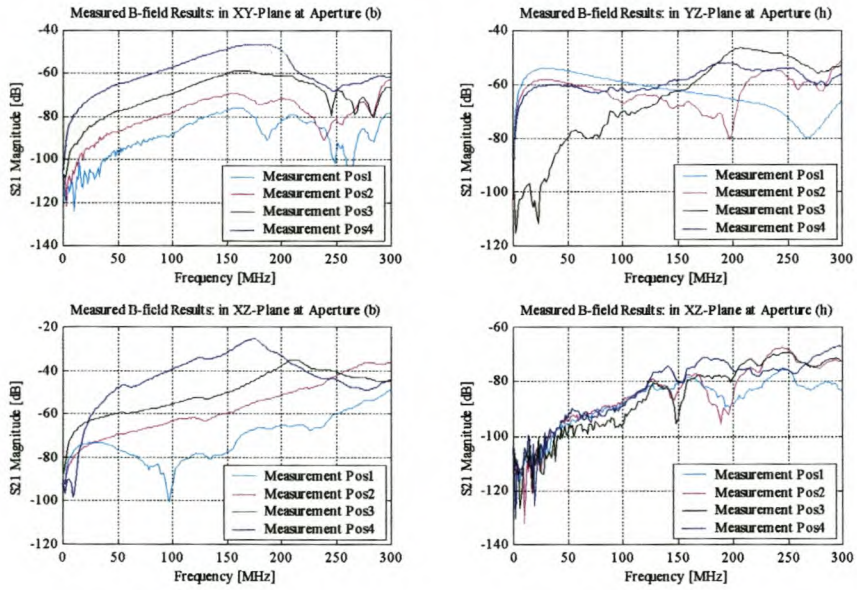

Figure D.1.3: Measured induced *B*-field strength from a current-driven single-wire loop at aperture (b) and (h).

D.2 Measurement of *B*-field with the Single-Wire Transmission Placed Approximately 5cm from the Chassis

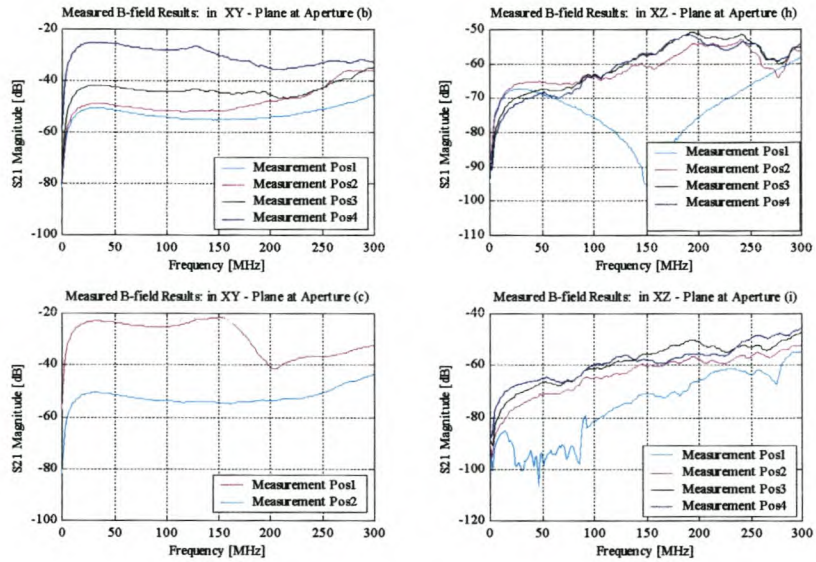

Figure D.2.1: Measured induced *B*-field strength from a current-driven single-wire loop at aperture (b), (c), (h) and (i).

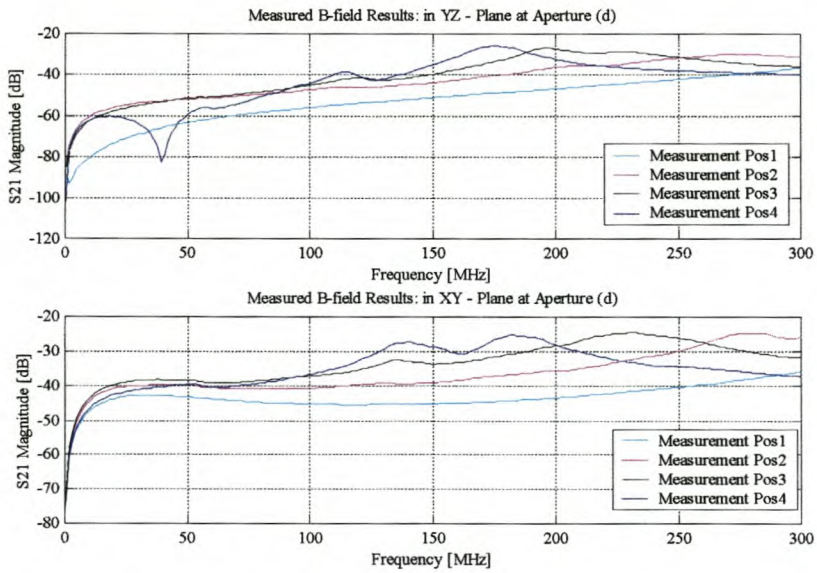

Figure D.2.2: Measured induced *B*-field strength from a current-driven single-wire loop at aperture (d).

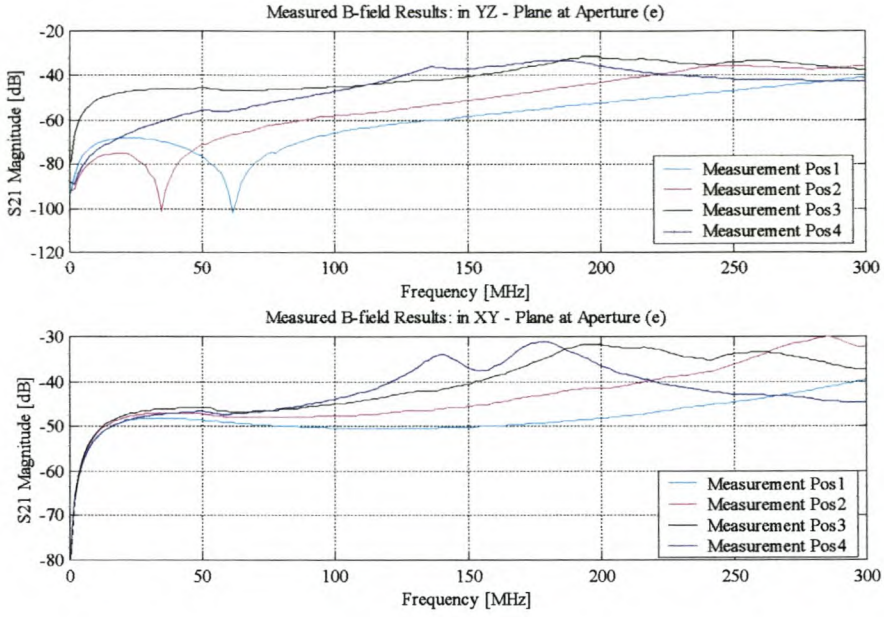

Figure D.2.3: Measured induced *B*-field strength from a current-driven single-wire loop at aperture (e).

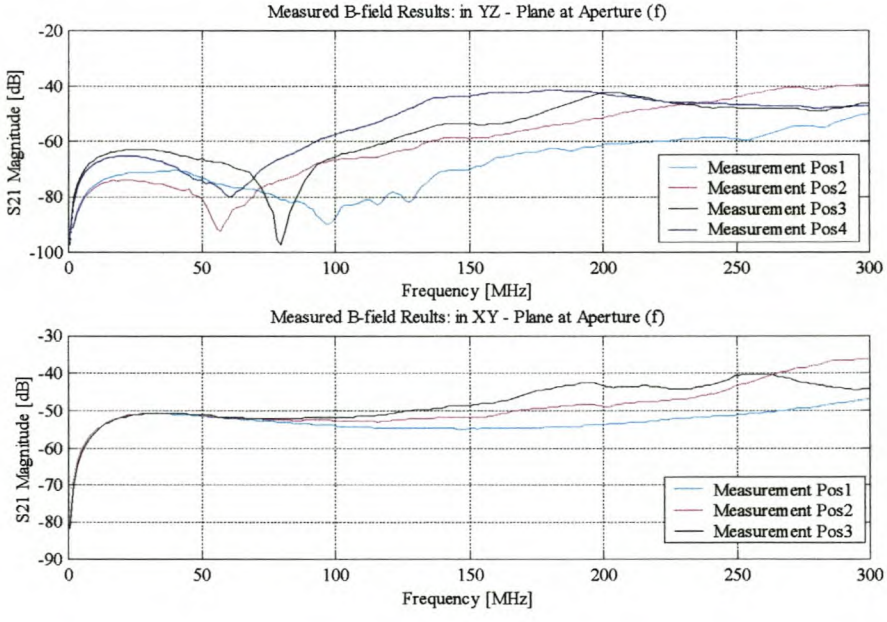

Figure D.2.4: Measured induced *B*-field strength from a current-driven single-wire loop placed 5cm above chassis at aperture (f).

D.3 Measurement of *E*-field with the Single-Wire Transmission Placed Approximately 5cm from the Chassis

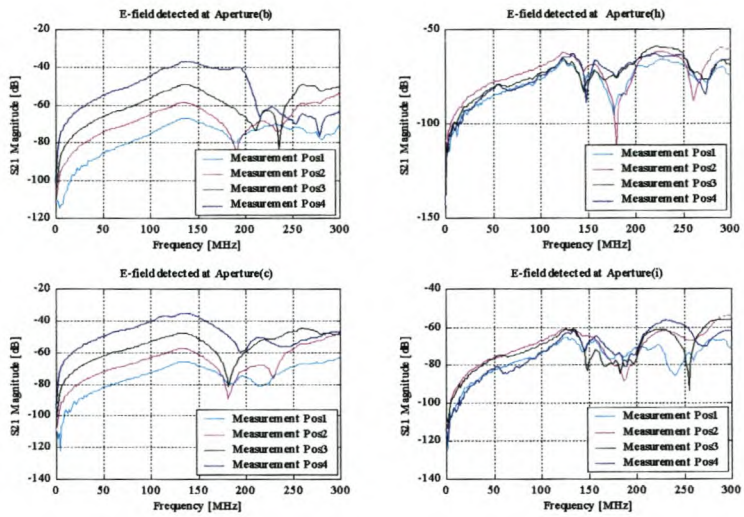

Figure D.3.1: Measured *E*-field strength from a voltage-driven single-wire at aperture (b), (c), (h) and (i).

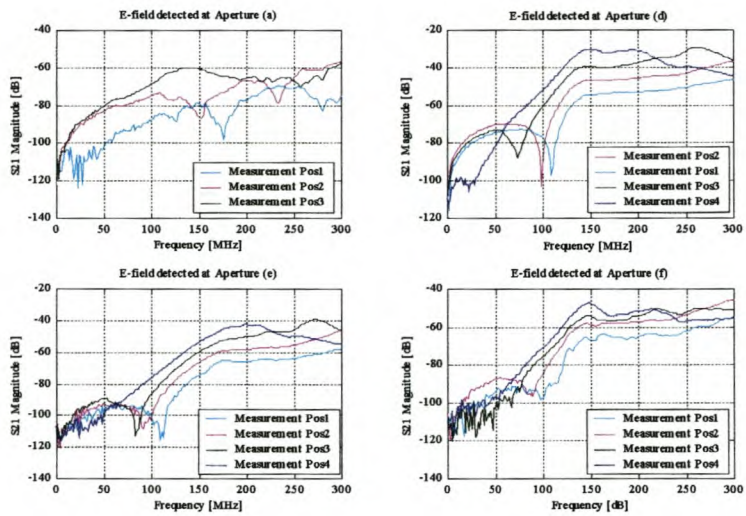

Figure D.3.2: Measurement of *E*-field strength from a voltage-driven single-wire at aperture (a), (d), (e) and (f).

D.4 *B* and *E*-field Measurement from the RG 316/U Placed Approximately 5cm from Chassis

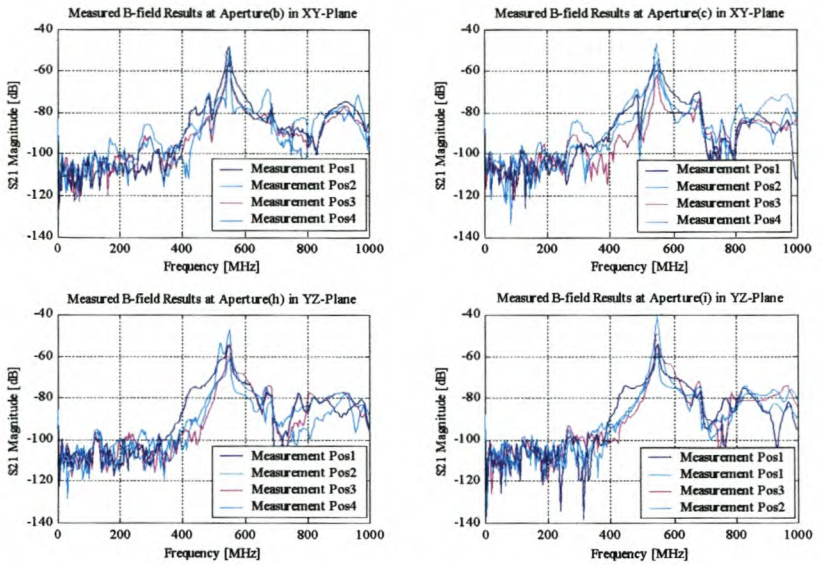

Figure D.4.1: Measured induced *B*-field strength from a coaxial cable at aperture (b), (c), (h) and (i).

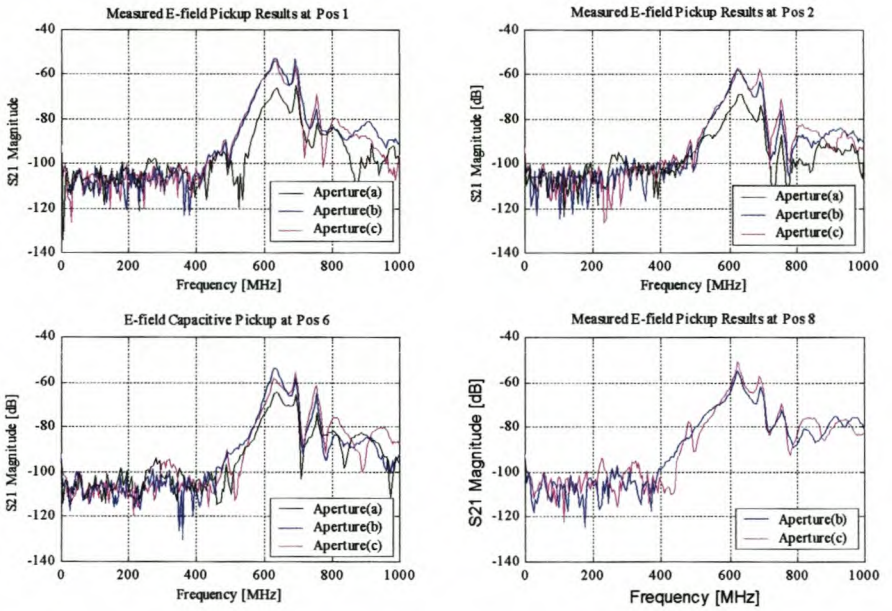

Figure D.4.2: Measured induced *E*-field strength from a coaxial cable.

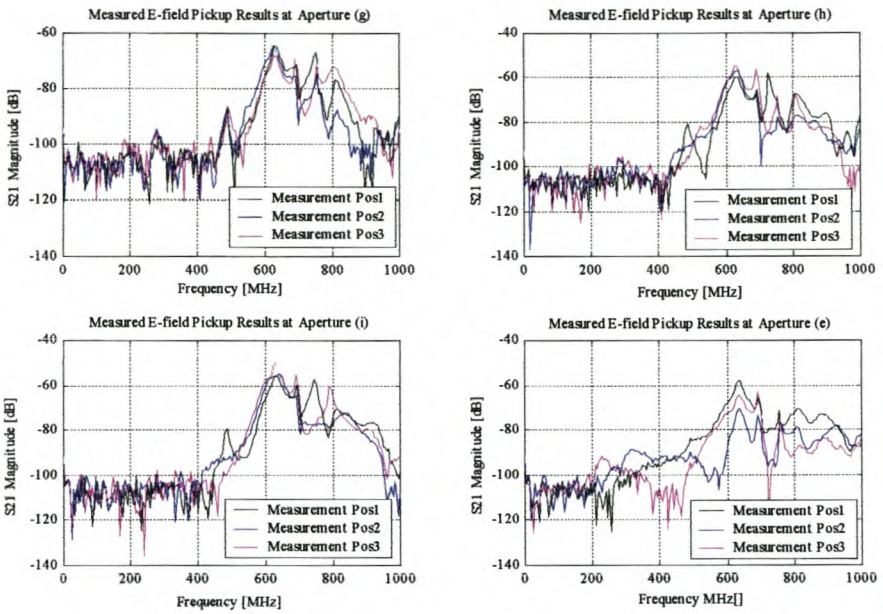

Figure D.4.3: Measured induced field strength from a coaxial cable at aperture (b), (c), (h) and (i).

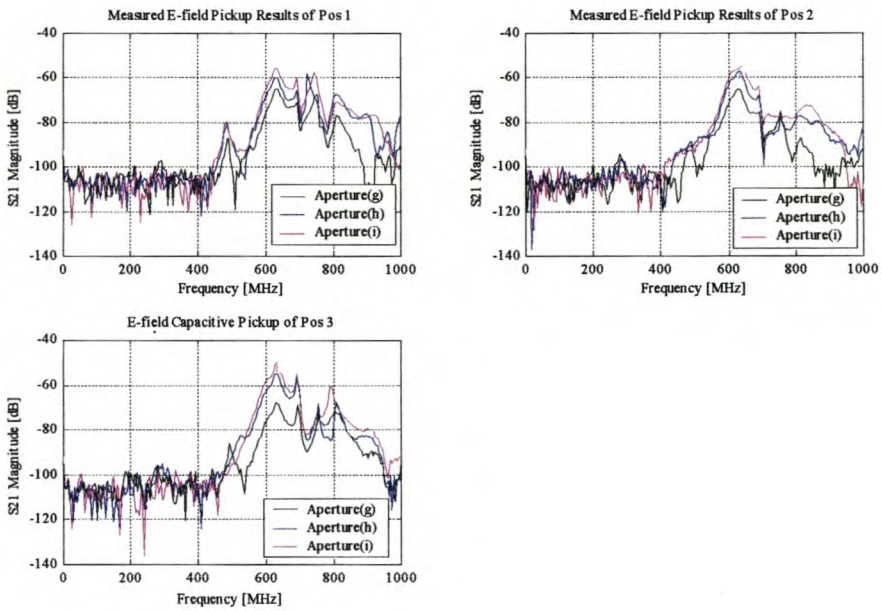

Figure D.4.4: Measured induced field strength from a coaxial cable.

D.5 Harmonic Measurements

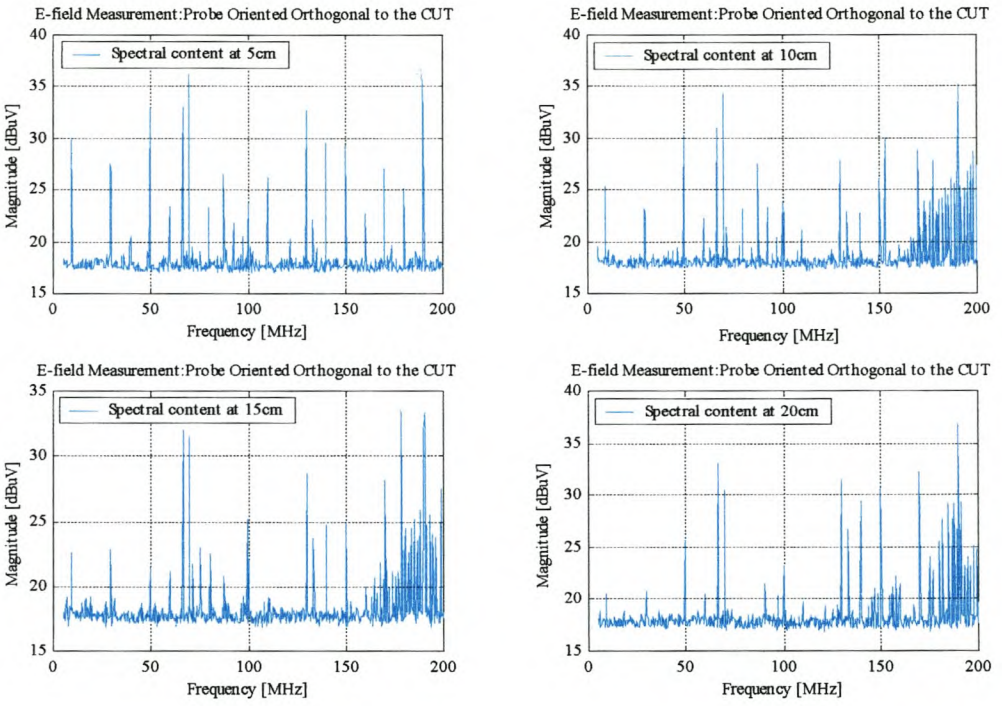

Figure D.5.1: Spectral content response of relative CM current emissions detected with an *E*-field probe positioned orthogonal to the ribbon cable.

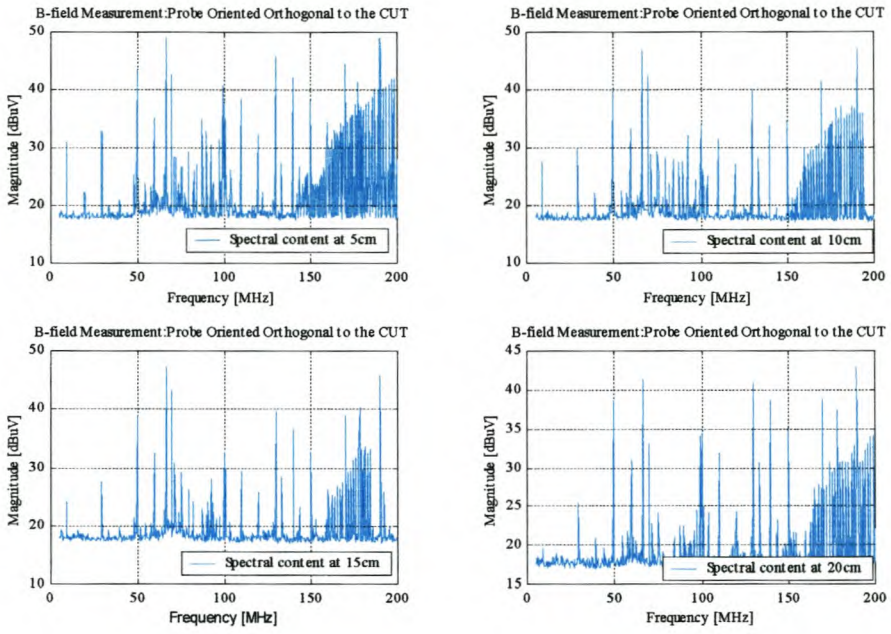

Figure D.5.2: Spectral content response of relative CM current emissions detected with a *B*-field probe positioned orthogonal to the ribbon cable.

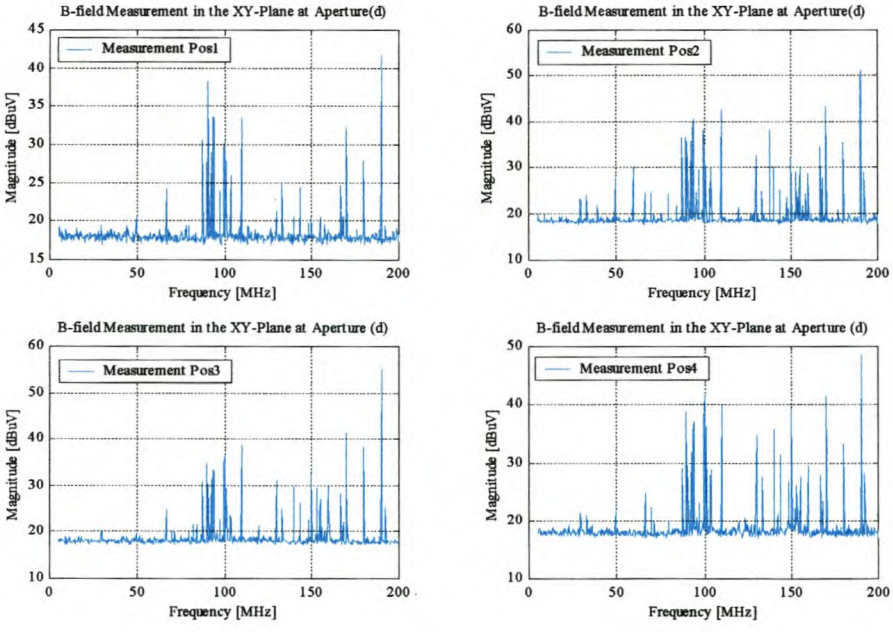

Figure D.5.3: Spectral content response of relative CM current emissions detected with an *B*-field probe within the EMC ITS.